A New Approach to Monitor the Integrity of Grounding Grids

Yury Chikarov

A thesis submitted to

Auckland University of Technology

In fulfillment of the requirements for the degree of

Doctor of Philosophy (PhD)

2013

School of Engineering

TABLE OF CONTENTS

LIST OF FIGURES

LIST OF TABLES

LIST OF SYMBOLS

A- Area of the grid in m^2

a- Distance in perpendicular direction between any point P on the surface and the conductor in m

a- angle between the element dx and D

B- Magnetic flux density, magnetic field value, in T

C - Capacitance of the element in F

D - Distance between elements, spacing between current carrying conductors in m

D_m- Maximum distance between any two points on the grid in m

d - Diameter of the conductor in m

$dx=|dp|$- length element

d_{hor} - Diameter of the horizontal element in m

d_{ver} - Diameter of the vertical element in m

Em- The actual maximum mesh potential in V

$Estep$- Step potential in V

$Etouch$- Touch potential in V

f - Frequency in Hz

f_0 - Cut off frequency in Hz

H- Magnetic field intensity, strength in A/m

h_1 - Thickness of the first layer in m

h_2 - Thickness of the second layer in m

I- Current injected into the grid or conductor in A

Ie- Current that flows through the element in A

I_f- Fault current in A

I_b- Current in a branch of the grounding grid

K_i- Irregularity factor

K_m- Geometrical factor

k- The ratio of actual frequency to the fundamental one

L - Inductance of the element in H

L_C- Total length of the conductor in the horizontal grid in m

L_p- Peripheral length of the grid in m

L_m- Effective buried length of elements in m

L_x- Maximum length of the grid in the x direction in m

L_y- Maximum length of the grid in the y direction in m

LED- Light-emitting diode

l - Length of the conductor in m

l_1 - Length of the first conductor in m

l_2 - Length of the second conductor in m

l_{ver} - Length of the vertical electrode in m

M- Mutual inductance in μH

P- Point on the soil surface

PCIU- Phase comparison and indication unit

PLC- programmable logic controller

PLR- programmable logic relay

R - Resistance of the conductor in Ω

R_{cont} - Contact resistance between soil and the element in Ω

R_f - Resistance of failure in Ω

R_{hor} - Resistance of horizontal element in Ω

R_{leak} - Resistance to the leakage current in Ω

R_{me} - Self-resistance of the element (resistance of metal) in Ω

R_{soil} - Soil resistance in Ω

R_{ver} - Resistance of vertical element in Ω

r - Radius of the conductor in m

S - Switch

S_f- Current division factor

SI- Signal indicator

s- Cross section of the conductor in mm^2

t - Depth of the grounding grid in m

V - Voltage in V

V_Δ- Voltage drop from a node of the grid to remote ground in V

X_C - Capacitive reactance in Ω

X_L - Inductive reactance in Ω

X_{LM} - Inductive reactance taking into account mutual coupling in Ω

x_e- Inductive reactance of the conductor per meter in Ω/m

Y- Admittance of the conductor in S (1/Ω)

Z - Total impedance of the element in Ω

Z_b- Total impedance of a branch of the grounding grid in Ω

Zm- Mutual impedance in Ω

Z_p- Total impedance of a system in parallel to the grounding grid in Ω

Z_s- Total impedance of a power system before the injecting point in Ω

ε_r - Relative soil permittivity

μ_0 - Vacuum permeability

μ_r - Relative soil permeability

ρ - Soil resistivity in Ωm

ρ_0 - Soil resistivity at low frequency in Ωm

ρ_1 - Equivalent soil resistivity of first layer in Ωm

ρ_2 - Equivalent soil resistivity of second layer in Ωm

ρ_e - Resistivity of the conductor in Ωm

ρ_{eh} - Equivalent soil resistivity for the horizontal element in Ωm

ρ_{ev} - Equivalent soil resistivity for the vertical element in Ωm

ω - Angular frequency in rad/s

ATTESTATION OF AUTHORSHIP

"I hereby declare that this submission is my own work and that, to the best of my knowledge and belief, it contains no material previously published or written by another person (except where explicitly defined in the acknowledgement), nor material which to substantial extent has been submitted for the award of any other degree or diploma of a university or other institution of higher learning"

Yury Chikarov ______________________________

Date ______________________________

ACKNOWLEDGEMENTS

Every thesis is not a work of only its’ author. There have been a lot of people who helped me on my way through both professionally and morally. Foremost I would like to express my deep gratitude and appreciation to my primary supervisor, Professor Tek Tjing Lie for his guidance and enormous support within the whole period of study. Without his attitude, patience and help it will not be possible to fulfil this work.

Also I am thankful for my secondary supervisor, Dr. Nirmal-Kumar C Nair from The University of Auckland for his encouragement, understanding and support towards completion of this work.

I also would like to thank Mr. David Nutt, Professor Krishnamachar Prasad and Dr. Adam Taylor from School of Electrical Engineering for their patience and great professional advices sometimes even in complicated technical questions.

Crucial technical support, especially in respect to the experimental part of the thesis, was provided with help of technical staff of our School. I would like to express my appreciation to Mr. Dave Crofts, Mr. Steven Hartley, Mr. Danny Moore and many other people for their help in this regards.

I also would like to thank the officials of School of Engineering and AUT for the financial support in terms of scholarships and grants that kept me focused on the thesis and for all the other opportunities extended for the PhD students. My respect and gratitude to Professor Zhan Chen, Kath Mills, Armida Pobre, Richard Nelson, Shirley Liew and many other people from our School who helped me in my work.

ABSTRACT

Connection of the potentially hazardous conducting parts of electric power plants with ground is the cheapest and most reliable way of providing safe conditions for staff and equipment of the power plant. The performance of the grounding mostly depends on the soil structure and its characteristics such as temperature, salts and acids presence, dampness etc. A grounding grid is buried in soil surface so that a visual inspection of its condition is difficult.

One of the main goals for grounding is to provide a continuous path for currents that may otherwise present hazard to the staff and equipment by dissipating the energy to the soil. For some cases it is to provide equipotential distribution throughout the territory of the power plant (substation). Both criteria can be met by only physically integrated grounding device. In situations of damaged grounding, safety parameters may be breached which may potentially result in electrocution of the staff and failure of the equipment.

Nowadays standardized and scientific techniques allow us to investigate a wide range of the grounding devices' characteristics but unfortunately it is not enough for a comprehensive representation. Using technical data, it is only possible to estimate an area where damaged elements can potentially be. But they do not provide the information about exact location of the damaged element and its' failure.

The proposed study sets up electric characteristics and features of the processes in grounding for different regimes. One of the parts of the analysis is dedicated to the determination and description of the processes with respect to a single horizontal element of the grounding grid. It then describes the features of the current and magnetic field distribution for the integrated and damaged horizontal element of the grid. A novel frequency response part of the analysis has also been carried out in order to establish a future investigative method using frequency of a test signal. The final part combines the parameters of the horizontal and vertical elements and their mutual coupling for the purpose of safety parameters evaluation. This part also describes distinctive features of the current and potential distribution in case of presence of the damaged horizontal elements. It includes not only mathematical but also a computer modelling of the processes. The exploration is intended to establish comparative performance of grounding with and without damaged horizontal elements.

The experimental part of the work validates and justifies the afore-described mathematical theory and formulation. It is also aimed at determination of the most appropriate parameters of the test signal for monitoring the health of the grounding devices.

This work also suggests a technical solution in terms of sequence of steps for the grounding devices' investigation and a device which is capable of location of the damaged elements and position of failure.

Overall, this research is focused on creation of a new approach towards establishing condition monitoring of grounding integrity. Considerable benefits such as time and labour reduction for the grounding devices investigation with increase of accuracy of failures location can be achieved by using this proposed technique.

CHAPTER 1: INTRODUCTION

1.1 Introduction

The widespread use of electricity in all sectors of industry, transport, agriculture and households has led to a significant increase of personnel associated with the operation of electrical infrastructure. In this regard, issues of electrical safety when servicing electrical equipment has acquired growing importance. The ways to improve electrical safety conditions are the establishment of new principles and methods of protection, taking into account advances in science and practice of electrical safety.

Electric power plant itself is a complex system consisting of high voltage apparatus, switchgear equipments, buildings and auxiliary units. It is necessary to provide normal and safe operating condition for staff and equipment. One reason for increased risk during a short circuit condition is due to ineffective integrity of the grounding devices.

A grounding device is one of the most important parts of electric power plants. It is not only protection from electrocution of staff and equipment damages but also in some cases a return circuit for load current.

The performance and reliability of grounding devices depends on its structural integrity. If grounding conductors are damaged, it may malfunction protective relay operation and therefore circuit breaker nuisance tripping. It also may result in failure of the grounding device itself, secondary circuits' cables and elements such as protection devices and etc. The circuits may attain unacceptable values when short-circuit fault currents occur in the network.

Since grounding grids are buried in the ground and their characteristics are influenced by surroundings it is challenging to find damaged horizontal elements in them.

The main purpose of this work is to investigate, describe and understand grounding devices' behavior for a range of scenarios and develop a new way to carry out their condition monitoring.

The features of the current and potential distribution in the grounding grids with damaged horizontal elements revealed within this research have never been described or investigated before.

The mathematical and computer modeling undertaken in this study explains new scenarios and regimes of the damaged grounding grids and compares them with the regimes of the grounding without damages. This analysis shows new distinctive patterns of the electrical characteristics of the grids with and without damaged horizontal conductors. It also enables safety parameters' prognosis in case of damaged elements presence which can significantly improve safety conditions at power plants.

Above mentioned features of the current and potential distribution in the grids with damaged horizontal elements are used for the development of a new technique and a device for the grounding investigation. Technical solutions described as sequence of steps for the grounding investigation technique are unique as well as main functional blocks of the device for such investigation. This new technique and the device can be implemented in conjunction with existing tools for the grounding investigation with significant improvement of accuracy for damages pinpointing and reduction of labor and time for the monitoring.

1.2 Background

Undoubtedly earlier development in regards to electric safety appeared during the initial days of electric power use in the 19th century. It was during those times when first grounding systems were implemented in order to prevent people from electric shocks. There have been a lot of changes, evolutions and choices of grounding systems but the main principle of connecting frames with the ground to provide safety remains the same.

Along with the development and evolution of these systems different criteria for their technical performance evaluation have been implemented. The main standardized parameters for such evaluation became: resistance of the grounding device; value of the potential in the most dangerous points of electric power plant and in the grid of the grounding device; testing the integrity of the ground grid (*IEEE Guide for Measuring Earth Resistivity, Ground Impedance, and Earth Surface Potentials of a Grounding System*, 2012; *IEEE Guide for Safety in AC Substation Grounding*, 2000; *IEEE Recommended Practice for Grounding of Industrial and Commercial Power Systems*, 2007). Meanwhile there has been a substantial scientific research as well in the area of the grounding devices integrity assessment (Jowett, 2008; Ma & Karady, 2009; Ma, Karady, & Kucuksari, 2010; B. Zhang, Zhao, Cui, & Li, 2002). The main focus of the research is to develop a condition monitoring technique that will provide the best solution for the grounding devices in terms of lowest time and labour needed and the highest accuracy for failures detection. So it is very important and necessary to find new distinctive features of the grounding devices' behavior in order to establish a new way of their condition monitoring.

1.3 Rationale

Growth of power systems networks and increasing level of the power consumption has resulted in increase of the short circuit power as well. Higher level of the short circuit currents' magnitude, in its turn, leads to higher voltage on the grounding and on the surface of ground as well. Even though initially the grounding device complies to all standard requirements, with passage of time due to influence of aggressive environment and above-mentioned features there is a probability of failure of horizontal elements of the grounding grids. In turn, it can result in safety parameters deterioration with hazardous operating environment for the equipment and staff.

The research work presented in this thesis will apply a mathematical analysis, computer modeling and experimental investigation to describe the processes in grounding grids due to violation of the integrity of its' horizontal elements compared with the scenario without damaged horizontal elements. Revealed features will be identified as the basis of a new technique and help developing a device to monitor the technical integrity of grounding.

1.4 Significance

Several significant outputs have been identified through this research. Firstly it is a development of fundamental understanding of the differences in processes of the current and potential distribution in certain horizontal element when it is damaged or physically integrated. Also it is a creation of the current and potential distribution "pattern" over the whole grounding grid with or without damaged horizontal elements by means of analysis calculation and computer modeling taking into account various system operating conditions. This will provide a possible prognosis of the safety parameters changes at the territory of electric power plant due to presence of the damaged elements. Main distinctive features of the above mentioned processes will benefit not only towards locating each damaged horizontal element but also a certain point of its failure. This will help to increase the accuracy of the grounding investigation and reduce time and labour needed for it compared with the existing methods and techniques. Also it will eliminate any diggings and tripping to access buried grounding.

1.5 Structure of the thesis

This thesis comprises 7 chapters. The first introduction chapter which presents the background of this research describes rationale and significance of the conducting this work and finally, presents an overview of the structure of the thesis.

The second chapter is a literature overview that provides a summary of the historical development and evolution of the grounding, its importance for providing safety and parameters that are used for the safety conditions evaluation. The literature review continues with the possible issues in case of violation of connection between different parts of the grounding grid compared with the normal operating regime. The overview is extended with the description of modern technical methods and techniques which are able to investigate the grounding devices technical characteristics. This review comprises both standards and scientific resources. Finally, this chapter explores potential ways of improvement for the grounding devices monitoring methods.

Chapter 3 is dedicated to mathematical analysis of the processes of current and potential distribution over a certain horizontal element when it is damaged compared with the case of its normal integrity. This part of the chapter presents the methodology to model a magnetic field distribution behavior as a function of current distribution in the conductor. The chapter also includes frequency response analysis of the grounding elements and a comparison of its parameters with that using the fundamental one.

Chapter 4 deals with the safety parameters evaluation and a potential distribution “pattern” over the grounding device as a whole with and without damaged horizontal conductors. Both mathematical and computer modeling are used. The chapter concludes with remarks on the characteristic features revealed during the analysis.

Chapter 5 presents the experimental study on the processes in the grounding grids. The chapter begins with the investigation of the most suitable characteristics for a test signal used for integrity monitoring. Then the research proceeds with the description of the grounding device under test, experiments carried out and the equipment required for the experiment. The chapter moves ahead with highlighting of the results of each experimental part to be done and concludes with remarks on investigation conducted.

Chapter 6 starts by listing main principles and requirements that provide the basis of a new technique and a device for the grounding monitoring. A possible structure of this device and sequence of technical steps of the technique are described. The research continues with a detailed explanation of the device units’ design schemes and timing diagrams of its performance. The chapter concludes with an algorithm for the new technique’s procedure in order to provide a complete investigation of the grounding device technical condition.

Chapter 7, the last chapter, briefly summarizes the research carried out and draws relevant conclusions. Finally, the chapter proposes the recommendations for further research and future work.

CHAPTER 2: GROUNDING DEVICES

The chapter reviews main aspects of the grounding devices’ performance, its role in providing safety, historical evolution from early days when grounding was used in order to provide safety and the main parameters that were utilized to estimate safety condition at the electric power plants.

2.1 Importance and role in industrial area

According to world statistics, annually there are 3-10 fatal accidents per million inhabitants in different countries per year. Deaths from electrocution in different countries vary between 9%-10%, which is 10-15 times greater than from other injuries. Annually from 1,000 to 1,200 people die due to electrocution in the US and about 250,000 people throughout the world. Electric shocks are 2%-2.5% among other injuries, 60% of all electrical accidents occur as a result of safety violations, 40% are the result of slack in safety aspects in designing power networks, equipment and installations (U.S. Department of Health and Human Services, 2008).

One of the reasons of ineffective operation or failures in operation of relay protection circuits or secondary commutation circuits in case of short circuits’ appearance is the ineffective condition of grounding devices.

Because of an increasing penetration of modern microelectronic devices at electric power plants, in industry, transport and communication the problem of their electromagnetic compatibility appeared (Haddad, Warne, & Institution of Electrical Engineers, 2004). The problem solution to address this is not possible without the correct operation of the grounding devices.

And of course, the main function that the grounding provides is safety for people who may be in contact with equipments of the power plant. Human operating safety is paramount and therefore keeping the grounding in order is vital (Cooper & Dolbey Jones, 1997).

A reliability of electric equipment operation and electric safety of a staff depends on the technical condition of the grounding devices. A peculiarity of the grounding devices is that their characteristics are changing constantly because of an influence of factors such as soil structure, dampness, presence of salts and acids, electric corrosion, some separate elements destruction because of freezing process etc. Meanwhile a visual assessment of the grounding devices' technical condition is not possible without actual digging. As a result, in time, there is a possibility of rise of the grounding devices current spreading resistance, horizontal elements ruptures that can lead to failures in operation of secondary commutation circuits in case of short circuits under abnormal operating conditions and also to a high voltage appearing on electrical equipments' frames, damages of insulation, thermal and electrical injuries of people. There is even a possibility of events when grounding devices meets the regulatory requirements but are often unsuitable for use in terms of the electromagnetic compatibility - when faults can damage or lead to malfunction of the secondary circuits' cables and relay protection and automatic systems.

2.2 Historical development and evolution

Towards the end of 19th century following initial installations and use of electric energy led to better understanding of high voltage (more than some dozens volts) use hazard especially with respect to AC current. There were no standards that could provide adequate information for people and fire protection (Bernard Lacroix & Calvas, 1998).

In the early period of development of three-phase power systems, it was a common practice to isolate neutral points and operate the system in an ungrounded state. In the UK, the majority of the high voltage systems were operated this way until 1912, and in Germany this was the case until 1917. However, as power systems grew in size, problems with this method of operation emerged because the magnitude of ground fault current in an ungrounded system increases with the phase-to-ground capacitance of the network. Above a certain current threshold, persistent intermittent arcing will occur during the fault resulting in damage to equipment close to the arcing fault. Also, damage can occur to the other parts of the network as a result of high magnitude overvoltages that are developed. Therefore, the permanent single-phase-to-ground fault on such systems becomes unmanageable and fast fault detection and isolation, or alternatively methods of suppressing the arc, are required.

The first requirements to ground equipment frames appeared in France in a "standard" for electrical installation in 1923. The standard provided absolutely no information on grounding conditions or on the value of ground connection resistance, and stipulated no protection device. Meanwhile the requirement for a ground leakage trip operating at 30mA or less was introduced in the UK in 1930.

Subsequently with a wide spread and growth of power supply industry in many countries standardized requirements to grounding improved significantly.

Nowadays, some parts of high voltage networks still operate ungrounded because it can be advantageous, under certain circumstances. However, the most commonly recommended practice is to ground at list one neutral point of the network, and there are important advantages in operating the systems in this way. The main advantage is that the power system is safer because ground faults are easier to detect, to clear and to locate (Jones, Jones, & Mastrullo, 2011).

According to how the neutral is connected to ground, grounded systems are categorized as either solidly grounded or impedance grounded. Impedance grounded systems can be classified as resistance, reactance or resonant type.

The three grounding systems (TN, TT and IT) internationally standardized finally have been adopted in many national standards. Each of these systems had its own advantages and disadvantages but they all ensured safety of persons (*Electrical Installations for Buildings*, 2005). All the three systems described above are defined as follows:

- The **TN** system: The transformer neutral is grounded. The frames of the electrical loads are connected to the neutral.
- The **TT** system: The transformer neutral is grounded. The frames of the electrical loads are also connected to the ground connection.
- The **IT** system: The transformer neutral is not grounded. The frames of the electrical loads are connected to the ground.

2.3 Soil resistivity

The ground is a poor conductor and, therefore, when it carries high magnitude current, a large potential gradient will result and the grounding system will exhibit a ground potential rise (GPR).

Soil and rock resistivity may vary considerably from region to region, and it is rarely constant either vertically or horizontally in the area of interest around an electrical installation. The magnitude of power frequency ground fault currents can range from a few kA up to 20-30 kA, and ground impedances of high voltage substations may lie in the range from 0.05Ω to over 1Ω (*IEEE Guide for Safety in AC Substation Grounding*, 2000).

The following factors will affect the resistivity of the ground and, hence, the resistance to ground of the electrodes:

1. Type of soil (e.g., sand, clay, rich soil, swamp).

2. Moisture content (e.g., after a rain or during a drought).

3. Salt content.

4. Temperature.

5. Frequency of injected signal and its waveshape (e.g., dc, 60 Hz, or transient signals).

6. Stratification (e.g., layer of top soil, followed by clay, followed by rock).

7. Density of soil (i.e., packing of the soil) and grain size (e.g., fine soil, large clumps).

8. Depth.

9. Season.

10. Nearby objects (e.g., metal pipes, concrete slabs, buried tanks, fences).

11. Surface topography.

Since water is conductive and electrolytic, it should not be surprising that the quantity and type of water and salts in the ground will influence the ground's resistivity. When the moisture content increases from nearly 0% up to about 14-18%, the resistivity decreases considerably. After this percentage, the rate of decrease is very slow. Usually, soil has moisture content above 40%. A large quantity of water does not imply that the resistivity is low. Sand saturated with distilled water does not have the same low resistivity as garden soil lightly watered with well water. Compared to metals, the conductivity of most soils is extremely poor.

The conductivity of the upper layer of the ground can be greater than the lower layers, especially when the top layer is a rich top soil. In this case, generally the upper layer will carry most of the current of an electrode (if not driven too deeply). Sand and bedrock near the surface usually imply a high resistivity (Yacobs, 1981).

For shallow grounding electrodes, the temperature is important. Generally, the resistivity decreases as the temperature increases. At low temperatures, the ground water can freeze increasing the resistivity of the soil. This increase in the resistivity is (one reason) why it is recommended that the tip of a grounding rod be placed at least below the frost line. As the water is evaporated from the soil, the resistivity can also increase. The stability of the grounding system (i.e., variation of the resistance over time) is often enhanced by increasing the depth of the electrodes.

High levels of current can dry up the soil, increasing its resistivity. In some older power systems, the neutrals may be connected via the earth ground. This can be a continuous source of high level current (Kaiser, 2005)

Apart from satisfying electrical safety, the grounding system should also have sufficient mechanical strength and be corrosion resistant, and the system should have adequate thermal capability for carrying the maximum fault current. These aspects are dealt with in detail in most standards about grounding (Short, 2003).

2.4 Safety parameters

Grounding devices apart from providing safety and in some cases a return circuit for load currents also provide an equipotential distribution of the voltage on the surface of the ground at power plants (Natarajan, Imece, Popoff, Agarwal, & Meliopoulos, 2001).

As seen from Figure 2.1, when two parts of the grounding grid of AC transit substation are bonded together with proper integrated conductors there will be no substantial potential difference amongst the point of enclosures. But if one of the conductors is damaged, it will increase the value of the current and the voltage in the other one. Such overvoltage can create the situation when the second conductor will be damaged due to overheating. Once this happens the integrity of the grounding is affected.

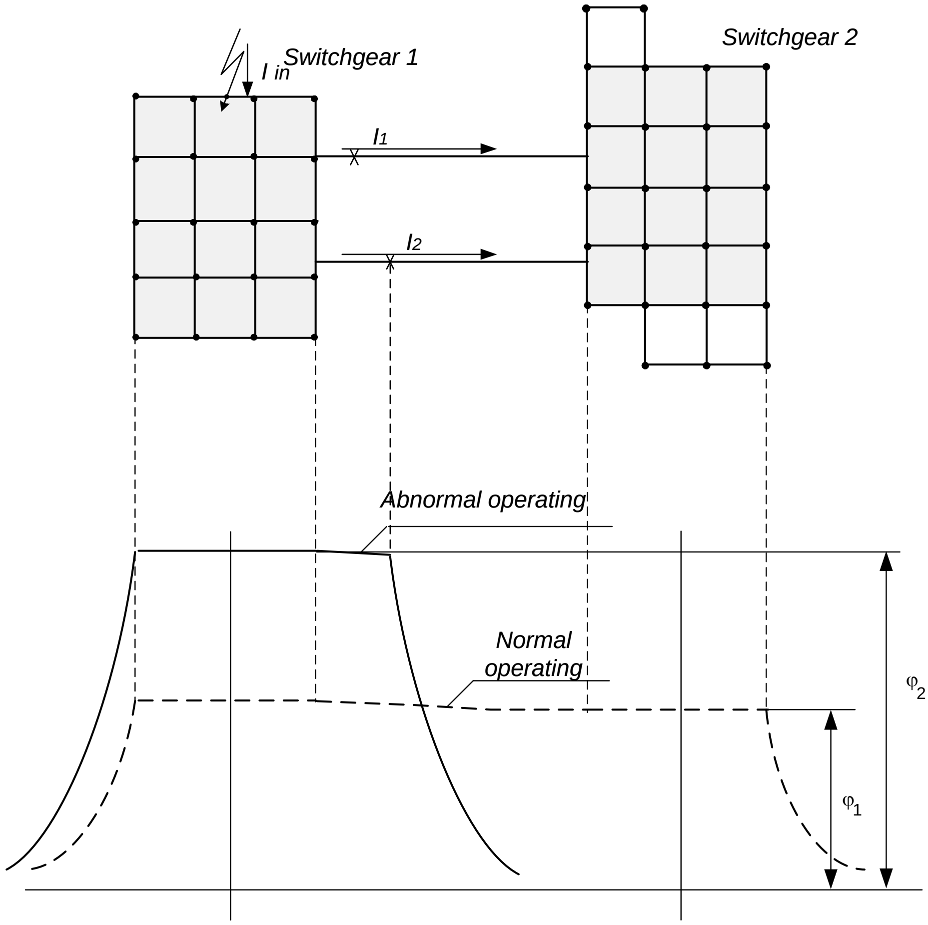

Figure 2.1: High potential appearance in a transit substation

The picture in Figure 2.1 is an example of the grounding device of AC substation when switchyards of different voltages and parts of the power plant are connected together by means of horizontal conductors or sheaths of cables.

The most important parameters of electric safety at power plants are touch voltage and step voltage (Cooper & Dolbey Jones, 1997; *IEEE Guide for Safety in AC Substation Grounding*, 2000) as shown in Figure 2.3.

As from (*IEEE Guide for Safety in AC Substation Grounding*, 2000):

> *Step voltage: The difference in surface potential experienced by a person bridging a distance of 1 m with the feet without contacted any grounded object.*
>
> *Metal-to-metal touch voltage: The difference in potential between metallic objects or structures within the substation site that may be bridged by direct hand-to-hand or hand-to-feet contact.*

Step voltages are normally less hazardous than touch voltages for two reasons:

(1) The human body can tolerate higher voltages across the foot-to-foot current path (step) compared to the hand-to-feet path (touch);

(2) For any given position, the step voltage is lower than the prospective touch voltage.

According to the experimental data described in (*IEEE Guide for Safety in AC Substation Grounding*, 2000), the resistance of the human body for hand-to-hand contact is equal to 2330Ω. The hand-to-feet resistance is equal to 1130Ω. But in general for the human body, it is suggested to use value of 1000Ω.

> *It should be remembered that the choice of 1000Ω resistance value relates to paths such as those between the hand and one foot or both feet, where a major part of the current flowing from one foot to the other is far less dangerous. It is generally agreed current flowing from one foot to the other is far less dangerous.*

Usually the grounding grids' construction for power plants is a grid buried into the soil at approximately 1 meter depth. This grid contains horizontal elements bonded together and connected to the equipment enclosures and other parts of the plant. The grid includes meshes of the horizontal elements located throughout the territory of the power plant. In addition to the horizontal grid, sometimes vertical electrodes can be added to it. The number of vertical electrodes, their length (several meters), diameter and location are determined by the climate conditions, geometry of the power plant, resistivity of the soil and some other reasons. The vertical electrodes are also bonded to the horizontal grid.

The location of the worst-case step voltage is accepted by both UK and US standards to be the potential difference across the ground surface one meter diagonally out from the corner of the grid (*IEEE Recommended Practice for Grounding of Industrial and Commercial Power Systems*, 2007).

While the grounding grid does not have damaged elements, the ground potential is not uniform but it has rates of change that are sufficiently limited so that a step or touch potential is not fatal as shown in Figure 2.2. When the vertical electrodes are close to each other, the curve of the potential distribution will be close to an ideal horizontal line.

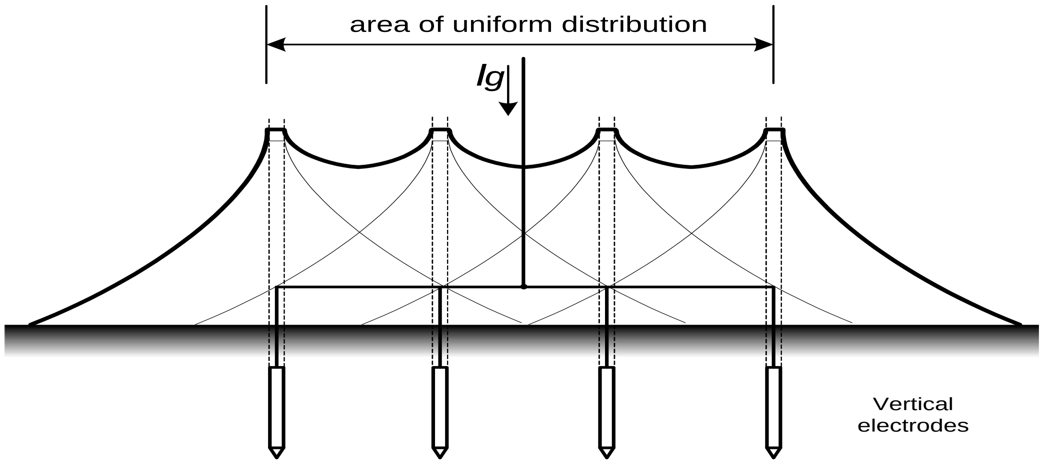

Figure 2.2: A curve of potential distribution on the surface

This means that under both normal and abnormal operating conditions all the equipment enclosures and staff will have no potential difference among the perimeter of a power plant (V_{step} and V_{touch1} in the Figure 2.3).

In case of the presence of horizontal elements' damages an uneven potential distribution appears on the surface of the ground. The profile of the potential curve in Figure 2.3 in such conditions will not have uniform distribution and this fact can lead to the substantial step voltage appearance. Especially it can be dangerous on the surface above the edge meshes of the grid. Value of the potential difference may exceed the breakdown voltage of the secondary circuits' cables insulation and in the worst situation may result in the common-mode failure of relay protection and circuit breakers. Such situation can result in the most dangerous consequences for staff and equipment (V_{touch2} in Figure 2.3).

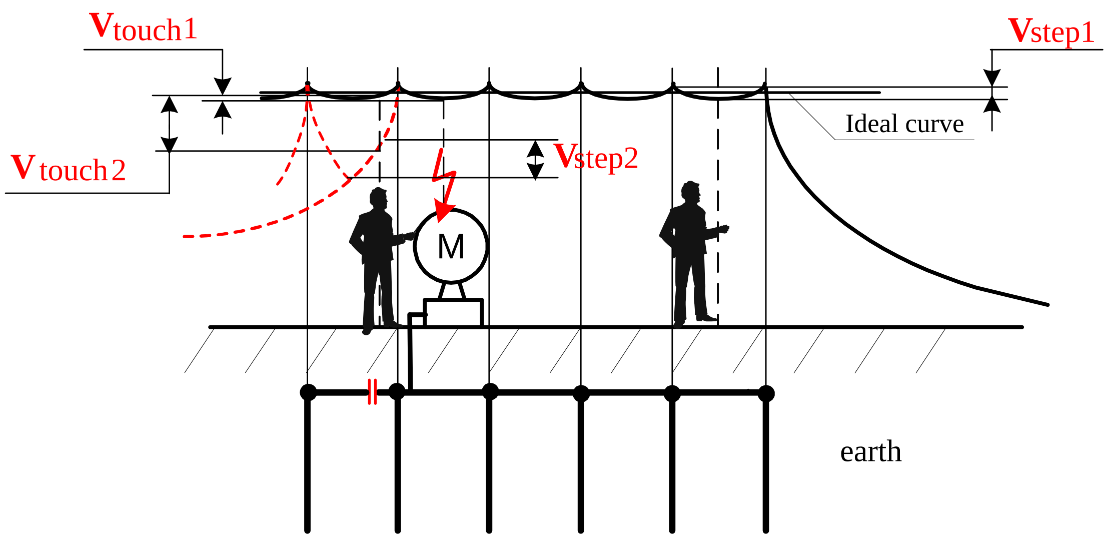

Figure 2.3: Touch and step voltage exposure

As it can be seen from Figure 2.3, if the grounding grid is integrated then the values of step and touch voltages are small (V_{touch1} and V_{step1}). If the grid has a damaged horizontal element then the curve of the potential is not uniform anymore and thus, one can expect an increase of safety parameters values (V_{touch2} and V_{step2}).

Some of the main examples of the elements breakages are shown in Figure 2.4.

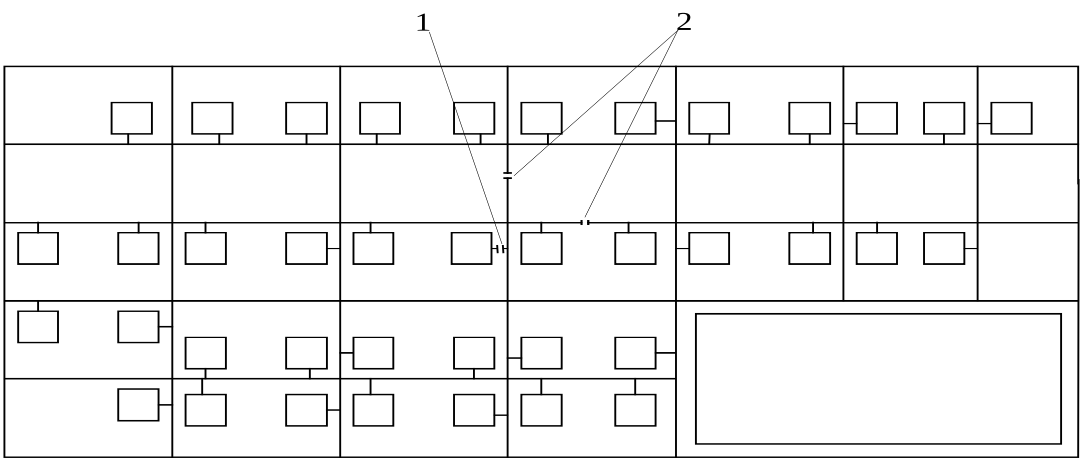

Figure 2.4: Grounding device with damaged horizontal elements and grounding conductors (pigtails).

The figure represents possible damages of the grounding elements. The damaged horizontal elements are shown as 2 in the figure when 1 is a damaged grounding conductor which connects the enclosure with ground.

2.5 Existing techniques and methods for the grounding devices' investigation and calculation

Typically, approximately 80%-90% of the whole elements of a grounding device are horizontal elements. It means that integrity of the whole grounding device depends on the integrity of its horizontal elements.

The grounding device's horizontal elements are to be more susceptible to deterioration in a corrosive environment than the vertical ones. Being in a soil superficial stratum, the horizontal elements are exposed to air oxygen more than vertical elements. As a result, the horizontal elements are more prone to be corroded.

The existing technology of grounding devices is currently determined by measuring their parameters as follows: (i) resistance of the grounding device to ground; (ii) value of the potential in the most dangerous points of electric power plant and in the grid of the grounding device; and (iii) testing the integrity of separate parts of the grounding (*IEEE Guide for Measuring Earth Resistivity, Ground Impedance, and Earth Surface Potentials of a Grounding System*, 2012; *IEEE Guide for Safety in AC Substation Grounding*, 2000; *IEEE Recommended Practice for Grounding of Industrial and Commercial Power Systems*, 2007).

It means that all grounding devices associated with the processes of safe electric energy generation, conversion, transformation, transmission, distribution and consumption and also associated with the lightning protection must satisfy the basic rule of electric safety. All available touch exposed conductive parts of grounding devices, adjacent conductive parts, grounding conductors and also conductive parts of the return circuits, including rails, cable sheathing must be safe for direct contact with them under normal operation, in case of hazardous insulation damages and with an impact of the lightning current as well (O'Riley, 2002).

Unfortunately, the above mentioned measurements do not show a complete picture of the grounding devices state, because the actual configuration of the grids and characteristics of its elements change within the period of operation and may do not meet the requirements of normative documents. It may result in the outages of the grounding devices main functions and growth of GPR, touch and step voltages, uneven potential distribution. And at the same time, even if the resistance of the grounding device is low with a tendency of single-phase-to- ground current increasing the GPR can be substantial and exceed limited values especially when some horizontal elements are damaged.

There are several existing publications highlighting proper design, use, maintenance and monitoring of the grounding devices' characteristics which provides information about proper evaluation, installation and connection at the initial stage of the grounding devices' "life" (*IEEE Guide for Measuring Earth Resistivity, Ground Impedance, and Earth Surface Potentials of a Grounding System*, 2012; *IEEE Guide for Safety in AC Substation Grounding*, 2000; *IEEE Recommended Practice for Grounding of Industrial and Commercial Power Systems*, 2007).

According to (*IEEE Guide for Measuring Earth Resistivity, Ground Impedance, and Earth Surface Potentials of a Grounding System*, 2012), the objective is to determine whether the various parts of the ground grid are interconnected with low resistance copper. This copper is shunted by the surrounding ground, which usually has very low impedance.

The ammeter-voltmeter method, using alternating current, cannot be used satisfactorily for this test. The reactance of a large copper wire in this case is shunted by the surrounding ground, a path which may have slightly less reactance than the wire. Therefore, a continuity test for buried wire would give indeterminate results if alternating current was used.

The practical integrity test consists of passing about 5 A into the ground grid between two points to be checked. The voltage drop across these points is measured with a millivoltmeter or portable potentiometer and the effective resistance is calculated from the current and voltage readings.

This method is able to approximately identify the fact of integrity failure but cannot identify the location or establish if all elements are fine.

Other methods discussed in literature are summarized as follows: (Dawalibi, 1986; Ma et al., 2010) introduces the method when current with value about 150-200 A and frequency not 60 Hz is injected in a grounding device between two points (pigtails) that are located not far from each other. This method is different from (B. Zhang et al., 2002) in that the injected current is required to be around 200 A and its frequency is not 60 Hz or 60 Hz harmonic. Conclusion about the possibility of broken (corroded) element is made when weak magnetic field is captured above the elements.

However, all experiments were conducted when a substation was under construction and there was no power frequency magnetic field influence on the experimental setup.

Another method is described in (Jowett, 2008) when broken conductors are identified by substantial difference between the theoretical and simulated magnitudes of the leakage currents. In the method a high frequency current (up to 1 MHz) is injected into the ground grid and potential values are measured over the surface of the grid. A similar approach is highlighted in (Giannini & Dzapo, 2004) where faults are not precisely pinpointed, but by isolating a faulty current path, the work of excavation and repair is markedly reduced.

A device introduced in (L. D. Grcev, 1996) is designed to perform all required voltage measurements under conditions described in standards (*IEEE Guide for Measuring Earth Resistivity, Ground Impedance, and Earth Surface Potentials of a Grounding System*, 2012; *IEEE Guide for Safety in AC Substation Grounding*, 2000). It is based on the heavy current method procedure in large substation grounding systems inspections when the measuring current of the main frequency (50 Hz or 60 Hz) is injected into grounding system, providing a source of induced surface potentials. The device consists of two parts, (i) the IMD (intelligent measuring device) and (ii) the accompanying IPE (integrated program environment) for a personal computer.

None of these methods determine a possible breakage indication, particularly the estimated location of the horizontal element's damage.

Details about the calculation of a grid resistance, effect of ground non-uniformity, the highest possible short circuit current and determining the substation GPR (ground potential rise) are available from (L. D. Grcev, 1996; Hickey, 2002; *IEEE Standard for Qualifying Permanent Connections Used in Substation Grounding*, 2003).

Most of the mathematical modeling for grounding devices is based on the circuit theory or electromagnetic field theory. The common feature of the models is currents calculation and evaluation of the potentials across the grids conductors.

One of the computer models, based on electromagnetic field theory, for transient analysis of a network of buried and above ground conductors is described in (Dzapo & Giannini, 2003). In this analytical model, the current distribution is determined by the sinusoidal approximating function when current is considered to be zero at the end points of the segments and rises sinusoidally to a maximum at the junction point of the segments.

Assumptions made include (i) the total current in the conductors is filamentary line current in the conductors' axis; (ii) the current on open end points is assumed to be zero; (iii) the soil is modeled as linear and homogeneous half-space characterized by conductivity, permittivity and permeability constants; and (iv) neglect of the soil ionization.

Reference (Yang & Pan, 2008) focuses on the description of a program support computer visualization model which helps a user to look at the whole ESP (ground surface potentials) map of power substations. In fact, it comes down to work on the image pattern of potential distribution on the surface of the ground with already pre-measured or calculated potential magnitudes.

The work shown in (Li, Chen, Fan, & Lu, 2006) and (Huang & Kasten, 2001; Selby & Dawalibi, 1994), introduces a mathematical model, based on the theory of electromagnetism, combined with the moment method and electrical network model techniques. The model for calculating of the magnetic source currents distribution of a grounding system with or without floating metallic conductors in AC substations is presented. Both leakage currents and their mutual coupling influence are considered in the calculation. The ground is considered as multilayer conductivity medium.

There is also a range of research papers regarding the problem of the grounding devices corrosion and its influence on the safety conditions.

In (Otero, Cidras, & Alamo, 1999), the authors proposed a new method of corrosion diagnostics of the grounding devices' elements with a similar approach to that of (Liu, Xiao, & Tian, 2010).

Major engineering project companies and grounding equipment manufacturers now have in-house computer programs to evaluate different substation grounding arrangements (Hu et al., 2000).

As one can see mathematical studies presented in the above referred papers do not reveal the processes taking place in the grounding devices with damaged horizontal elements and do not provide possible changes to safety parameters in such cases.

CHAPTER 3: MATHEMATICAL ANALYSIS OF THE PROCESSES IN ELEMENTS OF GROUNDING

Chapter represents several measures such as reviewing and investigating of the state-of-the-art of grounding devices design as presented in the previous chapter.

The study presented in this chapter is a development of a mathematical apparatus in order to clearly understand processes taken place in the grounding devices in different regimes of its operation. Such an analysis is paramount for the future understanding and detection of the processes' distinctive features.

The analysis carried out in the chapter comprises three stages. The first stage will be dedicated to a frequency response analysis of the grounding elements and a comparison of its parameters with the one considering the fundamental frequency. Furthermore, the results of this evaluation will be used to establish a test signal frequency for the monitoring of the grounding devices. The second stage will present the methodology to model a magnetic field distribution behaviour as a function of current distribution in a separate conductor. This analysis represents features of the magnetic field behaviour over the damaged element compared with that without failures. The final stage will present an evaluation of the grounding elements impedances and their mutual influence on each other.

3.1 Frequency response on the grounding elements' characteristics

The basic function of the grounding devices is to create a parallel path for faults currents (short circuit currents, induced currents, lightning etc) and effectively disperse them into ground without causing any hazard to people or damage to installation.

Grounding devices may be affected by currents of different frequencies due to a range of processes at power plants. They can be influenced by low frequency currents during normal operation and short circuits and they also may have high frequency influence during lightning strokes.

Under low frequencies, grounding devices are supposed to behave like pure resistances with very good and effective operation. But with the increase of the frequency factor inductive and even capacitive characteristics of the grounding devices can manifest. This may result in variation of the current and potential distribution along the grounding device and deterioration of its efficiency.

Figure 3.1 represents an example of 60 (50) Hz current distribution through the grounding grid. The current is distributed according to the resistance of the parts of the grid with respect to the current injection point. The total current flowing to the right hand side of the grid (see Figure 3.1) will have a higher percentage compared to the current flowing to the other parts of the grid because it has more elements compared with the other parts of the grid.

Taking into account the fact that elements of the grounding device can be evaluated as pure resistances it is possible to calculate voltage distribution throughout a power plant area. Please note that the curve represented in Figure 3.1 is an ideal case.

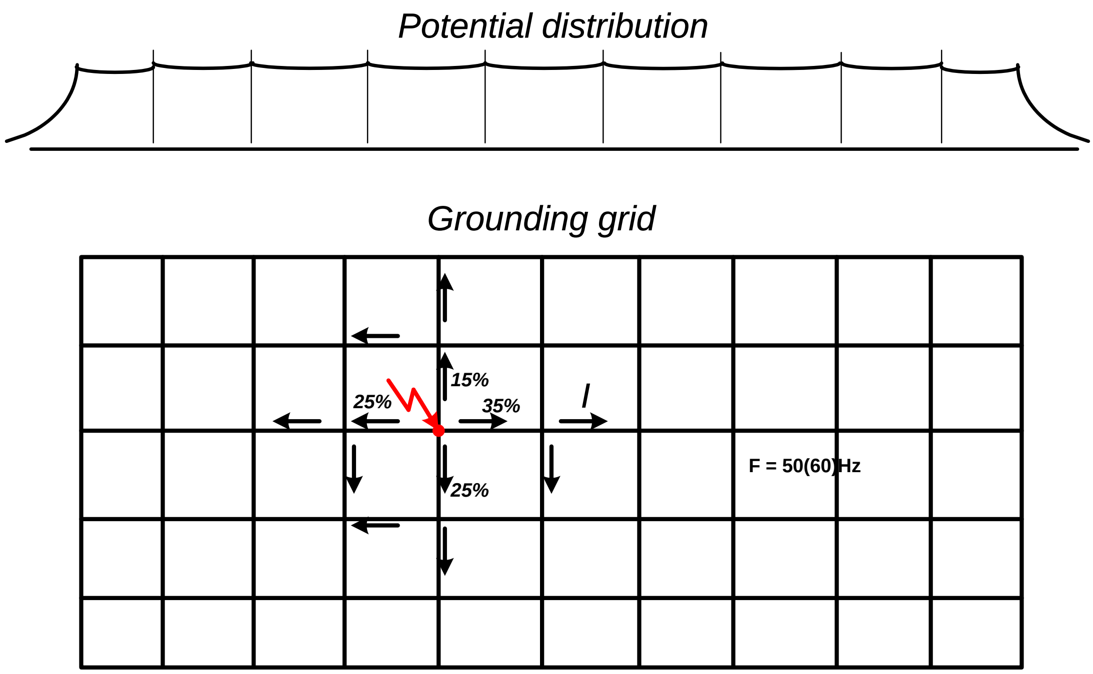

Figure 3.1: Current and potential distribution under 50 (60) Hz

Another figure representing the parameters distribution in grounding may have appeared when the frequency range differs from the fundamental one. In this case the impedances of grids elements may have another features and values. With the increase of frequency one can expect the increase of the reactive component and as a result a substantial influence of capacitance emerges. All of these can result in higher magnitudes of the hazardous potentials on the grounding grids.

Such an evaluation is also important to obtain a test signal frequency which will not change its pattern due to processes in the grids while monitoring.

The frequency-dependency of grounding systems have been addressed by means of different models that can be classified as: (a) models based on the quasi-static approximation and circuit models (e.g. (Olsen & Willis, 1996; Rudenberg, 1945)), (b) transmission line models (e.g. (Mentre & Grcev, 1994; Papalexopoulos & Meliopoulos, 1987)) and (c) full electromagnetic-models (e.g. (L. Grcev & Dawalibi, 1990)).

Initially, mathematical models with regards to currents flow from the grounding device into soil begun from R. Rudenberg and his work in this area (Rudenberg, 1945). He described a fundamental behavior of grounding in the soil. A number of other authors have dealt and worked on the same area as well (Bourg, Sacepe, & Debu, 1995; L. Grcev & Popov, 2005; Llovera, Lliso, Fuster, & Quijano, 2008) and (L. Zhang, Pan, Tan, & Wen, 2009). All of them have a common analysis approach of the impedance of the grounding devices' elements. They highlight three main components in the total impedance of the element which are Resistance, Inductance and Capacitance as a function of frequency (see Figure 3.2).

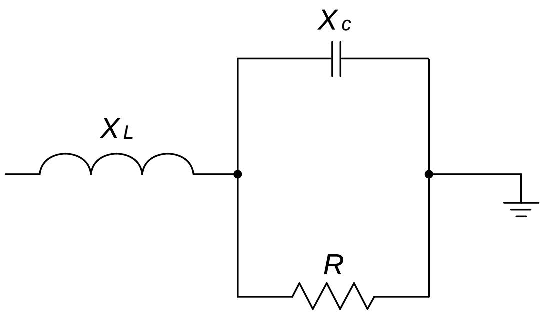

Figure 3.2: Equivalent scheme of the element

Expressions for *R*, *L* and *C* of the vertical ground rod as one of the simplest and most commonly used means for current dissipation have similar "nature" and consequently give approximately the same results. As from (L. Grcev & Popov, 2005), the following expressions are obtained.

$$R = \frac{\rho_0}{2\pi l}\left(\log\frac{4l}{r} - 1\right), \tag{3.1}$$

$$C = 2\pi\varepsilon_r l\left(\log\frac{4l}{r} - 1\right), \tag{3.2}$$

$$L = \frac{\mu_r l}{2\pi}\left(\log\frac{4l}{r} - 1\right), \tag{3.3}$$

According to (Bourg et al., 1995), general expressions for elements of the model are

$$R = \frac{\rho_0}{2\pi l}\left(\ln\frac{4l}{r} - 1\right), \tag{3.4}$$

$$C = \frac{2\pi}{\varepsilon_r l}\frac{1}{F_1(\frac{2l}{r})}, \tag{3.5}$$

$$L = \frac{\mu_r}{2\pi}\left(F_1\left(\frac{l}{r}\right) + \frac{l}{4}\right), \tag{3.6}$$

$$F_1(x) = \ln(x + \sqrt{1 + x^2}) + \frac{1}{x} - \sqrt{1 + \frac{1}{x^2}}\ . \tag{3.7}$$

As from (Llovera et al., 2008), equations are as follows

$$R = \frac{\rho_0}{2\pi l}\left(\ln\frac{8l}{d} - 1\right), \tag{3.8}$$

$$C = \frac{\varepsilon_r l}{18\ln\left(\frac{4l}{d}\right)}, \tag{3.9}$$

$$L = 2l\ln\left(\frac{4l}{d}\right). \tag{3.10}$$

As one can see all expressions are of similar "nature" and consequently give approximately the same results.

Finally, expressions of impedances calculation are as follows:

$$X_C = \frac{1}{\omega \cdot C} = \frac{1}{2\pi \cdot f \cdot C}, \tag{3.11}$$

$$X_L = \omega \cdot L = 2\pi \cdot f \cdot L. \tag{3.12}$$

Recent studies show that it is also important to consider soil parameters, conductivity and permittivity which are frequency dependent as it is described in (Pedrosa et al., 2010) and (Visacro & Portela, 1987) (see Eqns. (3.13) and (3.14)).

$$\rho = \rho_0 \left(\frac{100}{f} \right)^{0.072}, \tag{3.13}$$

$$\varepsilon_r = 2.34 \cdot 10^6 \cdot \rho_0^{-0.535} \cdot f^{-0.597}. \tag{3.14}$$

Within the calculation, it is assumed that a soil structure is homogeneous. Since the aim of the study is getting the percentage of impedance changing as a function of frequency it is acceptable to make such an assumption and by having the same value of the uniform soil resistivity one will get correct results.

In order to describe the grounding behaviour correctly, the calculation model performed in this work is based on the theory described in (Llovera et al., 2008) with modifications by taking into account as presented in (Pedrosa et al., 2010). Therefore, the final equations can be determined as a combination of above-described techniques.

The final equations for R and C parameters can be calculated as follows:

$$R = \frac{\rho}{2\pi l} \left(\ln \frac{8l}{d} - 1 \right), \tag{3.15}$$

$$C = \frac{\varepsilon_r l}{18 \ln \left(\frac{4l}{d} \right)}. \tag{3.16}$$

For the future study with respect to the experimental investigation and development of a new technique it is vital to evaluate possible variations of the grounding elements characteristics when the injected current flows through the horizontal elements but not into the ground. In this case one can determine a so called self-impedance of the elements.

The resistance of the current-carrying conductor for the fundamental frequency current is expressed as follows (Bayliss, 1996):

$$R_{50(60)} = \rho_e \cdot l / s \, , \tag{3.17}$$

Inductive reactance of the conductor is expressed as

$$X_{50(60)} = x_e \cdot l \, , \tag{3.18}$$

The resistance of the copper conductor at high frequency can be described from (Skilling, 1974) as

$$R = 83 \cdot 10^{-6} \cdot \frac{l \cdot \sqrt{f}}{d} \tag{3.19}$$

At the same time inductive reactance of the element is changing significantly as described in the following.

$$X = x_{50(60)} \cdot k \, , \tag{3.20}$$

3.2 Case study

For the purpose of numerical example to illustrate the mathematical models, the following parameters are chosen. Let ρ_0=100 Ωm (under low frequency f=100 Hz), μ_r=1, ε_r =11, l=3 m, d=0.016 m, material of the conductor is copper, ρ_e=0.0175 Ω·mm^2/m, x_e =0.000175 Ω/m.

By substituting the values in Eqns. (3.13) and (3.14), for instance, for the frequency 100Hz one can have

$$\rho = 100 \cdot \left(\frac{100}{100}\right)^{0.072} = 100 \ \Omega\text{m},$$

$$\varepsilon_r = 2.34 \cdot 10^6 \cdot 100^{-0.535} \cdot 100^{-0.597} = 12.741.$$

The results of calculations for frequencies up to 1.5 MHz are presented in Table 3.1 and Table 3.2 respectively. The diapason of frequencies up to 1.5 MHz was chosen in order to provide and compare the possible values of impedances for different regimes of the grounding grids operation including lightning. During the lightning strike frequencies of the currents flowing through the grounding grids are very high. They are considered to be 1Mhz and higher.

Table 3.1: Soil Resistivity as function of frequency

f, Hz	***ρ***, Ωm
100	100
150	97.1
300	92.4
450	89.7
600	87.9
750	86.5
900	85.4
1050	84.4
1200	83.6
$15 \cdot 10^3$	69.7
$150 \cdot 10^3$	59.1
$1.5 \cdot 10^6$	50.0

Table 3.2: Soil Permittivity as a function of frequency

f, Hz	ε_r,
100	12.7
150	10.0
300	6.6
450	5.2
600	4.4
750	3.8
900	3.4
1050	3.1
1200	2.9
$15 \cdot 10^3$	0.6
$150 \cdot 10^3$	0.2
$1.5 \cdot 10^6$	0.04

Graphically the results of calculations are shown in Figure 3.3 and Figure 3.4 respectively.

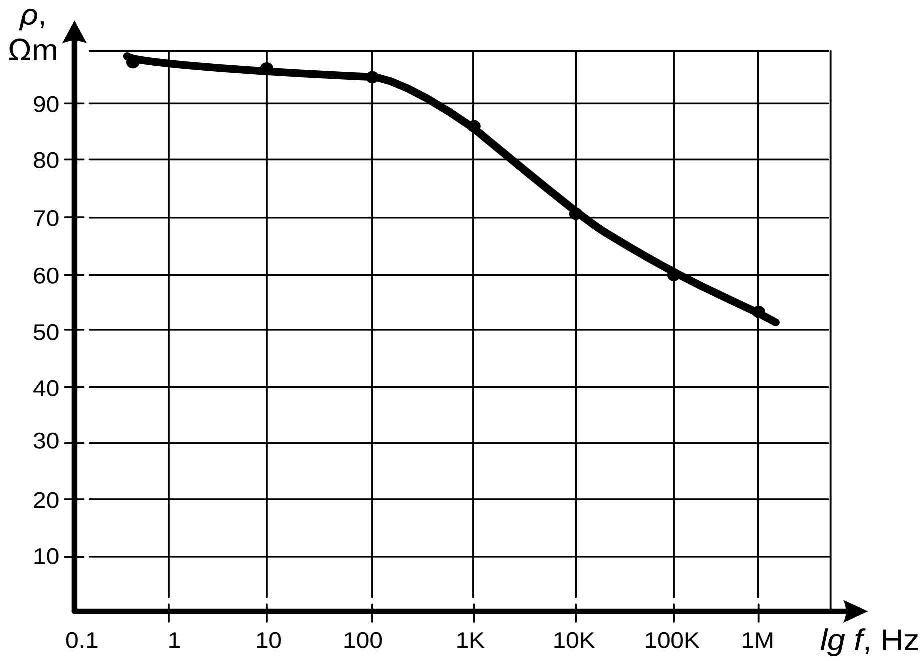

Figure 3.3: Soil resistivity against frequency

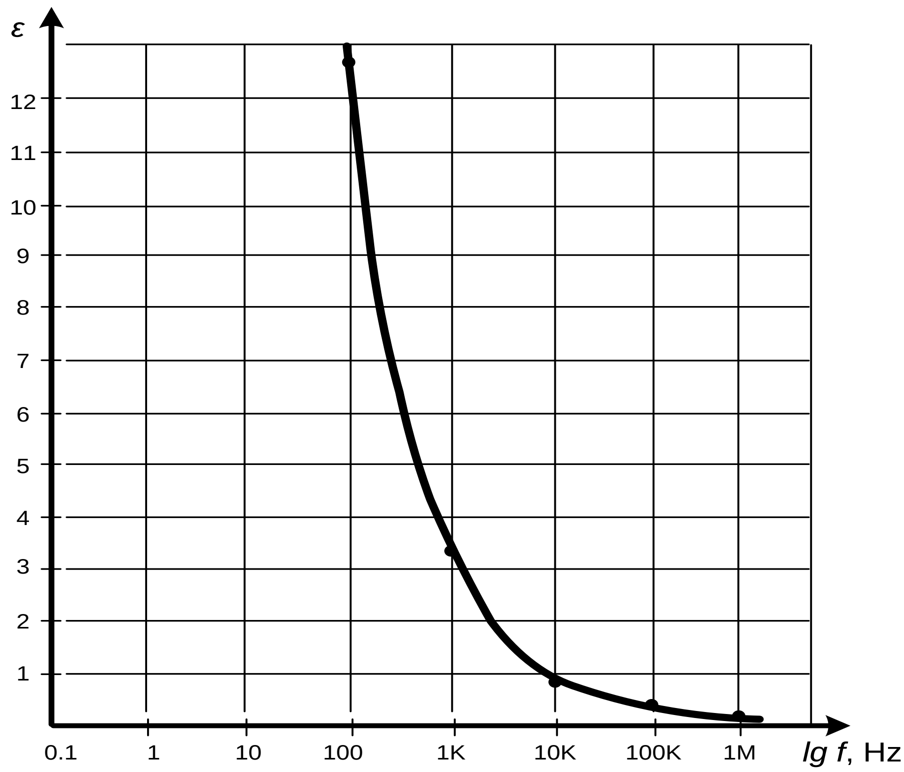

Figure 3.4: Soil permittivity against frequency

As one can observe from Figure 3.3 and Figure 3.4 both soil resistivity and permittivity decrease as frequency increases. It is because soil behaves as a brine or semiconductor. As for resistivity the difference of the value for 100 Hz and 1200 Hz is 16.4% which is quite small.

Meanwhile, for the frequency of 100 Hz one can obtain as follows:

$$L = 2 \cdot 3 \ln\left(\frac{4 \cdot 3}{0.016}\right) \cdot 10^{-7} = 3.972 \text{ μH},$$

$$C = \frac{12.7 \cdot 3}{18 \ln\left(\frac{4 \cdot 3}{0.016}\right)} \cdot 10^{-9} = 0.32 \text{ nF}.$$

The results of the "*C*" calculations for frequencies up to 1.5MHz are presented in Table 3.3. A curve of capacitance changes is shown in Figure 3.5.

Table 3.3: Capacitance of the conductor as function of frequency

f, Hz	***C***, nF
100	0.320
150	0.250
300	0.170
450	0.130
600	0.110
750	0.096
900	0.086
1050	0.079
1200	0.073
$15 \cdot 10^3$	0.016
$150 \cdot 10^3$	0.004
$1.5 \cdot 10^6$	0.001

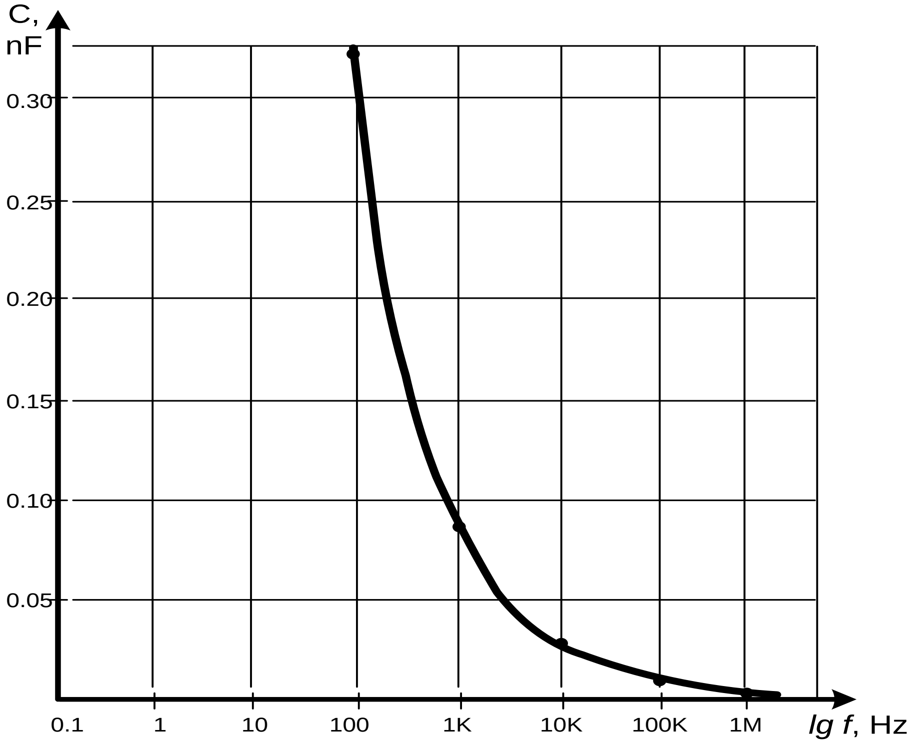

Figure 3.5: Diagram of capacitance against frequency

Finally all three components of the grounding device's element which are R, X_C and X_L can be calculated as follows

$$X_C = \frac{1}{2\pi \cdot 100 \cdot 0.32 \cdot 10^{-9}} = 4976.1 \text{ k}\Omega,$$

$$X_L = 2\pi \cdot 100 \cdot 3.972 \cdot 10^{-6} = 2.5\,\text{m}\Omega,$$

$$R = \frac{100}{2\pi \cdot 3}\left(\ln \frac{8 \cdot 3}{0.016} - 1\right) = 33.5\,\Omega,$$

The results of calculations for all frequencies are presented in Table 3.4.

Table 3.4: Resistance, inductive and capacitive reactance of the element as function of frequency

f, Hz	***R***, Ω	X_L, Ω	X_C, Ω	***Z***, Ω
100	33.5	0.0025	4976.1	33.5
150	32.5	0.0037	4246.3	32.5
300	30.9	0.0075	3122.3	30.9
450	30.0	0.0112	2701.2	30.0
600	29.5	0.0150	2412.7	29.5
750	29.0	0.0188	2211.6	29.0
900	28.6	0.0220	2057.3	28.6
1050	28.3	0.0260	1919.7	28.3
1200	28.0	0.0300	1817.8	28.0
$15 \cdot 10^3$	23.4	0.375	659.3	23.8
$150 \cdot 10^3$	19.8	3.750	260.8	23.6
$1.5 \cdot 10^6$	16.8	37.50	103.1	54.3

The results of calculations of the total impedance *Z* are presented in Table 3.4 as well.

Graphically the results of impedances evaluation are shown in Figure 3.6, Figure 3.7 and Figure 3.8.

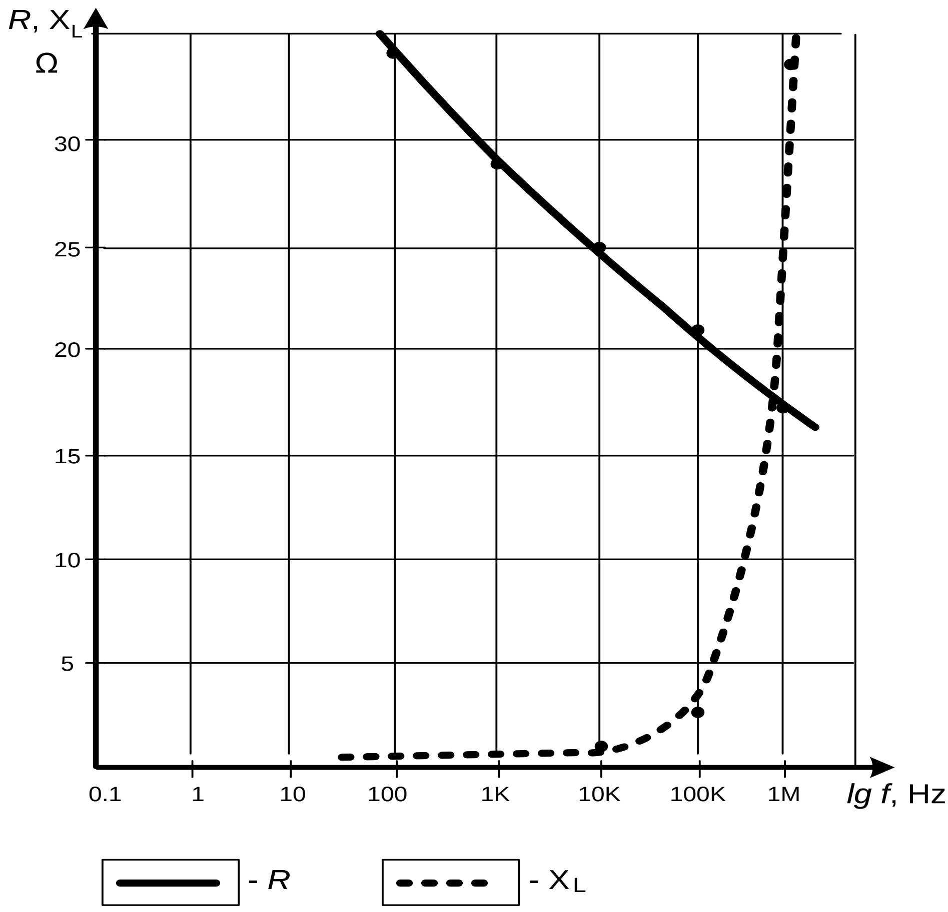

Figure 3.6: Diagrams of R and X_L against frequency

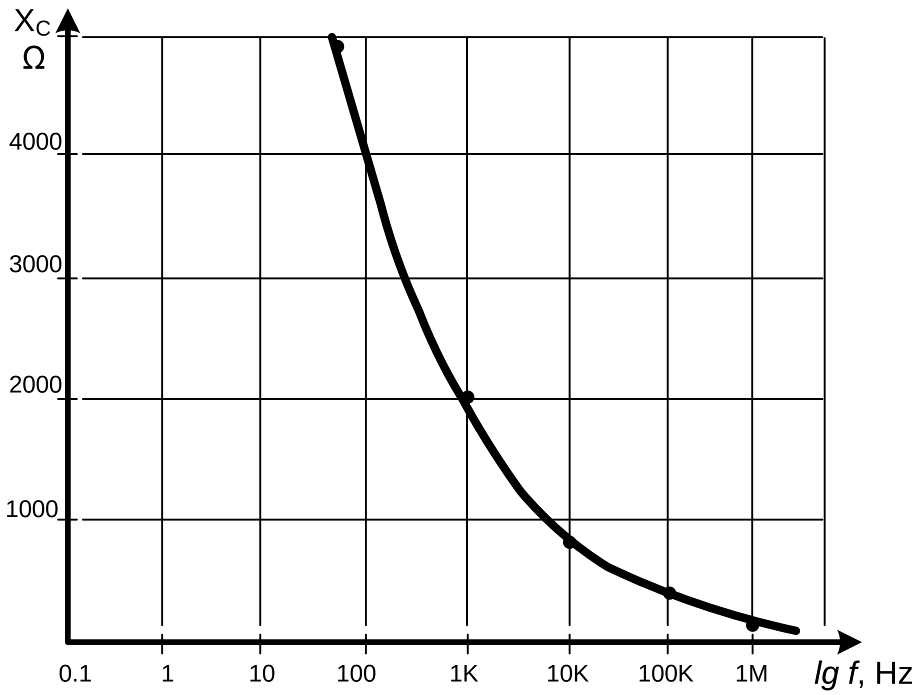

Figure 3.7: Diagram of X_C against frequency

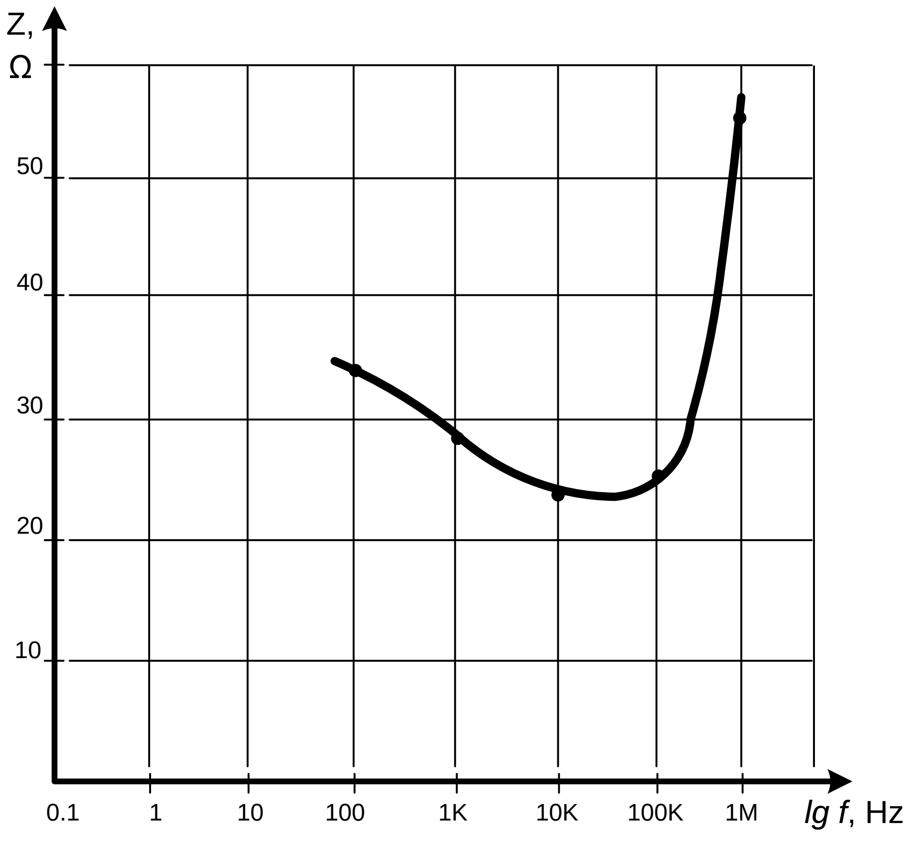

Figure 3.8: Total impedance of the element against frequency

Meanwhile according to the expressions described above the self-resistance of 3m copper conductor can be obtained as follows:

$$R = 0.0175 \cdot 3/200 = 0.000262 \ \Omega.$$

And the self-inductive reactance is as follows:

$$X = 0.000175 \cdot 3 = 0.000525 \ \Omega.$$

With the increase of frequency the reactance of the conductor will increase proportionally. Meanwhile, the value of the resistance will have almost the same value.

Figure 3.9 depicts these changes on the resistance and reactance as the frequency rises.

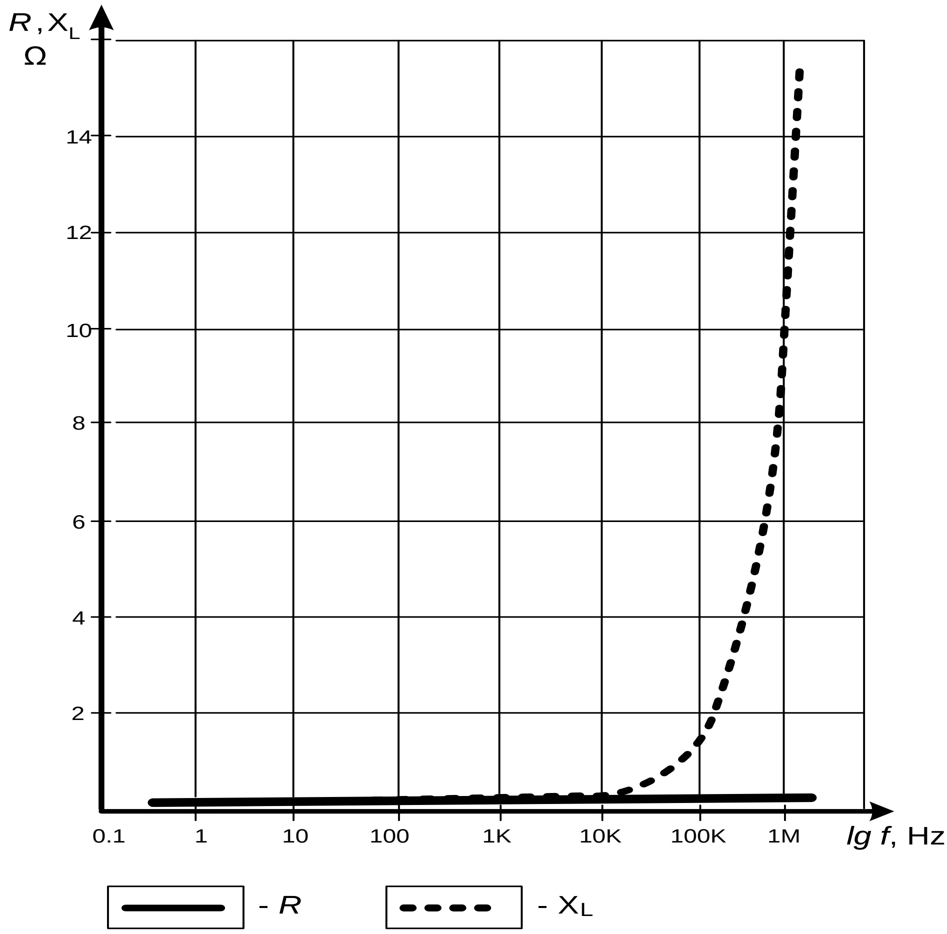

Figure 3.9: Self-resistance and self-inductance against frequency

3.3 Magnetic field distribution over the horizontal element

In order to conduct the analysis of the processes of the current and potential distribution in the grounding grid as a whole it is necessary to explain and describe these processes in a single element of the grid. Features revealed during such an analysis can be used in creation of a new approach to monitor the grounding devices' condition.

As the main base for evaluation, the Biot-Savart Law is used (Betts, 1981; Serway & Jewett, 2004). In accordance to this law the magnitude of the magnetic field strength is proportional to the current in the wire and varies as the inverse square of the distance from the source (see Eqn. (3.21) (Chikarov, Lie, & Nair, 2012)).

$$dH = \frac{I_e \cdot \sin\alpha}{4\pi D^2} dx \quad , \tag{3.21}$$

A horizontal element of the grounding device's mesh can be presented as a conductor with the initial current I_0 and length l (see Figure 3.10).

From the principles of geometry (Audin, 2003)

$$\sin \alpha = a/D. \tag{3.22}$$

Also, from the Figure 3.10

$$D = \sqrt{a^2 + x^2} \, . \tag{3.23}$$

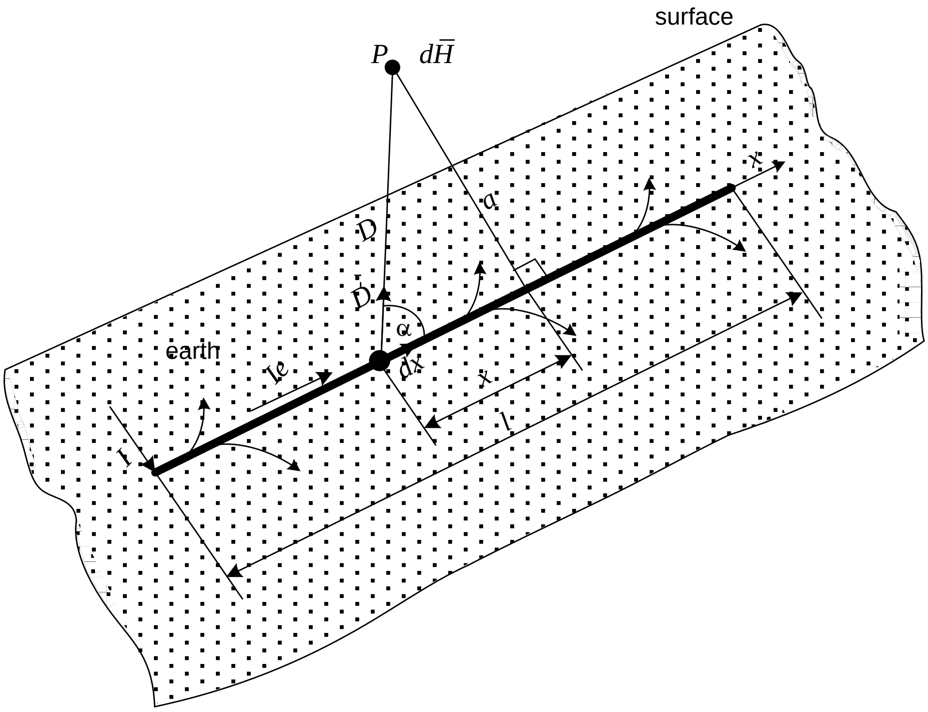

Figure 3.10: Scheme for magnetic field evaluation

Substitution of Eqs. (3.22) and (3.23) into Eq. (3.21) gives

$$dH = \frac{I}{4\pi D^2} \cdot \frac{a}{D} dx = \frac{I}{4\pi \cdot \left[\sqrt{a^2 + x^2}\right]^3} \cdot a \cdot dx \,. \tag{3.24}$$

But all these equations describe the magnitude of the field strength created by the current in only a small length element *dx* of the conductor. To find the total magnetic field strength *H* created at some point *P* by a current of finite value, the contributions of all current elements *I dx* must be added up to make up the current. That is, *H* must be evaluated by integrating Eq. (3.24)

$$dH = \int_0^l \frac{I_e}{4\pi \cdot \left[\sqrt{a^2 + x^2}\right]^3} \cdot a \cdot dx = \frac{I \cdot a}{4\pi} \int_0^l \frac{dx}{\left[\sqrt{a^2 + x^2}\right]^3} \,. \tag{3.25}$$

According to tables of indefinite integrals from (Poliyanin & Manzhirov, 2007)

$$\int \frac{dx}{(\sqrt{a^2+x^2})^3} = \frac{x}{a^2 \cdot \sqrt{a^2+x^2}} \, . \tag{3.26}$$

Taking the integral (3.25) by using (3.26) one will get

$$dH = \int_0^l \frac{I_e}{4\pi \cdot \left[\sqrt{a^2+x^2}\right]^3} \cdot a \cdot dx = \frac{I_e \cdot a}{4\pi} \int_0^l \frac{dx}{\left[\sqrt{a^2+x^2}\right]^3} \, . \tag{3.27}$$

$$H = \frac{I_e \cdot a}{4\pi} \cdot \frac{l}{a^2 \cdot \sqrt{a^2+l^2}} = \frac{I_e}{4\pi} \cdot \frac{l}{a \cdot \sqrt{a^2+l^2}} \tag{3.28}$$

With the assumptions that the current I in each element decreases uniformly because of leakage currents into the soil one can have

$$I_e = I \cdot (1 - x/l) \, . \tag{3.29}$$

The final expression is expressed as follows:

$$H = \frac{I \cdot (1 - x/l)}{4\pi} \cdot \frac{l}{a \cdot \sqrt{a^2+l^2}} = \frac{I \cdot (l - x)}{4\pi \cdot a \cdot \sqrt{a^2+l^2}} \, . \tag{3.30}$$

This expression can be written in relative values where: $a_* = a/l$, $x_* = x/l$, $I_* = I/l$

$$H = \frac{I_* \cdot l \cdot (l - x_* \cdot l)}{4\pi \cdot a_* \cdot l \cdot \sqrt{a_*^2 \cdot l^2 + l^2}} = \frac{I_* \cdot l^2 \cdot (1 - x_*)}{4\pi \cdot a_* \cdot l^2 \cdot \sqrt{a_*^2 + 1^2}} = \frac{I_* \cdot (1 - x_*)}{4\pi \cdot a_* \cdot \sqrt{a_*^2 + 1}} \, . \tag{3.31}$$

Profiles of magnetic field strength values *H(x)*, evaluated in accordance with the last expression for some values of a_* when I_* =1A, presented in Figure 3.11.

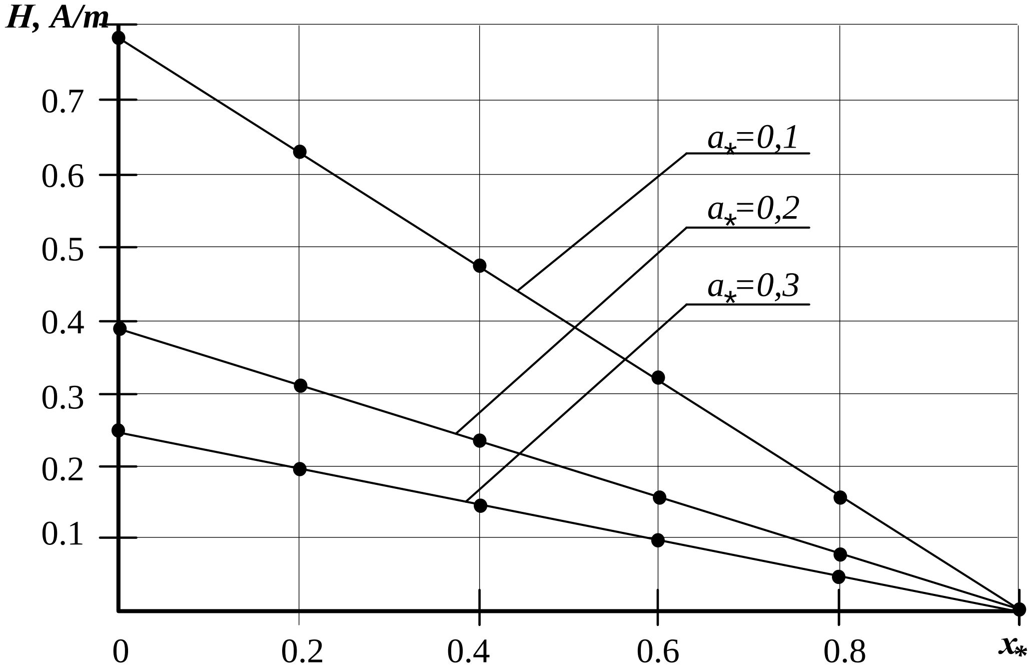

Figure 3.11: Dependence of magnetic field intensity on the distance from conductor

If one assumes that I = 1A, a = 0.4m (depth of the horizontal element), l=5m, then when the value of x is changing, in case when the horizontal element is integrated, one can obtain the following results of the magnetic field strength calculation on the surface of the ground (see Table 3.5).

Table 3.5: Calculation of the magnetic field strength value

Parameter	**Value**					
x, (m)	0	1	2	3	4	5
H (A/m)	0.198	0.159	0.119	0.079	0.040	0

Graphically, these changes are shown in Figure 3.12.

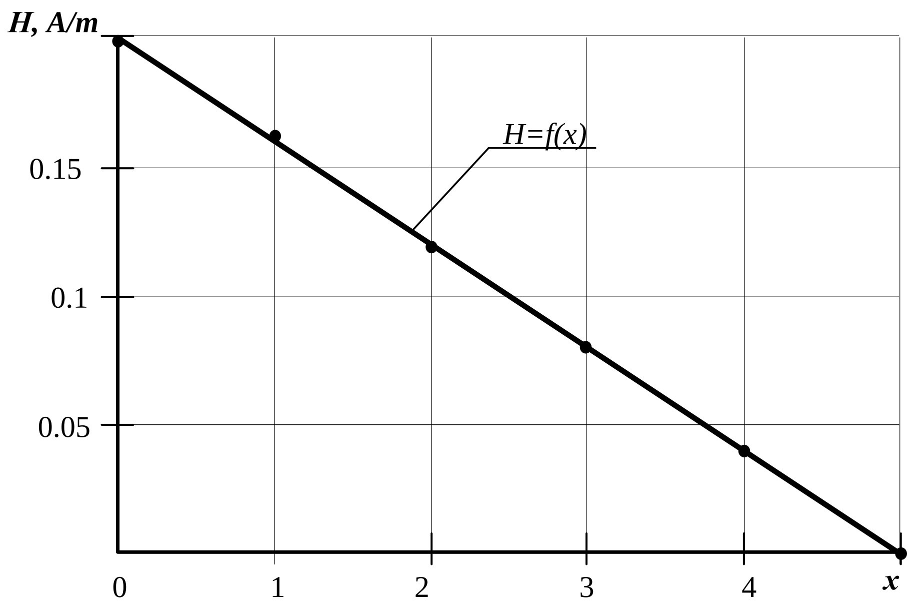

Figure 3.12: Magnetic field strength value over the integrated horizontal element

If the horizontal element has a breakage (failure) as shown in Figure 3.13 it can be presented as two pieces with lengths l_1 and l_2 and initial currents I_1 and I_2 respectively.

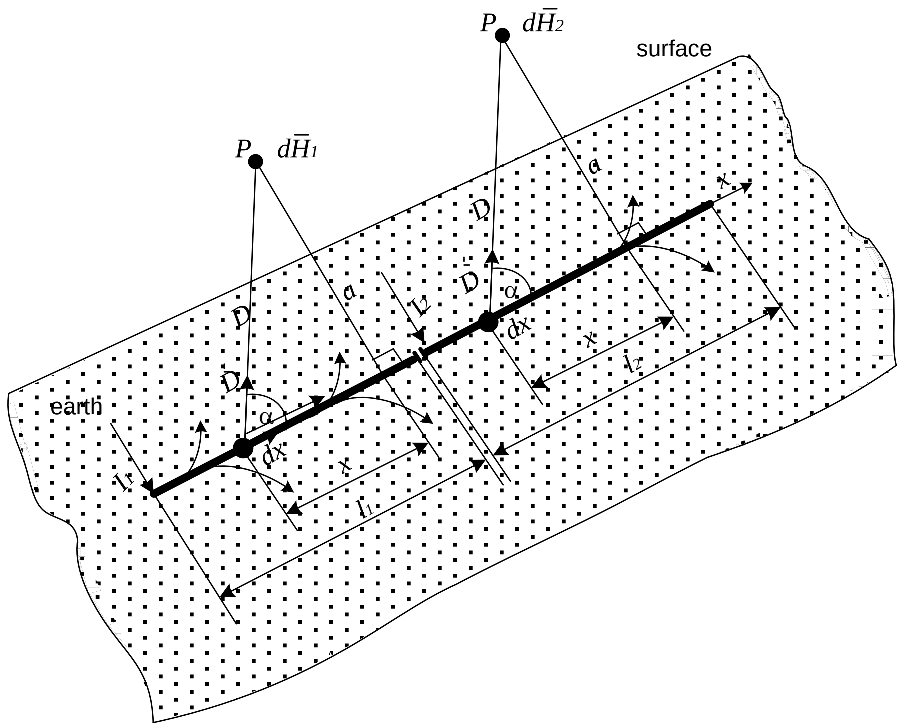

Figure 3.13: Model of the damaged element

Both parts of the element can be described analogically with the above mentioned expression (3.25).

$$dH_1 = \frac{Ie_1 \cdot a}{4\pi} \int_0^{l_1} \frac{dx}{\left[\sqrt{a^2 + x^2}\right]^3}; \quad dH_2 = \frac{Ie_2 \cdot a}{4\pi} \int_0^{l_2} \frac{dx}{\left[\sqrt{a^2 + x^2}\right]^3}. \tag{3.32}$$

The solution on the integrals can be represented as

$$H_1 = \frac{I_{e1}}{4\pi} \cdot \frac{l_1}{a \cdot \sqrt{a^2 + l_1{}^2}}; \quad H_2 = \frac{I_{e2}}{4\pi} \cdot \frac{l_2}{a \cdot \sqrt{a^2 + l_2{}^2}}. \tag{3.33}$$

After substitution of Eqn. (3.29) for each current the final expressions will be

$$H_1 = \frac{I_1 \cdot (l_1 - x)}{4\pi \cdot a \cdot \sqrt{a^2 + l_1{}^2}}; \quad H_2 = \frac{I_2 \cdot (l_2 - x)}{4\pi \cdot a \cdot \sqrt{a^2 + l_2{}^2}}. \tag{3.34}$$

For example, when I_1 = 0.7A, I_2 = 0.3A, a = 0,4m (depth of the horizontal element), l_1=2m, l_2=3m and if directions of the currents in different parts of the damaged element are different the curve of the magnetic field strength changes will be as shown in Figure 3.14

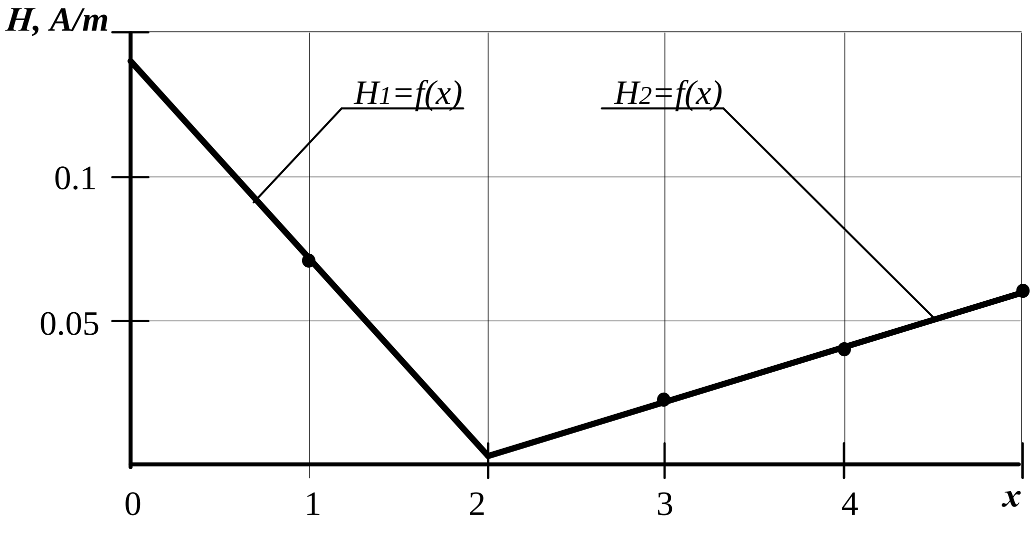

Figure 3.14: Magnetic field strength value over damaged horizontal element with opposite currents directions

But if the directions of the currents before and after the point of breakage are the same, the curve is shown in Figure 3.15.

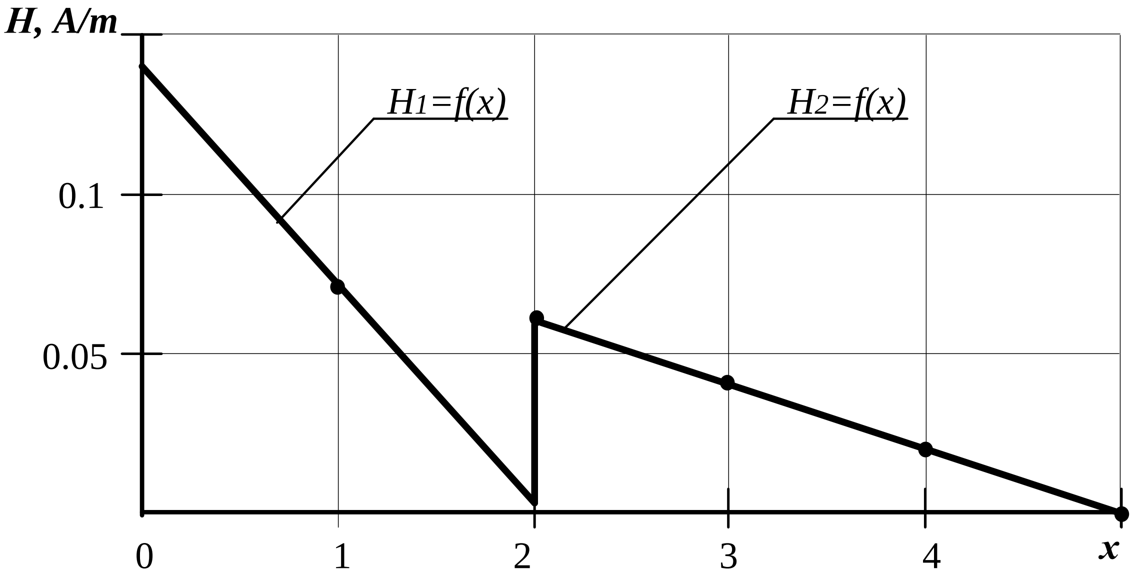

Figure 3.15: Magnetic field strength over damaged horizontal element when currents directions are the same

3.4 Impedance of the grid's elements and their mutual coupling

In general, the process of spreading of the current from an energized enclosure of the equipment to ground can be presented as shown in Figure 3.16.

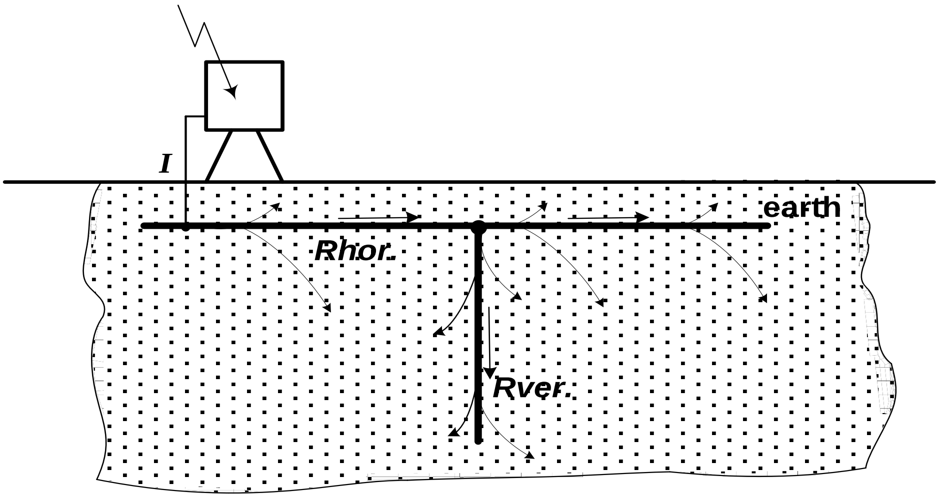

Figure 3.16: Horizontal and vertical elements in soil

Both, horizontal and vertical elements shown in Figure 3.16 represent not only self resistance of conductors themselves (steel, copper, copper clad etc.) but also lumped resistances to ground of the buried in soil conductors. The resistance of each conductor consists of three parts: (i) a self resistance of the conductor material, (ii) contact resistance between material of the element and soil and (iii) soil resistivity itself (Chikarov, Lie, & Nair, 2013). Thus, the full resistance to the current which leaks from the element to ground can be presented as

$$R_{hor.(ver.)} = R_{me} + R_{cont} + R_{soil} \, . \tag{3.35}$$

Please note the first two elements (R_{me} and R_{cont}) have very small values and often can be neglected.

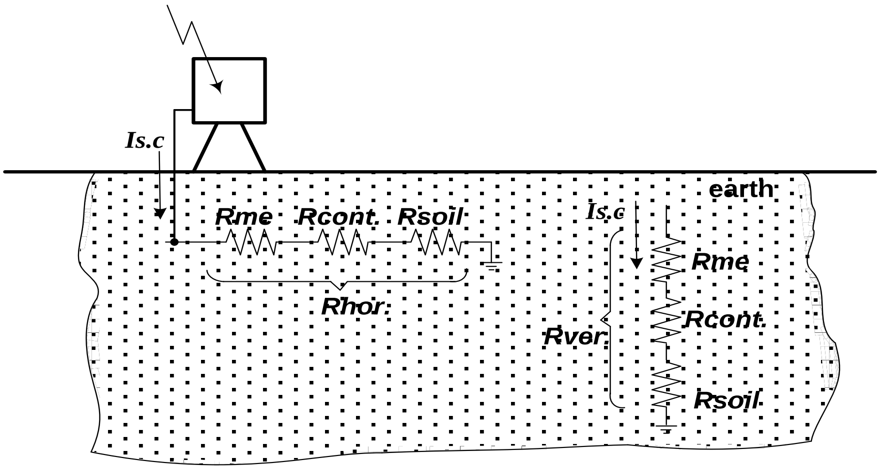

Figure 3.17: Equivalent schemes of horizontal and vertical elements in soil

In accordance with standards (*IEEE Guide for Measuring Earth Resistivity, Ground Impedance, and Earth Surface Potentials of a Grounding System*, 2012; *IEEE Guide for Safety in AC Substation Grounding*, 2000; *IEEE Recommended Practice for Grounding of Industrial and Commercial Power Systems*, 2007) and (Yacobs, 1981) the resistance of the vertical and horizontal elements they have with respect to current flowing from them into ground can be calculated as

$$R_{ver.} = \frac{\rho_{e.v.}}{2\pi \cdot l_{ver.}} \cdot \left(\ln\frac{2 \cdot l_{ver.}}{d_{ver.}} + 0{,}5 \cdot \ln\frac{4 \cdot l_{ver.} + 7 \cdot t}{l_{ver.} + 7 \cdot t} \right). \tag{3.36}$$

$$R_{hor.} = \frac{\rho_{e.h.}}{2\pi \cdot l_{hor.}} \cdot \ln\frac{l_{hor.}^{2}}{t \cdot d_{hor.}}. \tag{3.37}$$

When a vertical element crosses both layers of a two-layer soil, $\rho_{e.v.}$ can be determined as

$$\rho_{e.v.} = \frac{\rho_1 \cdot \rho_2 \cdot l_{ver.}}{(l_{ver.} - h_1 + t) \cdot \rho_1 + (h_1 - t) \cdot \rho_2}, \tag{3.38}$$

The resistance of ground depends on the resistivity of its soil stratums (ρ_1, ρ_2, ρ_3 etc.). The number of layers (stratums) can differ from one area to another depending on the soil structure. With an acceptable level of accuracy often multilayer structure of the ground is substituted with its two-layer soil equivalent (ρ_1, ρ_2). Eventually, the resistivity of the both layers (ρ_1, ρ_2) in the mathematical model is usually replaced with the resistivity of so called "equivalent" ground or its analogue (depending on techniques). For the purpose of modeling it is assumed that the structure of non-homogeneous ground is a two-layer soil.

An example of a single conductor buried at a depth below the surface is shown in Figure 3.18 along with the current distribution. The current density is practically constant for most of the conductor length and increases near the ends of the conductor (Melipoulos, Feng, Joy, & Cokkinides, 1993). In a practical grounding system, the current distribution is very complex. However, the picture shown in Figure 3.18 is applicable to practical grounding systems. There are two ways of the conductor representation: lumped or distributed equivalent circuits.

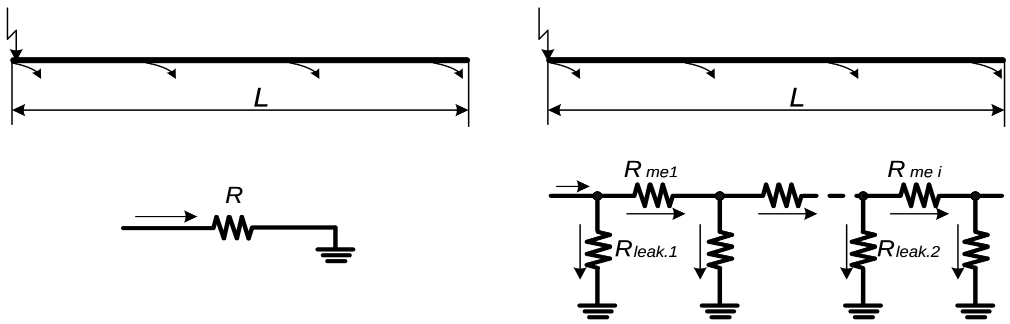

Figure 3.18: Equivalent scheme of horizontal or vertical element in the soil

These two parts of Figure 3.18 are equal in terms of the total resistance of the element so any scheme can be used for analysis of the processes in grounding grids. The only difference between these schemes is that the lumped resistance R_{hor} comprises all resistances as described in Eqn. (3.35).

In Figure 3.18 a distributed parameter R_{mei} is a resistance of the part of the horizontal element which represents the element's resistance itself (the resistance of the metal) or self resistance. $R_{leak.i}$ represents the resistance that each part has to leakage currents that flow from the element into soil. For the horizontal element

$$R_{hor.} = R_{me} + R_{leak.} \, . \tag{3.39}$$

One should also take into account a mutual electromagnetic coupling among elements due to influences of their electromagnetic fields on each other as a function of the distance among elements as shown in Figure 3.19. It results in artificial increase of the impedance of each element of the grid.

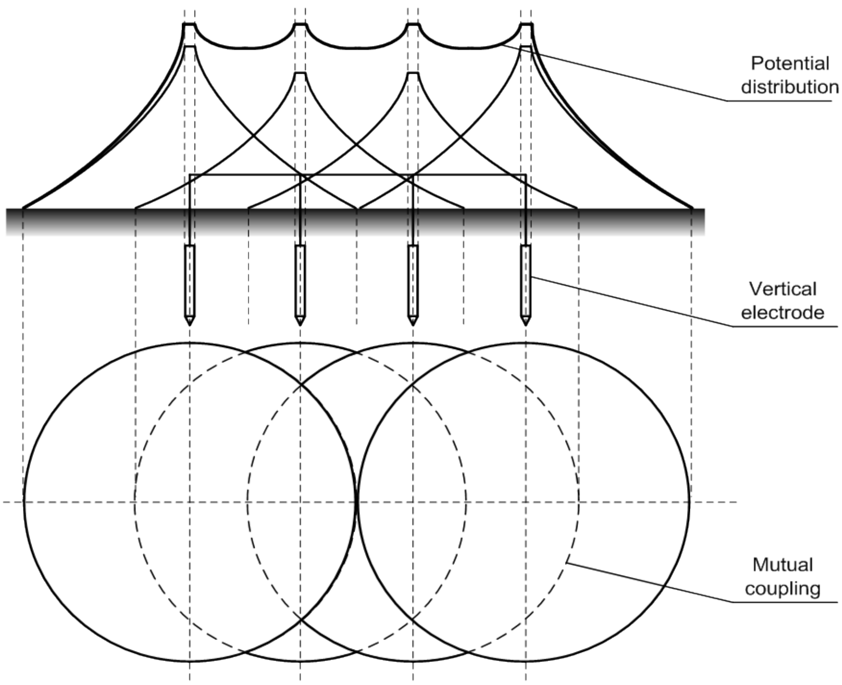

Figure 3.19: Influence of elements on each other

According to Sunde's formulas (Sekioka, Sonoda, & Ametani, 2005; Sunde, 1949) the mutual resistance can be evaluated by the following equations

$$R_m = \frac{\rho_{e.v.}}{4\pi \cdot l_{1.} \cdot l_2} \cdot \left[F(l_1 + l_2) - \left(\frac{F(l_1 - l_2) + F(l_2 - l_1)}{2} \right) - \sqrt{(l_1 + l_2)^2 + D^2} + \sqrt{(l_1 - l_2)^2 + D^2} \right] \cdot \quad (3.40)$$

$$F(l) = l \cdot \ln \left[\frac{\sqrt{l^2 + D^2} + l}{D} \right], \quad (3.41)$$

When electrodes are arranged in parallel axis (see Figure 3.20A), the mutual inductance can be assessed with the following equation.

$$M = \frac{\mu_0}{4\pi} \cdot \begin{pmatrix} a \cdot a\sinh\left(\frac{a}{d}\right) - \beta \cdot a\sinh\left(\frac{\beta}{d}\right) - \gamma \cdot a\sinh\left(\frac{\gamma}{d}\right) + \delta \cdot a\sinh\left(\frac{\delta}{d}\right) - \sqrt{a^2 + d^2} + \sqrt{\beta^2 + d^2} + \\ + \sqrt{\gamma^2 + d^2} - \sqrt{\delta^2 + d^2} \end{pmatrix} . \quad (3.42)$$

where $\gamma = m + \delta$, $a = m + n + \delta$, $\beta = n + \delta$.

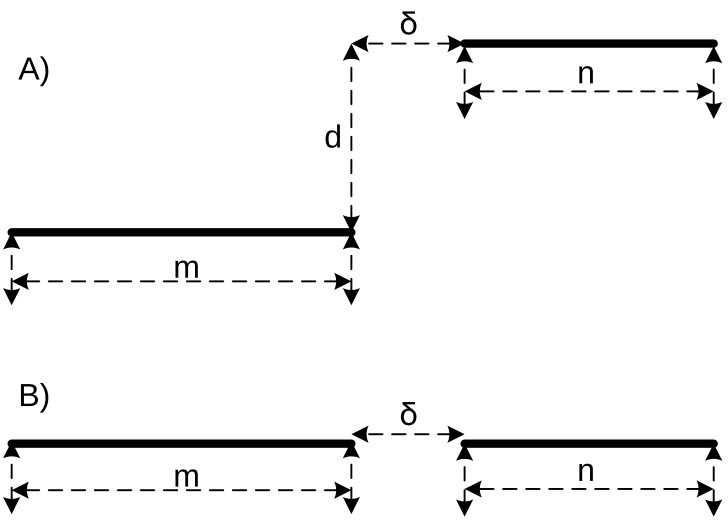

Figure 3.20: Different positions of electrodes

In case of elements arranged on the same axis (see Figure 3.20B) Eqn. (3.42) is no longer valid. The mutual coupling can be evaluated as follows:

$$M = 0.23 \cdot (a \cdot \log a + \delta \cdot \log \delta - \gamma \cdot \log \gamma - \beta \cdot \log \beta), \mu H \cdot \quad (3.43)$$

A mutual influence of vertical conductors is shown in Figure 3.21. In order to avoid overloading of the picture, only few samples of *M* connections are shown but all of them are considered during the calculations.

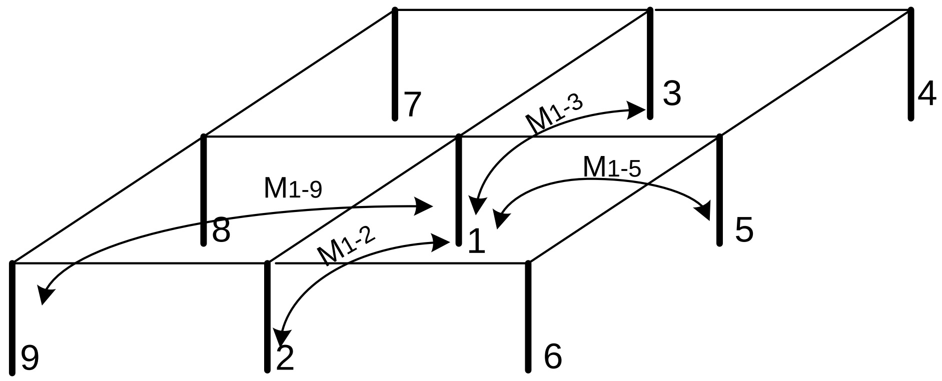

Figure 3.21: Mutual influence between vertical electrodes

As well as for vertical electrodes there is mutual coupling of the horizontal elements on each other as shown in Figure 3.22. Again not all the influences between elements are shown on the picture but all of them are included in the calculation.

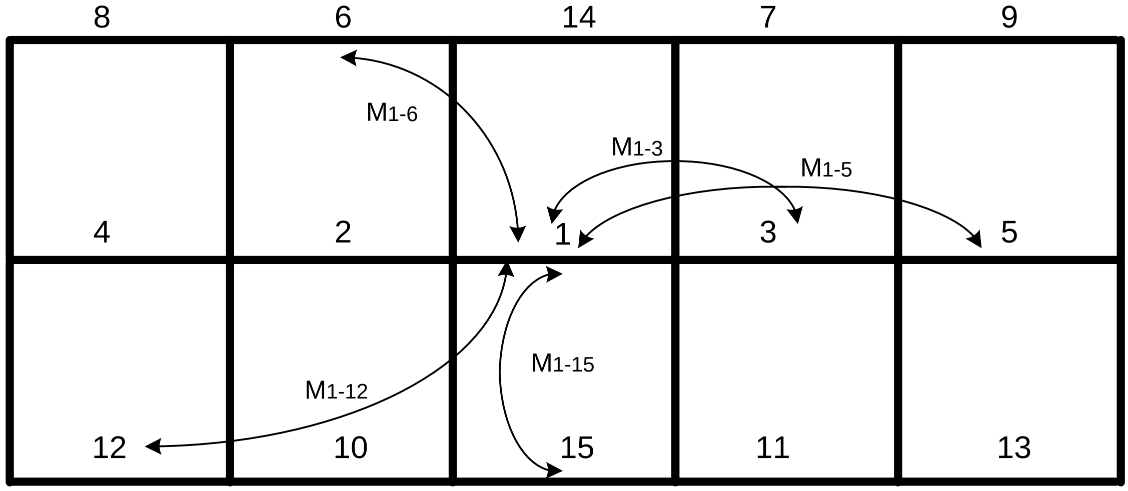

Figure 3.22: Mutual coupling of horizontal conductors

Numbering of the horizontal and vertical elements of the grid as shown in Figure 3.21 and

Figure 3.22 is chosen randomly. If the number of elements in the grid is large then such a numbering can be arranged in a specific way to simplify the representation and calculation of the shown values.

Of course not all the elements will have the same increment of their resistances since they are located in different places of the grid. One can expect that elements located in the middle meshes of the grid will have a maximum value of their resistances when elements in corner meshes will have the minimum ones.

Each pair of the vertical elements has impedance the same as for the parallel elements

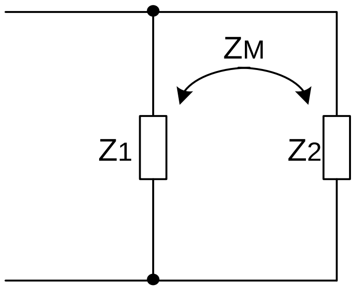

Figure 3.23: Total impedance of two conductors

The total impedance of these two conductors with mutual impedance is

$$Z_{\Sigma} = \frac{Z_1 \cdot Z_2 - Z_M{}^2}{Z_1 + Z_2 - 2Z_M}. \tag{3.44}$$

If Z_M=0

$$Z_{\Sigma M=0} = \frac{Z_1 \cdot Z_2}{Z_1 + Z_2}. \tag{3.45}$$

3.5 Case study

For the purpose of modeling it is assumed that the structure of non-homogeneous ground is a two-layer soil. The length of the vertical elements is 3m with a diameter

16mm. The length of the horizontal elements is 5m. Horizontal elements are located in the upper layer of the ground ρ_1, while vertical elements cross both layers ρ_1 and ρ_2. Resistivity of the soil stratums are ρ_1=250Ωm and ρ_2=30Ωm respectively. The thickness of the upper layer (h_1) is 2m. The thickness of the lower layer (h_2) is ∞.

For the horizontal elements, $\rho_{e.h}$ can be determined from (Yacobs, 1981).

Table 3.6: Equivalent resistance $\rho_{e.h.}/\rho_2$ of two-layer soil model for detection of the horizontal elements resistance

$\boldsymbol{\rho_1/\rho_2}$	$\boldsymbol{h_1}$, m	$\boldsymbol{t}$, m	Value $\boldsymbol{\rho_{e.h}/\rho_2}$ when the length of the horizontal elements l_{hor}=5m.
0.5	1	0.8	0.63
1	-	0.8	1.00
2	1	0.8	1.65
	3		1.89
5	1	0.8	3.03
	3		4.52
10	1	0.8	6.02
	3		9.45
20	1	0.8	11.40
	3		18.10

Substituting the values, one can define

$$\frac{\rho_1}{\rho_2} = \frac{250}{30} = 8.33 \cdot$$

From Table 3.6, one can obtain

$$\frac{\rho_1}{\rho_2} = 8.33; \qquad h_1 = 2 \text{ m}; \qquad \rho_{e.h.} / \rho_2 = 6.412,$$

$$\rho_{e.h.} = \left(\rho_{e.h.} / \rho_2 \right) \cdot \rho_2 = 6.412 \cdot 30 = 192.345 \ \Omega\text{m}.$$

Substitute the values into Eqn.(3.37), one can have

$$R_{hor.} = \frac{192.345}{2 \cdot 3.14 \cdot 5} \cdot \ln \frac{5^2}{0.8 \cdot 0.02} = 45.048\,\Omega$$

Similarly, for vertical rods

$$\rho_{e.v.} = \frac{250 \cdot 30 \cdot 5}{(3-2+0.8) \cdot 250 + (2-0.8) \cdot 30} = 77.160 \ \Omega\text{m}.$$

Then, from Eqn.(3.36), one can obtain

$$R_{ver.} = \frac{77.160}{2 \cdot 3.14 \cdot 3} \cdot \left(\ln \frac{2 \cdot 3}{0.016} + 0.5 \cdot \ln \frac{4 \cdot 3 + 7 \cdot 0.8}{3 + 7 \cdot 0.8} \right) = 25.741\,\Omega.$$

After substitution all values in Eqn.(3.40) one can have R_m = 2.2Ω when the distance between elements is 5m, R_m = 1.6Ω when the distance between elements is 7.5m and R_m=1.2Ω when the distance between elements is 10m.

The resistance of either horizontal or vertical element as a conductor is very low (approximately 0.01Ω). Thus, one can obtain the following equation for the horizontal element from Eqn.(3.39).

$$R_{leak.} = 45.048 - 0.01 = 45.038\,\Omega.$$

With regards to the second part of Figure 3.18 if one assumes that the element is represented by 3 sections the resistance of each section is as follows:

$$R_{me.i} = \frac{R_{me}}{3} = \frac{0.01}{3} = 0.0033\Omega \;\; R_{leak.i} = 45.038 \cdot 4 = 180.152\Omega$$

A mutual inductance and capacitance at low frequencies have very small contribution to the total impedance of the elements. According to (Celli, Ghiani, & Pilo, 2012) and (Terman, 1943) for perpendicular elements the mutual inductance is null.

Since vertical electrodes are straight in parallel to each other and *a* represents a total length of two vertical elements in parallel

$$\gamma = 5 \text{ m}, \; a = 5\text{ m}, \; \beta = 5\text{ m}.$$

When $\mu_0 = 4\pi \cdot 10^{-7}$, m=n=3m, d=5m, δ =0 m one can have

$$M_{1-3} = \frac{4\pi \cdot 10^{-7}}{4\pi} \cdot \begin{pmatrix} 5 \cdot 5 \sin 3\left(\frac{5}{5}\right) - 5 \cdot 5 \sin 3\left(\frac{5}{5}\right) - 5 \cdot 5 \sin 3\left(\frac{5}{5}\right) + 0 \cdot 5 \sin 3\left(\frac{5}{5}\right) - \sqrt{5^2 + 5^2} + \sqrt{5^2 + 5^2} + \\ + \sqrt{5^2 + 5^2} - \sqrt{0^2 + 5^2} \end{pmatrix} = 0.08\mu H$$

When $\mu_0 = 4\pi \cdot 10^{-7}$, m=n=3m, d=7.07m, δ =0 m one can have

$$M_{1-9} = \frac{4\pi \cdot 10^{-7}}{4\pi} \cdot \begin{pmatrix} 5 \cdot 5 \sin 3\left(\frac{5}{7.07}\right) - 5 \cdot 5 \sin 3\left(\frac{5}{7.07}\right) - 5 \cdot 5 \sin 3\left(\frac{5}{7.07}\right) + 0 \cdot 5 \sin 3\left(\frac{5}{7.07}\right) - \sqrt{5^2 + 7.07^2} + \\ + \sqrt{5^2 + 7.07^2} + \sqrt{5^2 + 7.07^2} - \sqrt{0^2 + 7.07^2} \end{pmatrix} = 0.07\mu H$$

In the study presented in this thesis, the processes in the grounding grids have frequency lower than 1 kHz. The maximum frequency taken into consideration is the 8-th harmonic frequency which is 400Hz or 480Hz depending on the fundamental frequency of the country (50/60Hz).

A self-inductance X_L of the rod as it is shown in Table 3.4 at 450Hz is 0.0112Ω. Mutual inductances between for instance elements 1-3 and 1-9 are

$$X_{M1-3} = 2\pi \cdot f \cdot M = 2 \cdot \pi \cdot 450 \cdot 0.08 = 226.1\mu\Omega$$

$$X_{M1-9} = 2\pi \cdot f \cdot M = 2 \cdot \pi \cdot 450 \cdot 0.07 = 197.8\mu\Omega$$

As one can see, the values of the mutual inductance are much smaller compared with the self-inductance of the element.

If one considers a pair of elements 1 and 3, their total inductance taking into account their mutual influence will be

$$X_{\Sigma(1-3)M} = \frac{0.0112 \cdot 0.0112 - 0.000226^2}{0.0112 + 0.0112 - 2 \cdot 0.000226} = 0.00571\,\Omega,$$

Without M

$$X_{\Sigma(1-3)} = \frac{0.0112 \cdot 0.0112}{0.0112 + 0.0112} = 0.0056\,\Omega.$$

3.6 Concluding remarks

The resistance *R* of the conductor in soil has decrease at all times when the frequency increases. Since *R* is a direct function of soil resistivity it behaves in the same manner. Meanwhile, the higher frequency the lower value of *R* and as one can see it is not a linear graph (see Figure 3.6). The difference between *R* under 100Hz and 1.2kHz is (-16.5)% as shown in Table 3.4 and in Figure 3.6.

The inductive reactance of the conductor is quite small under low frequencies and increases substantially with the frequency up to 1MHz (see Figure 3.6).

Total impedance of the element decreases as frequency increases up to the value of 150 kHz. After that due to high reactance of the conductor, the total impedance of the conductor, *Z*, increases substantially (+62.1%). As one can notice within the frequency range between 100 Hz and 1.2 kHz, the total impedance variation is -16.5% compared with the initial value. At the same time, the difference of the impedance value within the frequency range between 100 Hz and 450 Hz is just (-10.4)%.

One can see that at low frequencies (up to some dozens kHz), a major part of the conductor's impedance is resistance, *R*. But for frequencies close to 1MHz and higher, the conductor behaves more like inductance rather than pure resistance. At low frequencies the effect of soil resistivity and permittivity is small and can be neglected. However, it should be taken into account if the frequencies are greater than 10 kHz. Similar features of frequency response are also inherent to the horizontal elements of the grounding.

With respect to self-impedances, reactive component increases much faster compared with the resistance. Both parts increase with the rise of frequency. Under high frequency *R* can be neglected.

After analysis of the magnetic field distribution data and some calculations one can conclude that: a) the further the point of magnetic field measuring from the current-carrying conductor the lower value of the magnetic field strength is; b) with the assumption that the current in the integrated element has a linear decrease from its maximum value down to zero, due to leakage into soil, the magnetic field strength distribution over the element will have the same pattern. In a real life the current in the element subsides down not to a zero value since the element is paralleled by other elements; c) if the horizontal element is damaged, there will be two parts of the linear decrease (increase) of magnetic field strength over them depending on the direction of currents in those parts; d) due to some impedance (resistance) of the breakage (soil) and leakage currents, the magnitude of the magnetic field strength in different parts of the damaged elements will not have the same initial values (as shown in Figure 3.14 and Figure 3.15).

As one can notice from the impedances analysis, the additional inductive reactance due to mutual inductance is only 1.9%. From Figure 3.21, an influence from element #9 on the same element #1 is only 1.7%. If one sums up together all additional mutual inductances on the element #1, the answer will be 14.4% (0.0016Ω). It means that instead of the value X_L=0.0112Ω taking into account mutual electromagnetic coupling one can have

$$X_{LM} = X_L + X_M = 0.0112 + 0.0016 = 0.0128\ \Omega.$$

As one can conclude the total inductive reactance of the vertical element even with taking into account mutual coupling has a very small value compared with the element resistance (30Ω) and thus during the low frequencies analysis it can be neglected.

As for the horizontal elements (as from Figure 3.22), conducting the calculations in the same manner, their mutual inductance will result in 66% increase of the total inductive reactance for each element but again the total inductive reactance will be much smaller than resistance of the element. Moreover, the resistance of the horizontal elements is even bigger than the vertical ones.

As it can be seen from Table 3.4 the resistance has a huge value compared with the value of inductance. *Xc* of the element is much bigger but connected in parallel to the conductor and almost does not change the total impedance either. In this case even if one has tens of elements spread meters apart which can influence on each other due to their small inductance, value of their mutual inductance will be even smaller than their own.

CHAPTER 4: NETWORK MODEL AND ITS ANALYSIS

A realistic mathematical model of the grounding device will allow us to predict and explain the current and voltage distribution differences at the electric power plant due to the elements' failure. By means of such an analysis it will be possible to predict changes of the parameters' values which determine the main safety conditions at the power plants.

This chapter will describe overall characteristics of the potential and current distributions in the grounding grid with and without damaged horizontal elements. As the result of this part, a possible fluctuation of the main safety parameters will be evaluated. Features and new principles revealed in this study will be used for the establishment of a new monitoring technique for the grounding grids

There are a number of mathematical models with regards to the grounding devices' elements. All these theories use different approaches: Maxwell equations solutions (electromagnetic theory) (L. Grcev & Popov, 2005; Nekhoul et al., 1996), transmission line model (Bourg et al., 1995), antenna (full-wave) model (Cavka & Poljak, 2011), circuit theory (Llovera et al., 2008; Pedrosa et al., 2010; Visacro & Portela, 1987) and (Jambak & Ahmad, 2000). There are also some works with experimental data (Bourg et al., 1995; L. Grcev, 2007). While the circuit approximation can be considered to be simple but accurate enough, the transmission line model has advantage of relatively low computation compared with the other techniques. The main disadvantage of the model is limitation to a certain upper frequency, depending on the electrical properties of the ground and configuration of particular grounding system. On the other hand, the rigorous electromagnetic models based on antenna theory are the most accurate but more complicated in calculations. Most existing methods use circuit or electromagnetic field

representation of the processes. The common approach of these models is to firstly calculate currents following which an evaluation of the potentials above the grounding grids conductors can be made.
The applicability of these models is essentially driven by the ratio between the grounding system size and the minimum wavelength of the electromagnetic phenomenon involved in the study. These models state that for a typical grounding device a quasi-static theory can be used for frequencies below the megahertz range. Models determine that the grounding element's size in this case must be less than 1/10 of a wavelength in the ground. In (Olsen & Willis, 1996) the comparison of the authors' "exact calculations" with the quasi-static theory shows very small difference of the results' values up to some mega Hz frequency. In (L. Grcev & Dawalibi, 1990) the authors represent a combination of different theories and techniques in order to describe the grounding behaviour. They suggest that the ratio of the conductor length and its radius should be more than 1. In general, the ratio of about 10 is satisfactory.

The aim of this study is to model the current and potential distribution due to the horizontal elements' failures. Since the processes described in the study take place in grounding devices of not huge dimensions (not in the scale of kilometres) and the frequency range is lower than 1 MHz, the circuit theory and a quasi-static model can be utilized as a base of such an analysis.

The velocity of electromagnetic field propagation is determined by the electric and magnetic properties of the material through which it is propagating. Electrical and magnetic properties are described by complex quantities, in which the real part describes storage and the imaginary part describes loss. In free space vacuum, the imaginary part is zero. In all other materials, the real part is greater than that of free space (yielding a slower velocity of propagation than free space), and the imaginary part is non-zero, resulting in frequency dependent properties. Frequency dependence is a consequence of the finite velocities of charge motion by diffusion and scattering. At any change in material properties, some propagating energy is scattered. With the assumption that variation of the state variables, A and V, along the wire conductor is not fast the authors remark that there is no propagation for the frequencies lower 1MHz (Olhoeft, 2003)

As a result a quasi-static model used in this study will be limited to frequencies in the dozens of kHz range for non-negligible size of the grounding device in case of large ground permittivity and poor conductivity since in this case the propagation speed of the electromagnetic field can be much lower than the speed of light in free space.

Thus, regardless the fact that there has been a lot of work done in the area of the grounding devices' behaviour there are still no specifics that have place in the grounding grids in case of the horizontal elements damages. This study represents methodology of the grounding parameters' calculation in different regimes of the power plant. The analysis and modelling reveal main features of the mentioned processes in the grids with damaged horizontal elements compared with that without such failures in them. It also allows forecasting of possible hazard potentials which can appear on a human being body in case of the damaged elements presence in grids.

4.1 Current and potential distribution in grid

The main purpose of this study is to develop a mathematical explanation which helps to understand the processes of current and voltage distribution in the grounding devices for integrated and damaged conditions of its horizontal elements. The correct mathematical model of the grounding device will allow one to analyze and present the scenario when hazardous potentials (GPR – ground potential rise) can arise in the grounding grids and on the surface of ground due to failures of its horizontal elements. The information presented describes the worst case scenario of the potential distribution on the surface of ground in most hazardous regions of the grounding grid.

As it has already been described there are a number of mathematical models which can evaluate grounding performance parameters such as current distribution, potentials and touch and step voltages at various parts of a power plant. However there are no specifics about possible changes of the surface potentials in case of breakages or damages to the bonding of the horizontal elements in these theories.

A mathematical model of the current and potential distribution in the grounding grids is developed based on the graphs theory and matrix algebra (Skiling, 1967; Skilling, 1974). These are a versatile combination of tools for electric networks calculations and can be used for the grounding grids as well. As the final result of this part of the study possible values of safety parameters in case of damaged horizontal elements presence will be calculated. These values will be compared with that when the grounding grid does not contain damaged elements in a commode mode regime. Safety parameters in terms of step and touch voltages are the main factors that used in order to evaluate the performance of power plants.

The grounding device's grid is a complex system of parallel connected horizontal elements and joined vertical elements at the nodes. An example of the grounding grid that comprises not only horizontal but also vertical elements as a universal case of the grounding devices' structure is shown in Figure 4.1. The number of elements and meshes in grounding grids is depending on the specifics of certain power plant and can vary significantly.

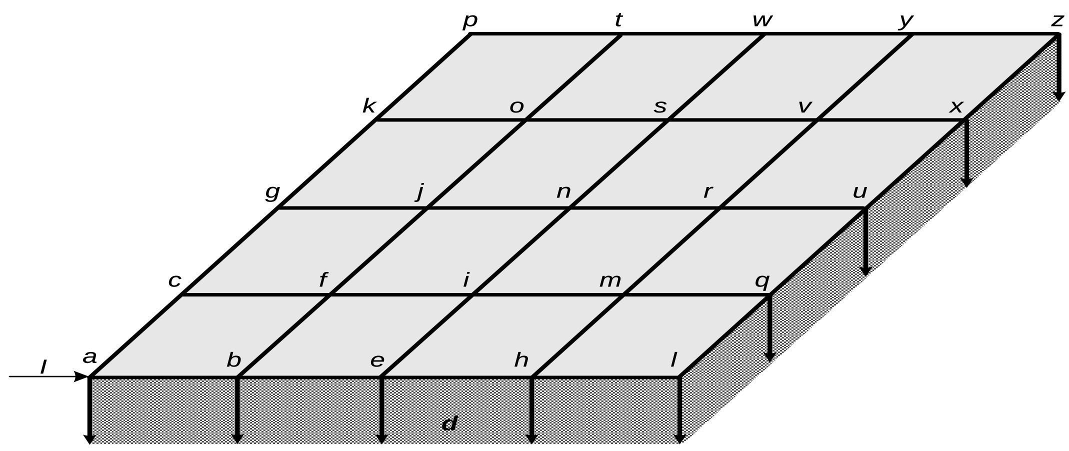

Figure 4.1: Grounding grid

As indicated in (*IEEE Guide for Safety in AC Substation Grounding*, 2000) and (Grigsby, 2001) the corner mesh voltage is higher than in the centre mesh and it is considered to be the worst-case scenario. The corner mesh voltage is higher in comparison with the centre mesh due to the fact that the current is dispersed through a number of paths. From Figure 4.1, it is very clear that the central part of the grid has more elements connected in parallel. As a result, the total resistance is low. As for the corner mesh, there are only three elements with a path to the ground. This is the main reason the point of the current injection was chosen at node "*a*" as shown in Figure 4.1.

A reference node "*d*" is so called remote ground where the potential is considered to be 0V.

The results of computer modelling provided in the case study bellow show that it is enough to take into consideration for future analysis only a part of the grounding grid that dissipates the major part of the injected current. Almost all current that flows through the grounding into ground is in the vicinity of 6 meshes from the point of injection.

The example of six meshes grounding device for analysis and its equivalent circuit are presented in Figure 4.2. A diagram of the grid's graph for analysis is shown in Figure 4.3. This number of meshes has been chosen as an optimal number for calculation due to the above-described features of the current and potential distribution.

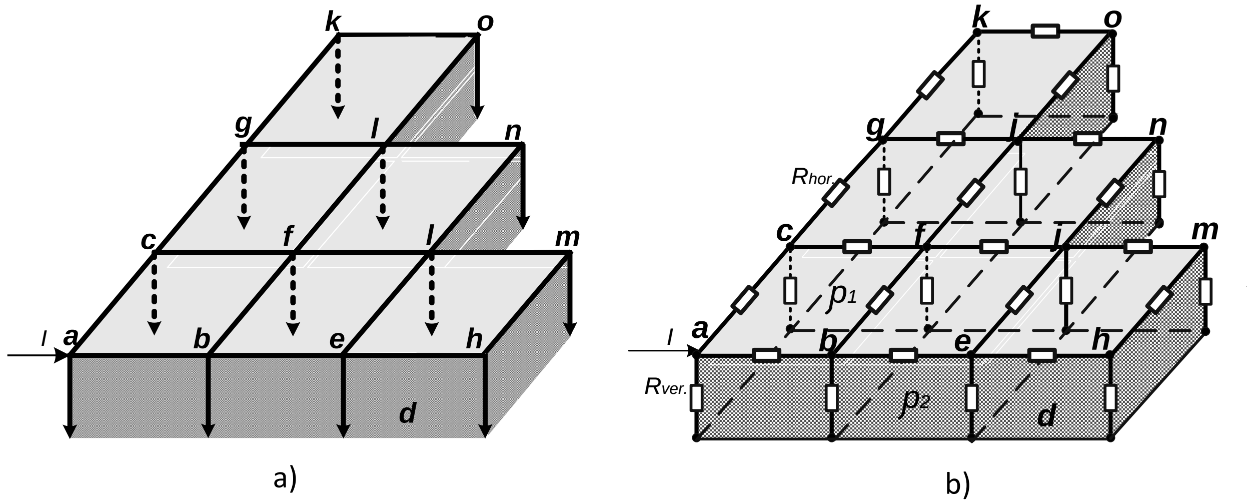

Figure 4.2: Grounding device for modelling a) and its equivalent circuit b).

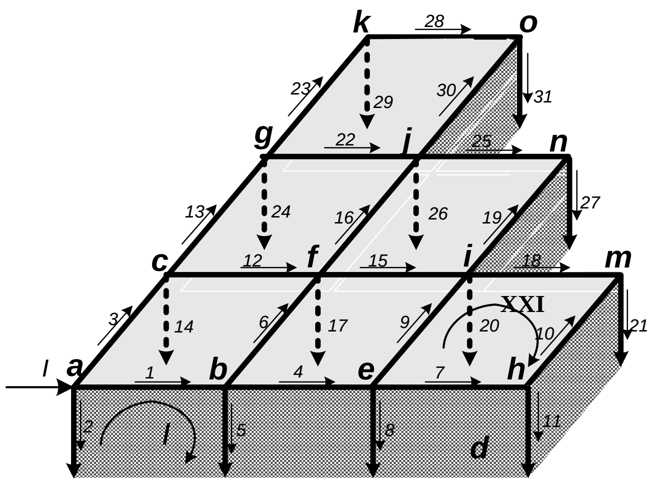

Figure 4.3: Graph of the grid for analysis

The numbering shown in the pictures is done arbitrarily (see Figures 4.3 and 4.4) since it does not have any impacts on the calculated results. Graph theory is a versatile tool that can be used to describe any electrical network, regardless of the number of branch-es and nodes of the network. According to this theory, any electrical system can be replaced by a graph with the same number of branches and nodes. Matrix analysis is implemented in order to simplify the calculation process because of the large number of the branches and nodes of the scheme.

By using created graph of the grounding device and Kirchhoff's and Ohm's Laws as a first step matrices "*M*" and "*N*" must be formed. "*M*" is the matrix of branches joints at the nodes. "*N*" is the matrix of branches joints in the independent loops.

The next step is to develop matrix of impedances "Z_n" or admittances "Y_n" of the horizontal and vertical elements joined at the nodes of the grounding device.

Setting the value of the short circuit current injected in the grid '*I*' current distribution of individual elements and voltage at the grid nodes can be determined.

There are two possible ways to calculate the current and voltage distributions through the elements of the grounding device. The first one is, at first, to determine "Y_n" and after that, inverse matrix "Y_n^{-1}".

Thanks to above-mentioned matrices one can define the voltage drop from each of the grounding device's nodes to the reference node "*d*".

$$\dot{V}_\Delta = Y_n^{-1} \cdot I \,, \tag{4.1}$$

After determination of the matrix's "$\dot{V}_\Delta$" components, it is necessary to define "Z_b^{-1}" – inverse diagonal matrix of the elements' impedances. So that the final equation for the current distribution calculation will be

$$\dot{I}_b = Z_b^{-1} \cdot M_t \cdot \dot{V}_\Delta \,, \tag{4.2}$$

where “ M_t ” – is a transposed matrix of “M”.

The second way of the currents determination is as follows: to multiply matrices “N” and “ Z_b ” and after that to create a combine matrix “A”

$$A = \begin{bmatrix} M \\ N \cdot Z_b \end{bmatrix}. \tag{4.3}$$

The last step is to calculate current in the elements

$$\dot{I}_b = A^{-1} \cdot I. \tag{4.4}$$

By using both of these methods one can have the same results of the current and voltage distribution.

Along with mathematical calculation in order to verify the main aspects of the current and potential distribution in grounding grids a computer modelling is conducted. The results of both mathematics and computer simulation are supposed to be the same. Computer simulation study is conducted using a well established MULTISIM software package (Berube, 2004). This software also will be used further in order to proceed with the processes in grounding with damaged horizontal elements.

4.2 Case study

The values of main parameters for calculations are as provided in the previous Chapter. Moreover in addition it is assumed that elements are made of copper-clad steel. The material of the grid elements is different and it depends on a country where the grounding is used. The copper-clad steel is the most common material being used in many countries. However, the choice of the conductors’ material does not change the calculations results since they are depending on the resistivity of soil. The grounding grid depth for calculations is 0.5m. The diameter of the horizontal element is 0.02m.

A computer model in MULTISIM for the scheme shown in Figure 4.1 is as bellow.

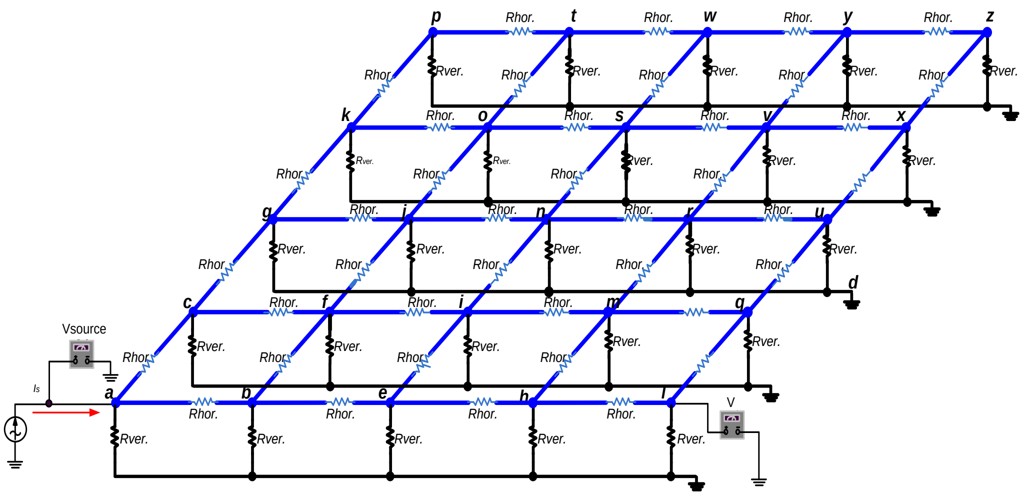

Figure 4.4: Equivalent circuit for Multisim software simulation

All the resistances shown in the Figure 4.4 have values calculated earlier in Chapter 3 Section 5 for vertical and horizontal elements of the grid.

In order to obtain the results of current and potential distribution in the scheme shown in Figure 4.2 matrices "*M*" and "*N*" must be determined.

The number of rows in matrix "*M*" equals the number of nodes in the scheme except the reference node. The number of columns in the matrix determines by the number of branches in the circuit.

$$M = \begin{array}{cc} \begin{array}{ccccccccccccccccccccc} 1 & 2 & 3 & 4 & 5 & 6 & 7 & 8 & 9 & 10 & 11 & 12 & 13 & - & 25 & 26 & 27 & 28 & 29 & 30 & 31 \end{array} & \\ \begin{bmatrix} 1 & 1 & 1 & 0 & 0 & 0 & 0 & 0 & 0 & 0 & 0 & 0 & 0 & - & 0 & 0 & 0 & 0 & 0 & 0 & 0 \\ -1 & 0 & 0 & 1 & 1 & 1 & 0 & 0 & 0 & 0 & 0 & 0 & 0 & - & 0 & 0 & 0 & 0 & 0 & 0 & 0 \\ 0 & 0 & -1 & 0 & 0 & 0 & 0 & 0 & 0 & 0 & 0 & 1 & 1 & - & 0 & 0 & 0 & 0 & 0 & 0 & 0 \\ 0 & 0 & 0 & -1 & 0 & 0 & 1 & 1 & 1 & 0 & 0 & 0 & 0 & - & 0 & 0 & 0 & 0 & 0 & 0 & 0 \\ 0 & 0 & 0 & 0 & 0 & -1 & 0 & 0 & 0 & 0 & 0 & -1 & 0 & - & 0 & 0 & 0 & 0 & 0 & 0 & 0 \\ - & - \\ 0 & 0 & 0 & 0 & 0 & 0 & 0 & 0 & 0 & -1 & 0 & 0 & 0 & - & 0 & 0 & 0 & 0 & 0 & 0 & 0 \\ 0 & 0 & 0 & 0 & 0 & 0 & 0 & 0 & 0 & 0 & 0 & 0 & 0 & - & -1 & 0 & 1 & 0 & 0 & 0 & 0 \\ 0 & 0 & 0 & 0 & 0 & 0 & 0 & 0 & 0 & 0 & 0 & 0 & 0 & - & 0 & 0 & 0 & -1 & 0 & -1 & 1 \end{bmatrix} & \begin{array}{c} a \\ b \\ c \\ e \\ f \\ - \\ m \\ n \\ o \end{array} \end{array}$$

The number of rows in matrix "*N*" is the same as the number of loops in the scheme (see Figure 4.3). The number of columns in the matrix determines by the number of branches in the circuit.

$$N = \begin{array}{cc} \begin{array}{ccccccccccccccccccccc} 1 & 2 & 3 & 4 & 5 & 6 & 7 & 8 & 9 & 10 & 11 & 12 & 13 & - & 25 & 26 & 27 & 28 & 29 & 30 & 31 \end{array} & \\ \begin{bmatrix} 1 & -1 & 0 & 0 & 1 & 0 & 0 & 0 & 0 & 0 & 0 & 0 & 0 & - & 0 & 0 & 0 & 0 & 0 & 0 & 0 \\ 0 & 0 & 0 & 1 & -1 & 0 & 0 & 1 & 0 & 0 & 0 & 0 & 0 & - & 0 & 0 & 0 & 0 & 0 & 0 & 0 \\ 0 & 0 & 0 & 0 & 0 & 0 & 1 & -1 & 0 & 0 & 1 & 0 & 0 & - & 0 & 0 & 0 & 0 & 0 & 0 & 0 \\ 0 & 0 & 0 & 0 & 0 & 0 & 0 & 0 & 0 & 1 & -1 & 0 & 0 & - & 0 & 0 & 0 & 0 & 0 & 0 & 0 \\ 0 & 0 & 0 & 0 & 0 & 0 & 0 & 0 & 0 & 0 & 0 & 0 & 0 & - & 0 & 0 & 0 & 0 & 0 & 0 & 0 \\ - & - & - & - & - & - & - & - & - & - & - & - & 0 & - & - & - & - & - & - & - & - \\ 0 & 0 & 0 & 0 & 0 & 0 & 0 & 0 & 0 & 0 & 0 & 0 & 0 & - & 0 & 0 & 0 & 0 & 1 & -1 & 0 \\ 0 & 0 & 0 & 0 & 0 & 0 & 0 & 0 & 0 & 0 & 0 & -1 & 1 & - & 0 & 0 & -1 & 1 & 1 & 0 & 0 \\ 0 & 0 & 0 & 0 & 0 & 0 & 0 & 0 & 0 & 0 & 0 & 0 & 0 & - & 1 & 0 & 0 & 0 & 0 & 0 & 0 \\ -1 & 0 & 1 & 0 & 0 & -1 & 0 & 0 & 0 & 0 & 0 & 1 & 0 & - & 0 & 0 & 0 & 0 & 0 & 0 & 0 \\ 0 & 0 & 0 & -1 & 0 & 1 & 0 & 0 & -1 & 0 & 0 & 0 & 0 & - & 0 & 0 & 0 & 0 & 0 & 0 & 0 \\ 0 & 0 & 0 & 0 & 0 & 0 & -1 & 0 & 1 & -1 & 0 & 0 & 0 & - & 0 & 0 & 0 & 0 & 0 & 0 & 0 \end{bmatrix} & \begin{array}{c} \mathrm{I} \\ \mathrm{II} \\ \mathrm{III} \\ \mathrm{IV} \\ \mathrm{V} \\ - \\ \mathrm{XVI} \\ \mathrm{XVII} \\ \mathrm{XVIII} \\ \mathrm{XIX} \\ \mathrm{XX} \\ \mathrm{XXI} \end{array} \end{array}$$

The next step is to develop impedances "Z_n" or admittances "Y_n" matrices of the horizontal and vertical elements joined at the nodes of the grounding device.

The matrix of admittances "Y_n" of the horizontal and vertical elements joined at the nodes of the grounding device is as follows:

$$
Y_n = \begin{array}{cc}
\begin{array}{ccccccccc} \boldsymbol{a} & \boldsymbol{b} & \boldsymbol{c} & \boldsymbol{e} & \boldsymbol{f} & - & \boldsymbol{m} & \boldsymbol{n} & \boldsymbol{o} \end{array} & \\
\left[\begin{array}{ccccccccc}
Y_1+Y_2+Y_3 & -Y_1 & -Y_3 & 0 & 0 & - & 0 & 0 & 0 \\
-Y_1 & Y_1+Y_4+Y_5+Y_6 & 0 & -Y_4 & -Y_6 & - & 0 & 0 & 0 \\
-Y_3 & 0 & Y_3+Y_{12}+Y_{13}+Y_{14} & 0 & -Y_{12} & - & 0 & 0 & 0 \\
0 & -Y_4 & 0 & Y_4+Y_7+Y_8+Y_9 & -Y_{11} & - & 0 & 0 & 0 \\
0 & -Y_6 & -Y_{12} & -Y_{11} & Y_6+Y_{12}+Y_{15}+Y_{16}+Y_{17} & - & 0 & 0 & 0 \\
- & - & - & - & - & - & - & - & - \\
0 & 0 & 0 & 0 & 0 & - & Y_{10}+Y_{18}+Y_{21} & 0 & 0 \\
0 & 0 & 0 & 0 & 0 & - & 0 & Y_{19}+Y_{25}+Y_{27} & 0 \\
0 & 0 & 0 & 0 & 0 & - & 0 & 0 & Y_{28}+Y_{30}+Y_{31}
\end{array}\right] &
\begin{array}{c} \boldsymbol{a} \\ \boldsymbol{b} \\ \boldsymbol{c} \\ \boldsymbol{e} \\ \boldsymbol{f} \\ - \\ \boldsymbol{m} \\ \boldsymbol{n} \\ \boldsymbol{o} \end{array}
\end{array}
$$

Diagonal elements of the matrix are admittances of all branches connected to this particular node. The rest of the matrix represents impedances of horizontal elements between each pair of nodes. All elements in the matrix include mutual coupling .

A certain value of a fault current injected in the grounding grid (as from (*IEEE Guide for Safety in AC Substation Grounding*, 2000)) depends on the certain scheme of particular power plant, its capacity, type of a fault, grounding resistance etc. Many different faults may occur in the system. For the calculations a fault current is usually a single-phase-to ground or two-phase-to ground fault current. So a certain value of a fault current can vary significantly. For this particular study as an example of a possible short circuit current that can appear for instance in the typical 20 kV substation the value of 1700A is taken. Undoubtedly, fault currents' values might be different as well as number of meshes of the grounding grid but in general, the certain current value is a linear function that influence on the grounding voltage to be calculated.

Not all the currents flow through the grounding as shown in Figure 4.5. Some of the currents flow through other elements of the power plant such as cables sheaths, metal constructions and etc into the soil. The impedance of these elements can be different depending on the specifics and features of the power plant. This impedance is shown as Zp in Figure 4.5. So, a current division factor S_f between Zp and Zg must be taken in the calculations.

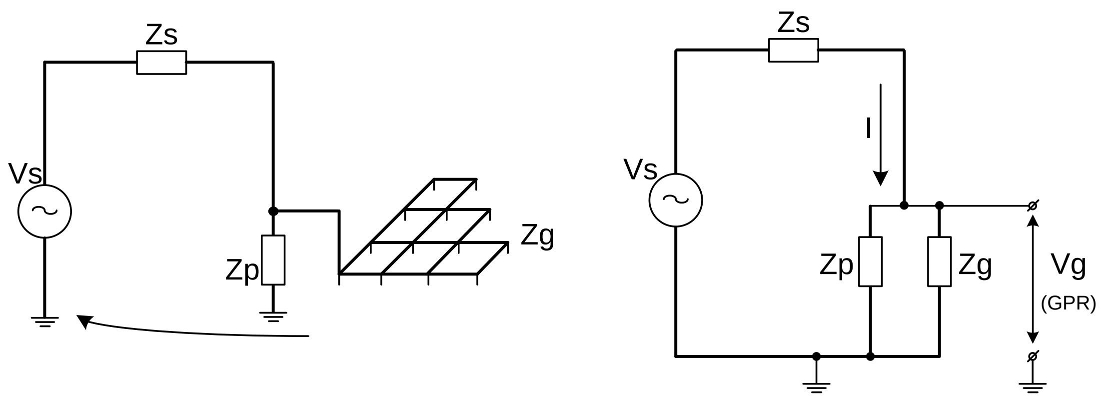

Figure 4.5: A part of fault current flowing through the grounding

Impedance "Z*s*" shown on the picture represents the total impedance of all elements of the system before the point of connection with grounding (fault point). In this particular example Zs=8Ω.

Thus, taking into account S_f = 0.36 the value of the current that flows through the grounding from (*IEEE Guide for Safety in AC Substation Grounding*, 2000)

$$I = I_f \cdot S_f = 1700 \cdot 0.36 = 610 \text{ A.}$$

After detection of the fault current value matrix of current injected in the grounding grid can be shown as

$$I = \begin{bmatrix} I_a \\ I_b \\ I_c \\ I_e \\ - \\ - \\ I_m \\ I_n \\ I_o \end{bmatrix} = \begin{bmatrix} 610 \\ 0 \\ 0 \\ 0 \\ - \\ - \\ 0 \\ 0 \\ 0 \end{bmatrix}, A$$

Substituting these values in Eqns. (4.1) and (4.2) thanks to Microsoft Office Excel and matrix analysis (Jordan, 2012; Vautier, Consulting, & New Zealand Institute of Chartered, 2008) one can have

$$V_\Delta = \begin{bmatrix} V_a \\ V_b \\ V_c \\ V_e \\ V_f \\ V_g \\ V_h \\ V_i \\ V_j \\ V_k \\ V_m \\ V_n \\ V_o \end{bmatrix} = \begin{bmatrix} 807 \\ 804 \\ 804 \\ 803 \\ 803 \\ 803 \\ 802 \\ 803 \\ 803 \\ 802 \\ 802 \\ 802 \\ 802 \end{bmatrix}, V \qquad I_b = \begin{bmatrix} I_1 \\ I_2 \\ I_3 \\ I_4 \\ I_5 \\ I_6 \\ I_7 \\ I_8 \\ I_9 \\ I_{10} \\ I_{11} \\ I_{12} \\ I_{13} \\ I_{14} \\ I_{15} \\ I_{16} \\ I_{17} \\ I_{18} \\ I_{19} \\ I_{20} \\ I_{21} \\ I_{22} \\ I_{23} \\ I_{24} \\ I_{25} \\ I_{26} \\ I_{27} \\ I_{28} \\ I_{29} \\ I_{30} \\ I_{31} \end{bmatrix} = \begin{bmatrix} 279 \\ 52 \\ 279 \\ 135 \\ 50 \\ 94 \\ 57 \\ 48 \\ 30 \\ 8 \\ 49 \\ 94 \\ 135 \\ 50 \\ 72 \\ 72 \\ 44 \\ 36 \\ 22 \\ 44 \\ 44 \\ 30 \\ 57 \\ 48 \\ 22 \\ 44 \\ 44 \\ 8 \\ 49 \\ 36 \\ 44 \end{bmatrix}, \mathrm{A}$$

A computer model of the same grounding device is presented bellow

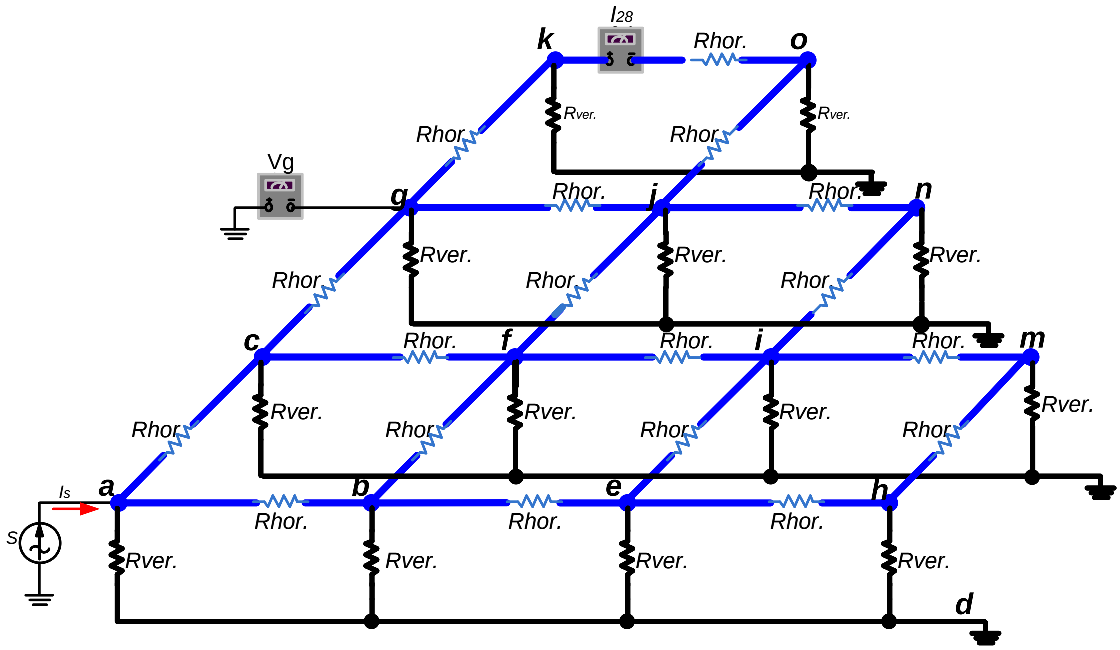

Figure 4.6: Computer model of the grounding grid

Measurements of the voltages and currents are made by means of voltmeters and ammeters as shown on the picture. The results of modelling of the potential and current distribution in the grid are presented in Table 4.1 and Table 4.2 respectively.

Table 4.1: Voltage distribution at nodes of the grounding device

Node	**Potential, *V***	**Node**	**Potential, *V***
a	807.8	*i*	803.2
b	804.8	*j*	803.2
c	804.8	*k*	802.9
e	803.5	*m*	802.8
f	803.8	*n*	802.9
g	803.5	*o*	802.8
h	802.9	-	-

Table 4.2: Current distribution through the grounding elements

Branch Number	**Current, *A***	**Branch Number**	**Current, *A***
1	279	*16*	72
2	52	*17*	44
3	279	*18*	36
4	135	*19*	22
5	50	*20*	44
6	94	*21*	44
7	57	*22*	30
8	48	*23*	57
9	30	*24*	48
10	8	*25*	22
11	49	*26*	44
12	94	*27*	44

13	135	*28*	8
14	50	*29*	49
15	72	*30*	36
-	-	*31*	44

As one can see, both, mathematical results and results of the computer modelling are the same and further for the more complicated processes' analysis a computer modelling is used.

The potential distribution graph (GPR) is shown in Figure 4.7.

If there is a damaged element in the mesh of the grid it will result in a different potential distribution since soil resistance in the gap can be substantially higher than the resistance of the integrated element. The results below provide information about the potential distribution in the grounding in case of the failure of the horizontal element presence. By "failure" one can mean breakage or rupture of the horizontal element due to mechanical, freezing, corrosion or other causes.

As an example of the worst-case scenario, horizontal elements 1 and 12 from Figure 4.7 are chosen as damaged elements. These elements are the closest elements to the current injection point that result in the highest potentials. Table 4.3 shows the results of the potential distribution in the grid for the case with two 4cm gaps with resistance of 0.624kΩ each. It is the resistance of the gap in the damaged element due to corrosion. The value of the gap's resistance is obtained thanks to the experiments. The experimental part conducted and its results are described in the next chapter. For the purpose of modelling gap's resistance is added to the resistance of above-mentioned horizontal elements in Figure 4.6 in series. The values in the Table 4.3 show nodes voltages and voltage fluctuation in percents compared with the scenario in Table 4.1 without failures.

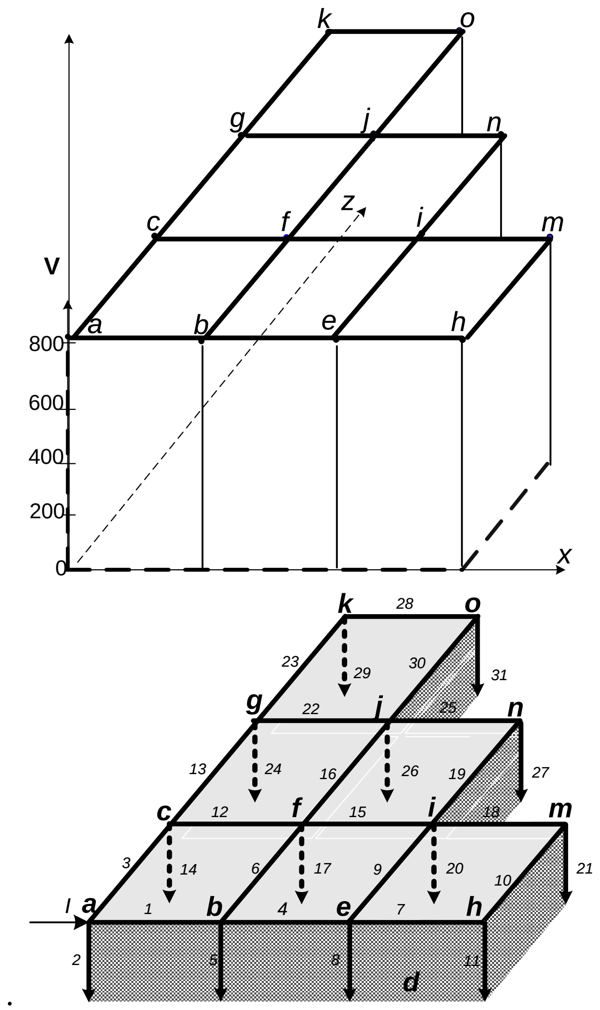

Figure 4.7: Grounding device's voltage distribution

Table 4.3: Voltage distribution with two damaged elements, V

Node	V_g, V	ΔV_g, %	**Node**	V_g, V	ΔV_g, %
a	819.8	+1.5	*i*	800.8	-0.3
b	800.6	-0.5	*j*	803.3	0.0
c	811.7	+0.9	*k*	806.0	+0.4
e	800.3	-0.4	*m*	800.2	-0.3
f	801.3	-0.3	*n*	801.8	-0.1
g	806.5	+0.3	*o*	803.9	+0.1
h	800.0	-0.3	-	-	-

The equivalent circuit and a curve of the potential distribution are shown in Figure 4.8.

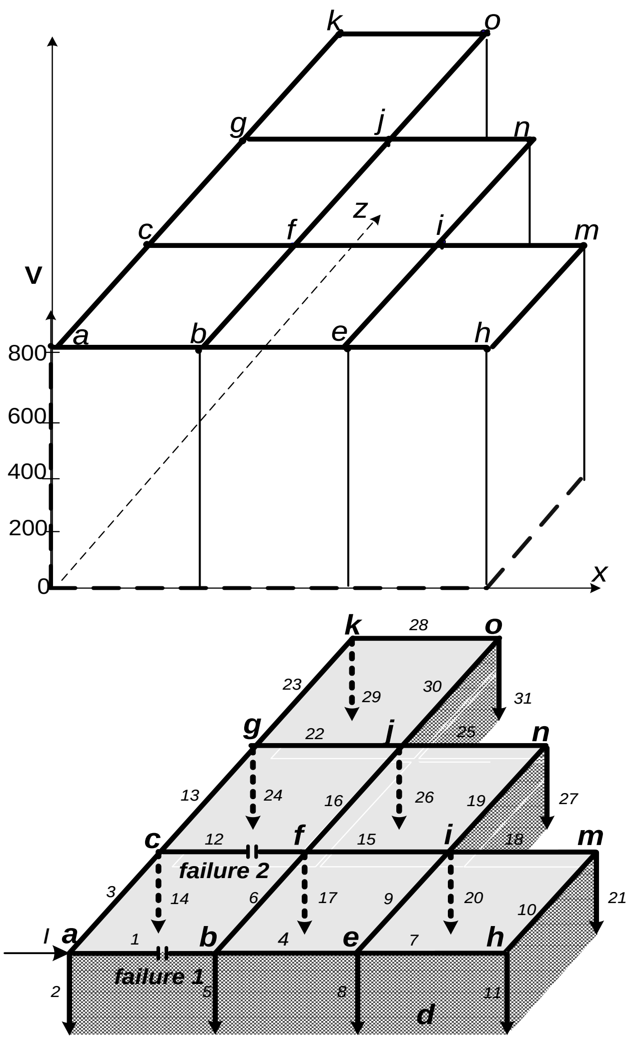

Figure 4.8: Potential distribution with damaged elements

In order to obtain more specific characteristics of the current and potential distribution the grounding circuit was narrowed down to 4 meshes (section A) as shown in Figure 4.9. It is possible to do like this since the process of current dissipation is similar in all meshes: current flows from the source through the elements into ground. The modeling circuit as it is shown in Figure 4.10.

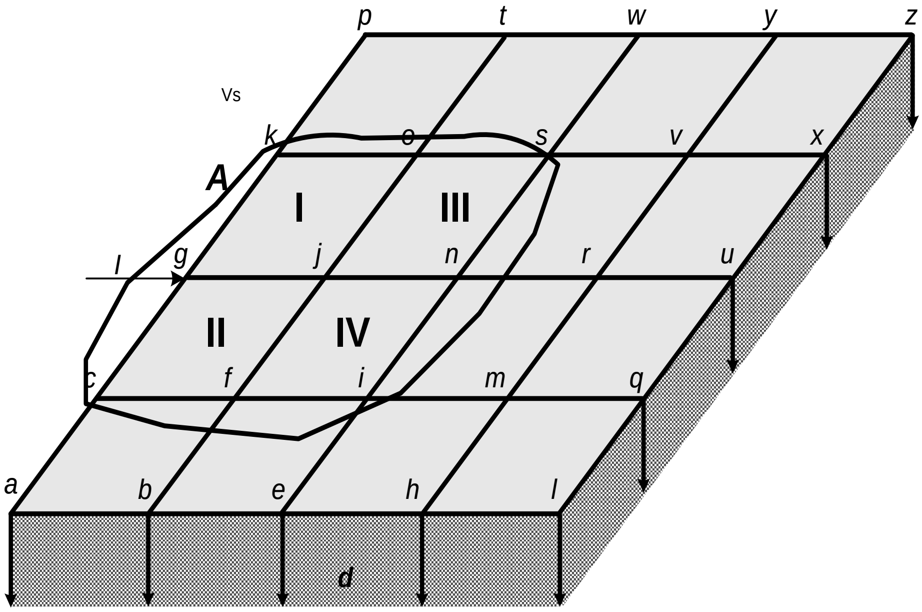

Figure 4.9: Four meshes section for analysis

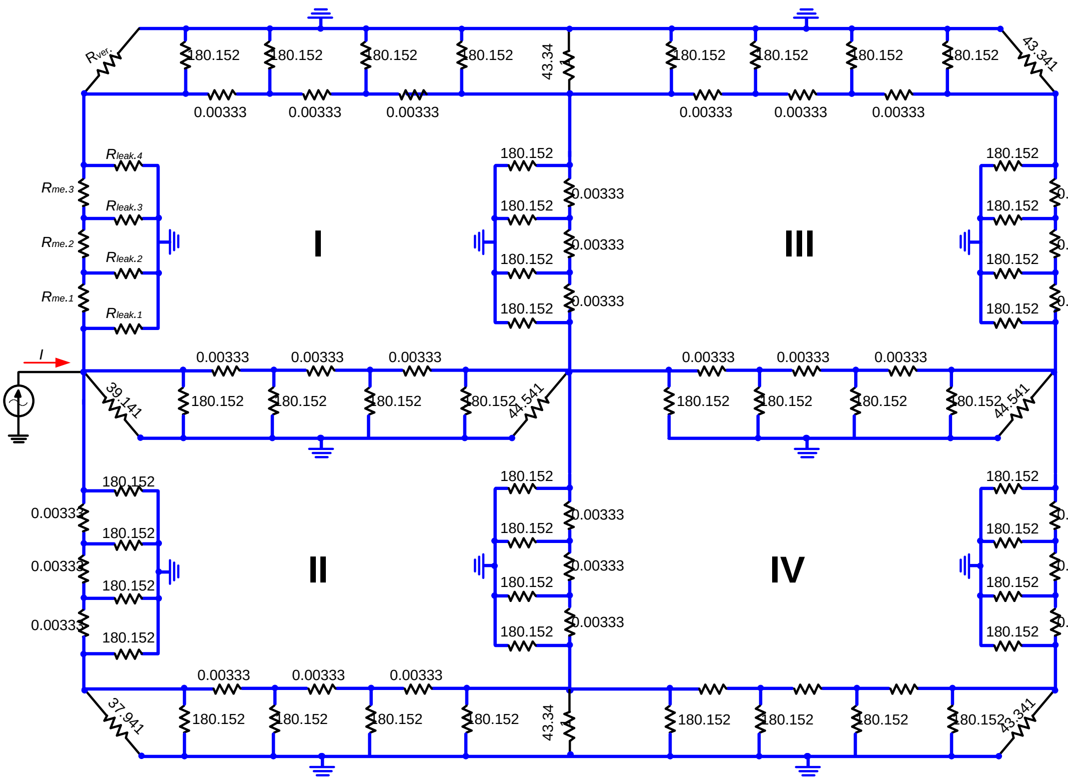

Figure 4.10: Four meshes section for simulation

Simulation studies are carried out not only for the case when all horizontal elements of the grid are physically integrated but also when there is a failure of the element. For such a purpose a gap between two parts of the damaged horizontal element is shown as an additional resistance in the circuit. The value of the failure varied depending on “nature” of the failure.

A modified scheme for the computer modelling is shown in Figure 4.11. The horizontal element between meshes I and II is chosen as a damaged one. To observe a current distribution in the element ammeters and oscilloscopes are installed in the circuit. The resistance of the middle element is recalculated taking into account possible failure’s resistance. Figure 4.11 shows first two meshes of the grid but takes into account all the above-described elements. The values of the elements $R_{me.i}$ and $R_{leak.i}$ are the same as shown in the other parts of the scheme.

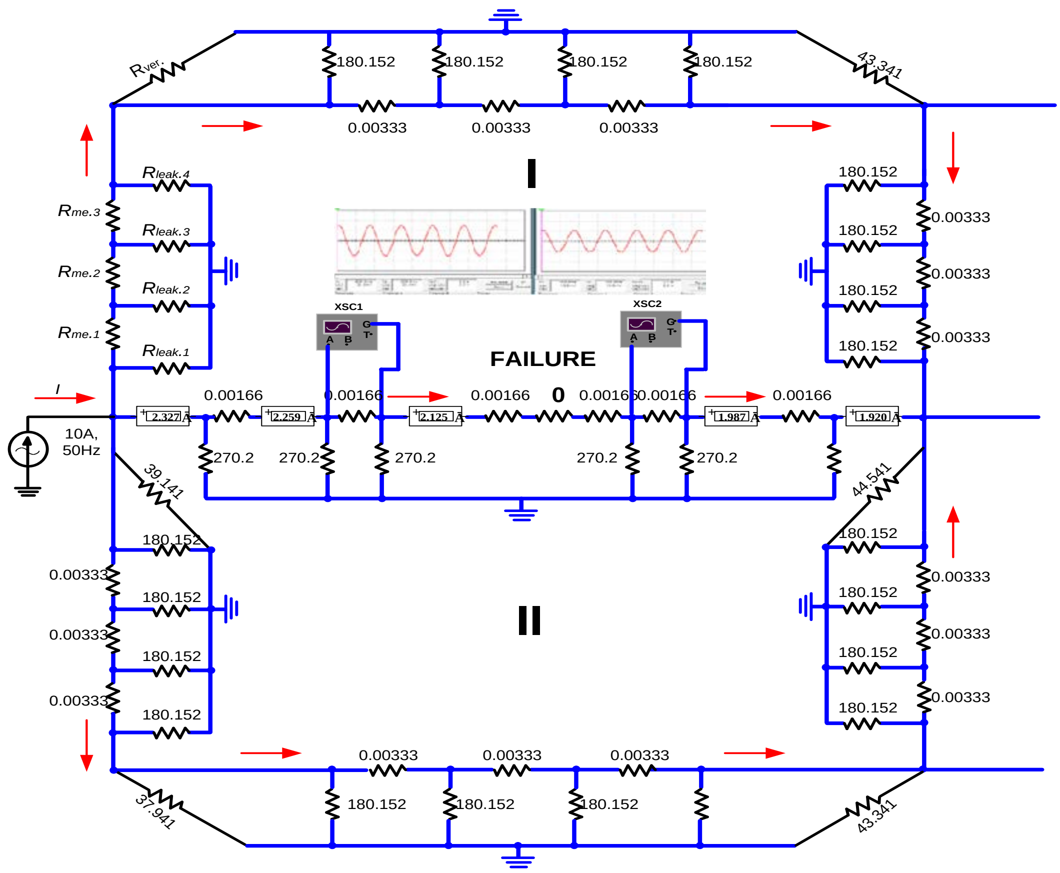

Figure 4.11: Simulation with integrated horizontal element (R=0Ω)

Figure 4.12 represents the regime when the horizontal element in the middle of the mesh is damaged. The resistance of the gap can be change in a wide range depending on the soil resistivity.

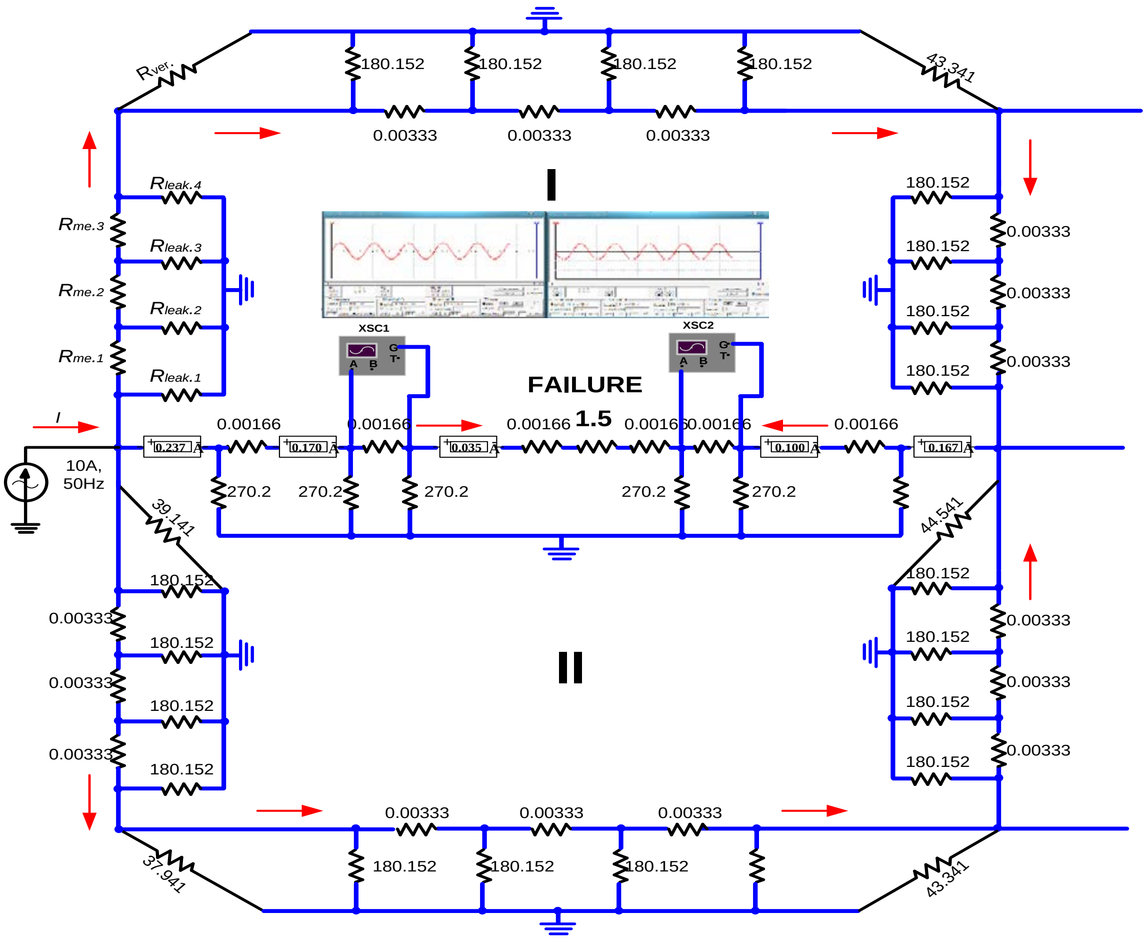

Figure 4.12: Simulation with damaged element (R=1.5Ω)

Graphically the results of the current processes' simulation can be presented as shown in Figure 4.13 and Figure 4.14 respectively.

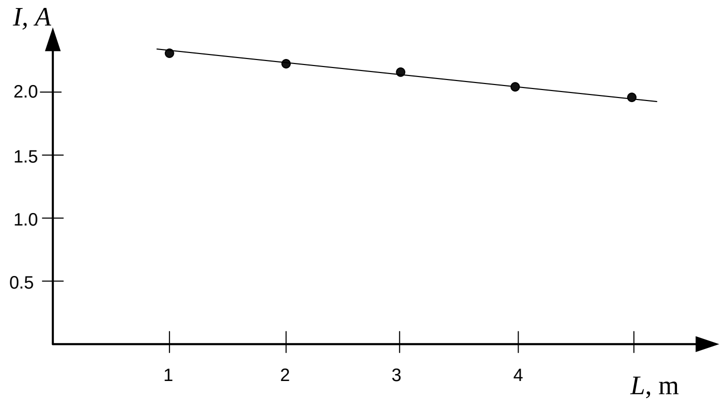

Figure 4.13: Current distribution along conductor without damages

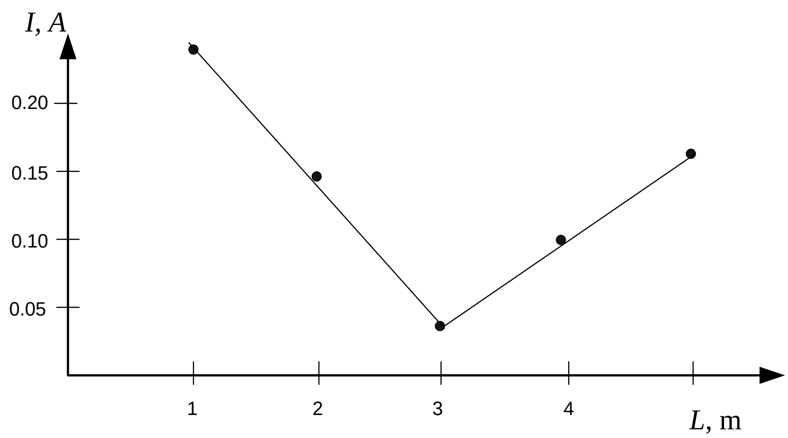

Figure 4.14: Current distribution along damaged conductor

In addition to the above-presented schemes, two more scenarios were analysed. The circuits were exactly the same as shown in Figure 4.11 and Figure 4.12 except a square-wave form with a test current of 1.5 A and a frequency of 400Hz was applied. The results from the above scenarios will be used to verify the experimental results which will be described in the later Section.

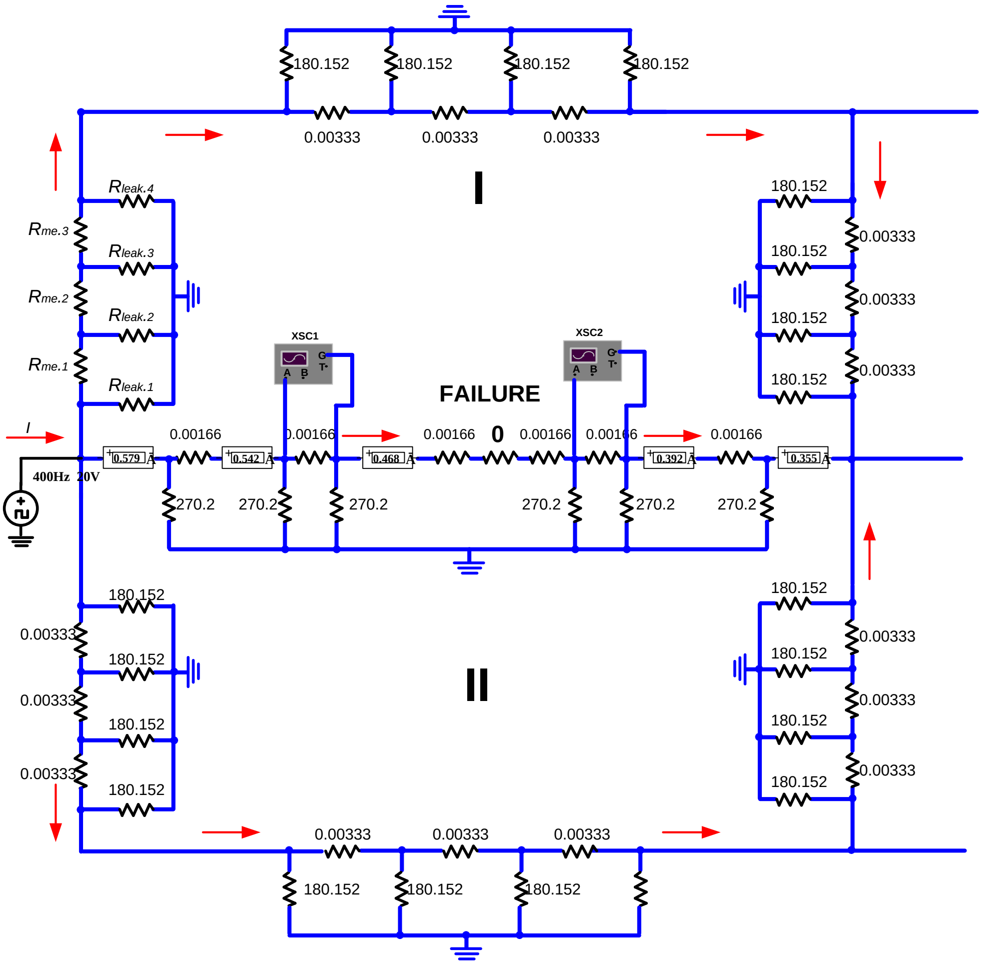

Figure 4.15: Simulation with integrated horizontal element (R=0Ω) and 400Hz generator

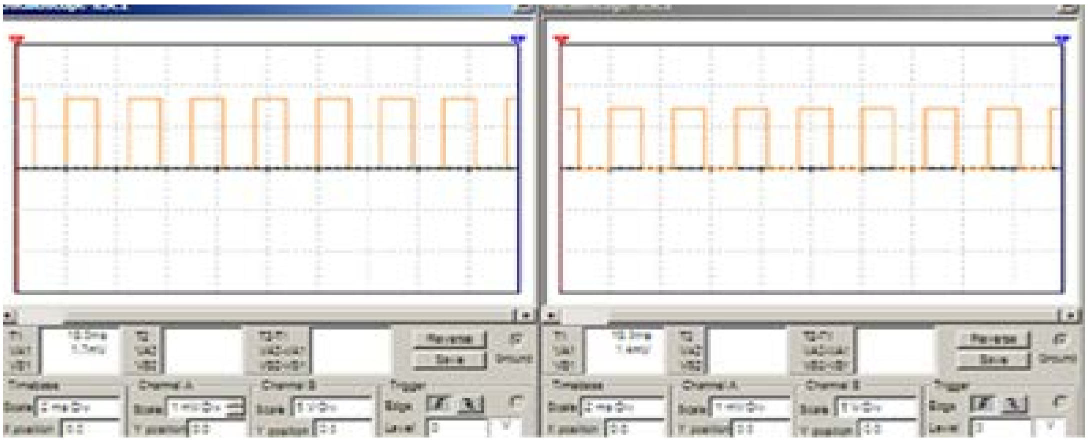

Figure 4.16: In phase direction of currents in element without failure

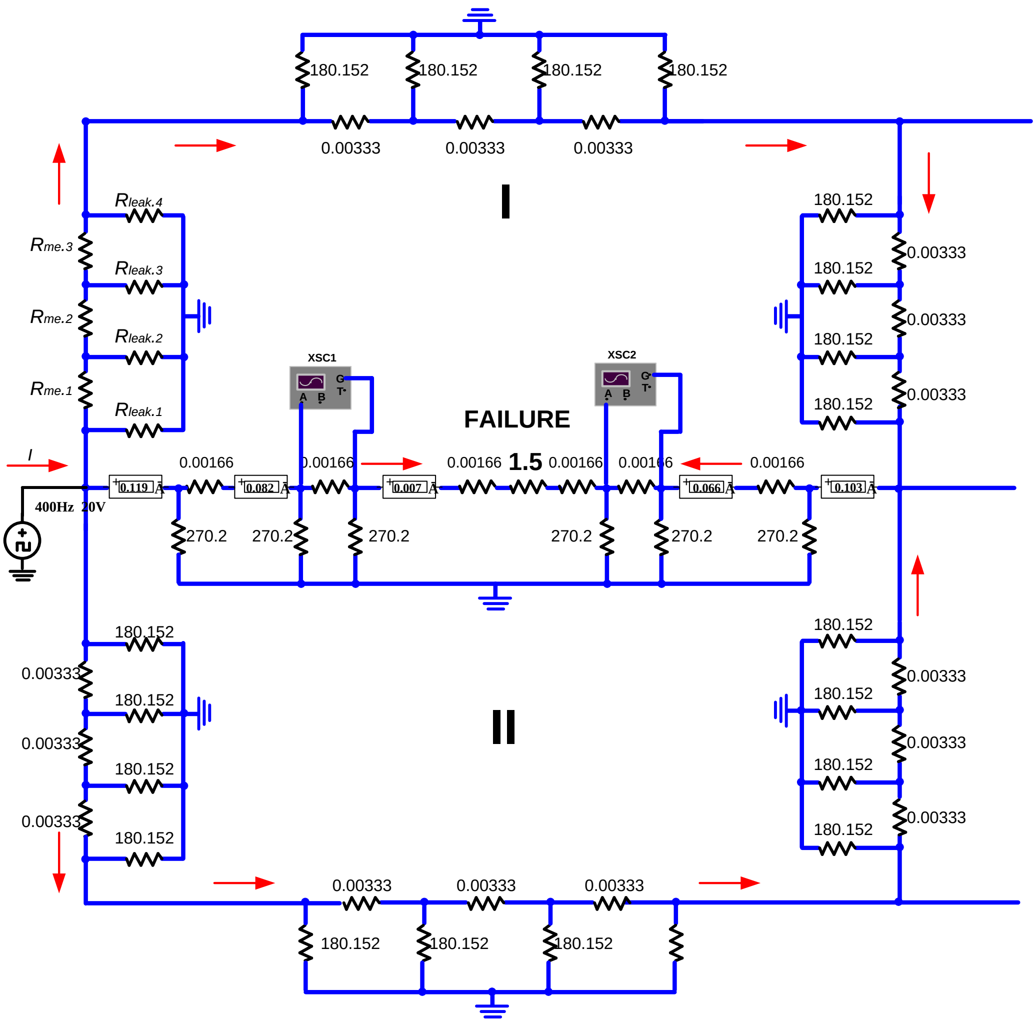

Figure 4.17: Simulation with damaged horizontal element and 400Hz generator

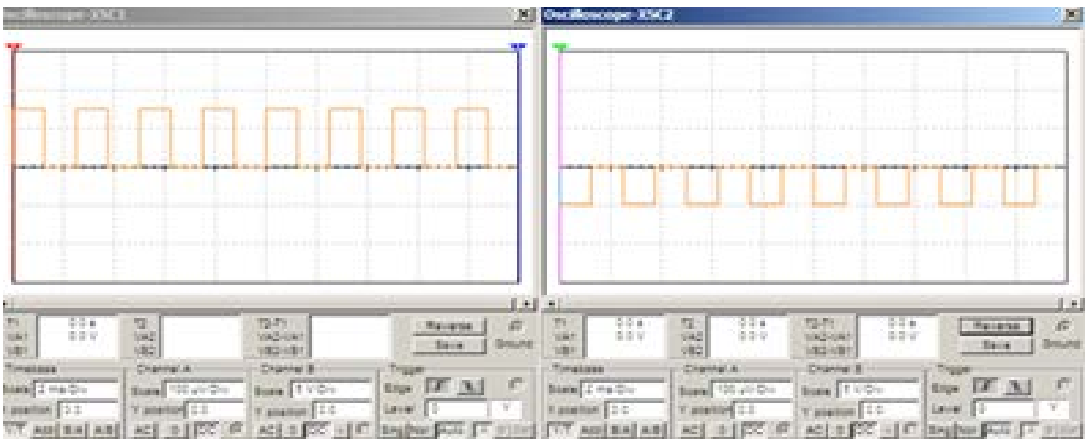

Figure 4.18: Out of phase direction of currents in element with failure

4.3 Safety parameters evaluation

The main parameters that usually taken for consideration in order to describe safety at the power plant are touch and step voltage. According to (*IEEE Guide for Safety in AC Substation Grounding*, 2000), the way of step and touch voltage determination is when one, setting the value of tolerable amount of electric shock energy for an average person (S_B), can calculate tolerable currents for a 50kg or 70kg human being. After that, permissible values of step and touch voltages can be calculated. The only variables that can influence upon the current through a body I_B, afore mentioned voltages E_{step} and E_{touch} are time, weight of a person and apparent soil resistivity.

The existing way described in the standard is good enough for the grounding devices at a stage of their projects' creation, for example, when one can determine the value of a tolerable E_{step}, E_{touch} and find the best design for the future grounding device. But after some period of time due to possible increase of a spreading resistance, damaged elements' appearance and not the same curve of the potential distribution E_m, E_{step} depend on voltage on the grounding device. With the same resistance of the person, increase of the grounding grid voltage will result in higher current through the body which of course is more hazardous.

According to (*IEEE Guide for Safety in AC Substation Grounding*, 2000) the maximum limit of touch voltage is:

For a body weight 50kg

$$E_{touch50} = (1000 + 1.5 \cdot \rho) \cdot \frac{0.116}{\sqrt{t_S}}\ . \tag{4.5}$$

For a body weight 70kg

$$E_{touch70} = (1000 + 1.5 \cdot \rho) \cdot \frac{0.157}{\sqrt{t_s}}. \quad (4.6)$$

In general, the maximum touch voltage may have several hundred volts value with a minimum clearance time (0.1s or less). The maximum limit of step voltage is:

For a body weight 50kg

$$E_{step50} = (1000 + 6 \cdot \rho) \cdot \frac{0.116}{\sqrt{t_s}}. \quad (4.7)$$

For a body weight 70kg

$$E_{step70} = (1000 + 6 \cdot \rho) \cdot \frac{0.157}{\sqrt{t_s}}, \quad (4.8)$$

where ρ - apparent resistivity of soil in Ωm, t_s – duration of shock current in seconds (0.5s).

Apparent soil resistivity may be calculated as follows

$$\rho = \frac{\rho_1 \cdot \rho_2 \cdot l_{ver.}}{\rho_1 \cdot (l_{ver.} + t - h_1) + \rho_2 \cdot (h_1 - t)}, \quad (4.9)$$

The actual mesh voltage E_m (maximum touch voltage) (*IEEE Guide for Safety in AC Substation Grounding*, 2000) can be evaluated as

$$E_m = \frac{\rho \cdot K_m \cdot K_i \cdot I}{L_m}, \quad (4.10)$$

The geometrical factor K_m as from (*IEEE Guide for Safety in AC Substation Grounding*, 2000):

$$K_m = \frac{1}{2\cdot\pi}\cdot\left[\ln\left(\frac{D^2}{16\cdot h\cdot d}+\frac{(D+2\cdot h)^2}{8\cdot D\cdot d}-\frac{h}{4\cdot d}\right)+\frac{K_{ii}}{K_h}\cdot\ln\left(\frac{8}{\pi(2\cdot n-1)}\right)\right], \qquad (4.11)$$

For grids with ground rods along the perimeter, or for grids with ground rods in the grid corners, as well as both along the perimeter and throughout the grid area,

$$K_{ii} = 1, \qquad (4.12)$$

$$K_h = \sqrt{1+\frac{h}{h_0}}, \qquad (4.13)$$

where h_0 = 1m (grid reference depth).

The effective number of parallel conductors in a given grid, n, can be made applicable to both rectangular and irregularly shaped grids that represent the number of parallel conductors of an equivalent rectangular grid:

$$n = n_a \cdot n_b \cdot n_c \cdot n_d, \qquad (4.14)$$

where

$$n_a = 2\cdot\frac{L_C}{L_p}, \qquad (4.15)$$

and n_b = 1 for square grids; n_c = 1 for square and rectangular grids; n_d = 1 for square, rectangular, and L-shape grids.

Otherwise,

$$n_b = \sqrt{\frac{L_p}{4 \cdot \sqrt{A}}}, \tag{4.16}$$

$$n_c = \left(\frac{L_x \cdot L_y}{A} \right)^{\frac{0.7 \cdot A}{L_x \cdot L_y}}, \tag{4.17}$$

$$n_d = \frac{D_m}{\sqrt{L_x^2 + L_y^2}}, \tag{4.18}$$

The irregularity factor, K_i, used in conjunction with the above defined n is:

$$K_i = 0.644 + 0.148 \cdot n, \tag{4.19}$$

For grids with ground rods in the corners, as well as along the perimeter and throughout the grid, the effective buried length, L_m, is:

$$L_m = L_C + \left[1.55 + 1.22 \left(\frac{l_{ver}}{\sqrt{L_x^2 + L_y^2}} \right) \right] \cdot L_R, \tag{4.20}$$

The maximum Step Voltage values are obtained as the product of the soil resistivity (ρ), the geometrical factor K_s, the corrective/irregularity factor K_i, and the average current per unit of buried length of grounding system conductor (I/L_S):

$$E_S = \frac{\rho \cdot K_S \cdot K_i \cdot I}{L_S}, \tag{4.21}$$

For the usual burial depth of 0.25m < h < 2.5m, then

$$K_S = \frac{1}{\pi} \cdot \left[\frac{1}{2 \cdot h} + \frac{1}{D+h} + \frac{1}{D}(1 - 0.5^{n-2}) \right], \tag{4.22}$$

For grids with or without ground rods, the effective buried conductor length, L_S, is written as follows:

$$L_S = 0.75 \cdot L_C + 0.85 \cdot L_R, \tag{4.23}$$

4.4 Case study

For the considered grounding device by substituting values in Eqns. (4.5)-(4.8) one can have

$$E_{touch50} = (1000 + 1.5 \cdot 54) \cdot \frac{0.116}{\sqrt{0.5}} = 177.3\,\text{V},$$

$$E_{touch70} = (1000 + 1.5 \cdot 54) \cdot \frac{0.157}{\sqrt{0.5}} = 240\,\text{V},$$

$$E_{step50} = (1000 + 6 \cdot 54) \cdot \frac{0.116}{\sqrt{0.5}} = 217.2\,\text{V},$$

$$E_{step70} = (1000 + 6 \cdot 54) \cdot \frac{0.157}{\sqrt{0.5}} = 294\,\text{V}.$$

Eqn. (4.9) gives

$$\rho = \frac{250 \cdot 30 \cdot 3}{250 \cdot (3 + 0.5 - 2) + 30 \cdot (2 - 0.5)} = 54\,\Omega.$$

As from Eqn. (4.20)

$$L_m = 90 + \left[1.55 + 1.22 \left(\frac{3}{\sqrt{15^2 + 15^2}} \right) \right] \cdot 39 = 157.2\text{m}$$

Since the shape of the grounding device example for calculation is not square

$$n_b = \sqrt{\frac{60}{4 \cdot \sqrt{150}}} = 1.1,$$

$$n_a = 2 \cdot \frac{90}{60} = 3,$$

$$n_c = \left(\frac{15 \cdot 15}{150}\right)^{\frac{0.7 \cdot 150}{15 \cdot 15}} = 1.2$$

$$n_d = \frac{21.2}{\sqrt{15^2 + 15^2}} = 1$$

$$n = 3 \cdot 1.1 \cdot 1.2 \cdot 1 = 4,$$

$$K_i = 0.644 + 0.148 \cdot 4 = 1.2,$$

$$K_h = \sqrt{1 + \frac{0.5}{1}} = 1.2,$$

$$K_m = \frac{1}{2 \cdot 3.14} \cdot \left[\begin{array}{l} \ln\left(\frac{5^2}{16 \cdot 0.5 \cdot 0.02} + \frac{(5 + 2 \cdot 0.5)^2}{8 \cdot 5 \cdot 0.02} - \frac{0.5}{4 \cdot 0.02}\right) + \\ + \frac{1}{1.2} \cdot \ln\left(\frac{8}{3.14(2 \cdot 4 - 1)}\right) \end{array}\right] = 0.7$$

Mesh voltage value is:

$$E_m = \frac{610 \cdot 0.7 \cdot 1.2}{157.2} \cdot 54 = 176 \text{ V}.$$

By substituting values in Eqns. (4.21) - (4.23) one can obtain

$$L_S = 0.75 \cdot 90 + 0.85 \cdot 39 = 100.65 \text{ m},$$

$$K_S = \frac{1}{3.14} \cdot \left[\frac{1}{2 \cdot 0.5} + \frac{1}{5+0.5} + \frac{1}{5}(1-0.5^{4-2}) \right] = 0.42 \text{ ,}$$

$$E_S = \frac{610 \cdot 0.42 \cdot 1.2}{100.65} \cdot 54 = 165 \text{ V}$$

4.5 Discussion

The results of mathematical and computer modelling in this chapter shows that in case of the damaged elements presence in the grounding grid increase of the ground potential rise can be 1.5% higher than that without damaged horizontal elements in the grid. It may result in a higher value of E_m and E_s. As it may be seen from Table 4.3 in case when some of the horizontal elements of the grid are damaged the maximum grounding device's voltage (GPR) will be at the point of the current injection. Of course, dimensions and design of the grounding and values of fault currents may vary but under the worst case scenario the grounding performance in terms of providing safety can be hazardous.

The higher voltage levels at points of the grid will result in higher levels of the mesh voltage. The bigger difference between potential values of nodes and steeper curves between nodes of the grid the higher values of touch and step voltage one can expect and the more unsafe conditions are at the power plant for personnel will be.

As shown in the last case study the value of mesh voltage is 176V which is just under the tolerable touch voltage E_{step50}=177.3V. As for the step voltage value (165V) it is lower than a permissible level of 217.2V.

But even if initially the grounding device was made according to all safety criteria and values of mesh and step voltages were permissible, in some period of time after the grounding creation, due to elements destruction GPR may increase. It will result in the increase of *Em* and *Es* as well and hazardous situation for personnel at the power plant. Moreover, with increase of the voltages at some nodes of the grid (i.e. node "*a*" and "*c*") potentials of the others drop significantly. It will result in steeper curve of the potential distribution and bigger difference between two points on the surface of ground. The situation will be even worse with increase of the fault currents values at the higher voltage range power plants. With increase of the fault currents' values, the GPR value also increases which will result in higher mesh and step voltages on the surface.

Graphically all these can be explained as shown in Figure 4.19 and Figure 4.20.

Figure 4.19 represents situation when there is a metallic connection between all the elements of the grid. In this case, the curves of their potential distribution graphically superimpose on each other. If one node has a bigger value of the potential in regards to the other nodes, it results in increase of touch voltage as shown in Figure 4.19(*Vtouch1*).

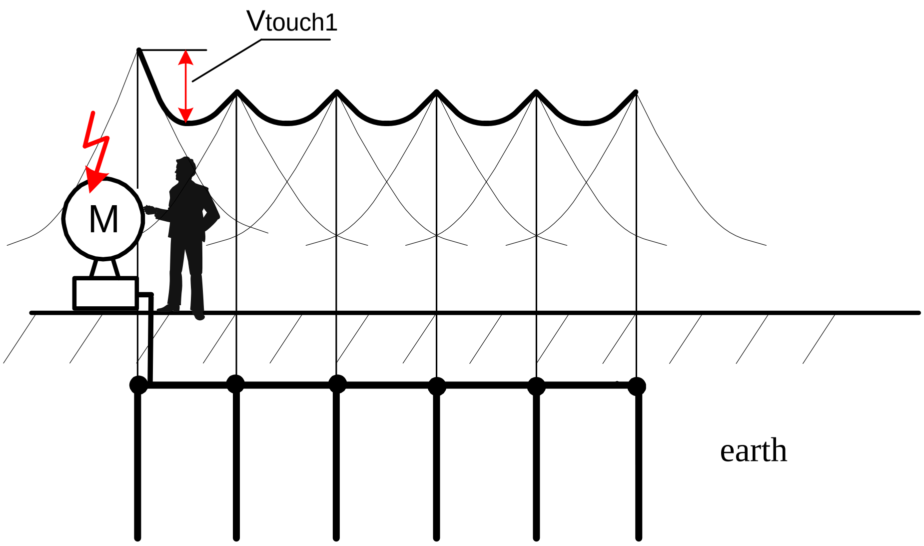

Figure 4.19: Potential distribution without damaged elements

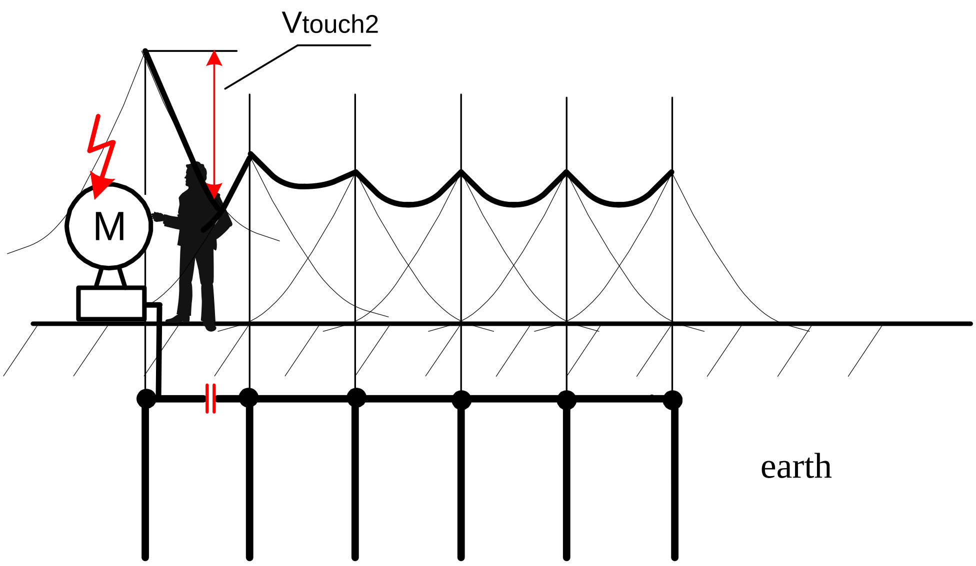

Figure 4.20: Potential distribution with a damaged element

The worst case scenario will be when elements of the grounding grid don't have an electrical connection (for instance due to physical damage of one of the horizontal elements (Figure 4.20). Their potential curves do not superimpose anymore. Each vertical element has its own curve. If this node is the same current injection point as from the previous example due to increase of the total grid resistance the voltage value will be even higher. Meanwhile nodes away from the injection node will have smaller values of potentials. All this will result in higher and more dangerous value of the total touch voltage (*Vtouch2*) as shown in Figure 4.20.

Thus, it can be seen that it is necessary to know not only the resistance of the grounding, soil resistivity etc. but also obtain the information about the integrity of the grounding grid and its horizontal elements. Existing methods and techniques are able to find out only whether or not different parts of the grounding grid are connected but not able to pinpoint the exact location of the damaged element.

Meanwhile, from Figure 4.11 and Figure 4.13 one can observe that the current value in the physically integrated element (R=0Ω) is almost the same with a slight drop of the current magnitude along the element with increase of the distance from the source.

Moreover, one can note that directions of the current along the element (except leakage currents) are the same. Sine waves of both oscilloscopes have the same phase with a small difference in peak-to-peak value.

On the contrary if the element is damaged and R more than a few Ohms (which is much smaller than obtained in the next chapter for the experimental part) one can determine that the current distribution along the element is uneven. There is a huge drop of the current and voltage magnitude at the point of failure with the substantial rise at the ends of the conductor (see Figure 4.12 and Figure 4.14).

As for the directions of the current in the element one can note that they are opposite to each other which represented by out of phase signals of the oscilloscopes. It means once the resistance of the failure (breakage) of the element achieves the value higher than the resistance of the rest of the circuit, the current distribution in the element is changing. The current chooses the direction with smaller resistance which is the resistance of the horizontal elements parallel to the damaged one. Due to draining of a portion of the current from each part of the damaged conductor into soil, current in both parts of the conductor flows from its ends to the point of failure which shown as out of phase currents in Figure 4.12 and Figure 4.18.

From the results, one can distinctly observe if there is a breakage in the horizontal elements.

4.6 Concluding remarks

Thus, according to the analysis provided, some features of the processes in the grounding with and without damaged elements were revealed, such as:

1) Over the physically integrated horizontal element of the grid values of sensors potentials are close to each other at all points of the element. Slight difference in these values is only a function of the leakage currents but taking into account soil resistivity which usually is much bigger than self-resistance of the element it will not result in a substantial influence on the potential distribution along the element. On the other hand when the element is damaged the curve of the potential distribution is not even with a minimum value at the place of failure (breakage).

2) In an undamaged horizontal element of the grid direction of currents along the element is the same. Once the element has a breakage with a gap filled with soil the direction of currents in the element before and after the location of the gap will be opposite to each other.

CHAPTER 5: EXPERIMENTAL STUDY OF THE PROCESSES IN GROUNDING

In order to verify and justify the results of the mathematics and computer modelling described in Chapter 3 and Chapter 4, experimental work on the grounding has been proposed, conducted and described in this chapter.

The chapter includes three main parts regarding the experimental research: a) investigation of the failure's impedance between parts of the damaged horizontal element, b) experimental evaluation of the most suitable characteristics and parameters of the current that will be used for the monitoring of the grounding grids and c) field study of the current and potential distribution processes in the grounding device under the test.

The chapter moves ahead with highlighting of the main results of each experimental part to be done and concludes with conclusions on investigations conducted.

5.1 Impedance of the element's failure

During the experimental assessment with respect to the elements failure's resistance, the current source *S* was connected to two small horizontal steel elements (bolts) buried in soil at 50cm – the horizontal grid's depth, as shown in Figure 5.1. As the source in setup shown in Figure 5.1, both AC and DC supply were used. Ends of both electrodes had a good contact with the soil. Water was added in those areas between two electrodes (bolts) where they had contact with the soil in order to provide good contact between metal and ground.

The soil structure had sandy loam top stratum (30cm) with the resistivity 250Ωm and clay as the bottom one with the resistance 30Ωm. The resistance of the connecting wires can be neglected since it was only 0.9Ω. The approximate temperature was 70 degrees *F* or 21 degree *C*, atmospheric pressure was approximately 99.750kPa or 750mmHg (torr). A diameter of the electrodes was 10mm. A distance between electrodes was varied in a range from 1 to 3cm.

These distances were chosen as possible value of a gap between two electrodes. Smaller values refer to such factors as corrosion and freezing processes in the soil when the gap between electrodes may have some centimetres value. Larger values (some dozens centimetres) may be caused by possible mechanical accidents during construction works.

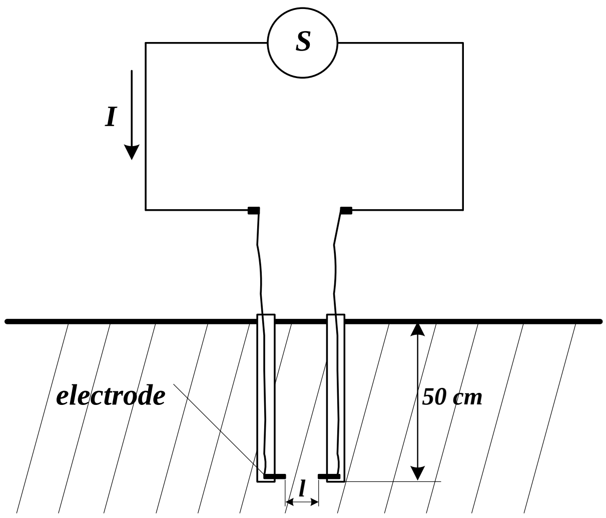

Figure 5.1: Experimental setup for measurement of failure's impedance

The experimental results of this study are shown in Table 5.1.

Table 5.1: Impedance of failure

Distance between electrodes, cm	***R*, kΩ**
1	0.226
2	0.445
6	0.120
26	1.100
60	4.260

As one can see from Table 5.1, the impedance of the gap filled with soil regardless the gap's length is much bigger than the impedance of the element itself. It happens because the area of the gap with soil between two parts of a damaged conductor is much smaller in comparison with the area that is involved in the current dissipation process for the element without damages.

Also, as it can be seen from Table 5.1, the impedance value of the gap in the damaged horizontal element increases nonlinearly with the increase of the distance between electrodes. The results of the breakage impedance from this experimental part were used for the mathematical and computer modelling in Chapter 4.

5.2 Determination of waveform parameters used for grounding monitoring

For analysis of the current and potential distribution processes and characteristics of the grounding it is necessary to employ a current of the certain waveform and frequency. It is much better to have a diagnostic or a test current which will have above mentioned characteristics different from the original current with fundamental frequency (50 or 60 Hz). By means of such a current it will be possible to eliminate any noise influence during investigation of the grounding device. Moreover, the use of such a test current will allow elimination of the power plant's tripping and forced outages to the load.

Experimental studies were conducted to determine the influence of the test current of different forms injected in the conductor on the signal that was picked up by an electromagnetic field coil (sensor) at some distance from the conductor. The results were evaluated by means of a double-beam oscilloscope. During the experiments, the sensor was located in the vicinity of the conductor connected to a signal generator.

Different forms of signals were taken into account (rectangular, sinusoidal, triangular, sawtooth waveforms). These experiments were conducted in one of the laboratories in the School of Engineering, Auckland University of Technology (AUT), Auckland, New Zealand. The experimental setup is shown in Figure 5.2.

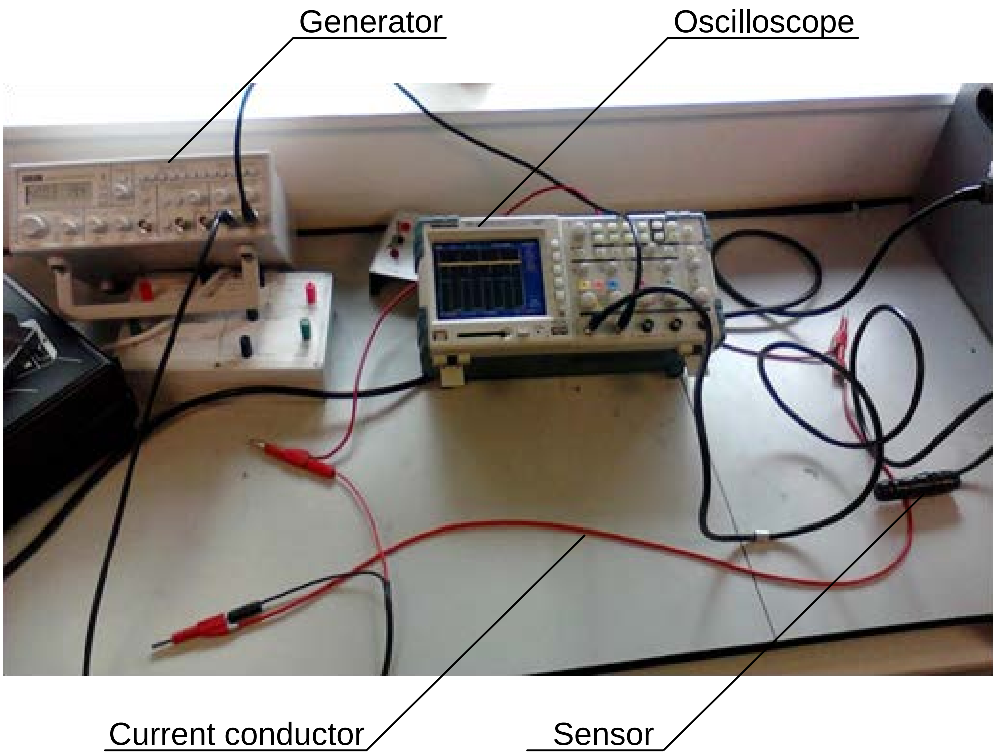

Figure 5.2: Setup to observe different form signals

During the experiment the output current from the signal generator flowed through the conductor connected to it. The sensor was located just above the current-carrying conductor. The output terminals of the sensor were connected to the first channel of the oscilloscope. The second channel of the oscilloscope was connected to the generator for its signal representation.

The output generator signal had 20V peak-to-peak value and 0.18A current. Examples of signals captured by the sensor are shown in Figure 5.4 to Figure 5.6. A yellow curve represents the signal picked up by the sensor. A blue curve is for the generator signal.

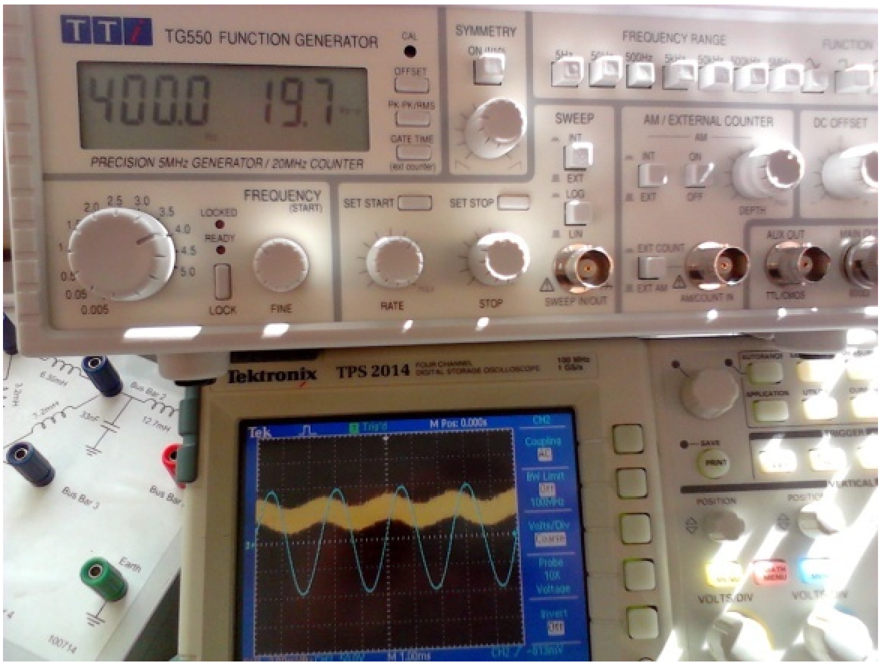

Figure 5.3: 400 Hz sine waveform generator signal

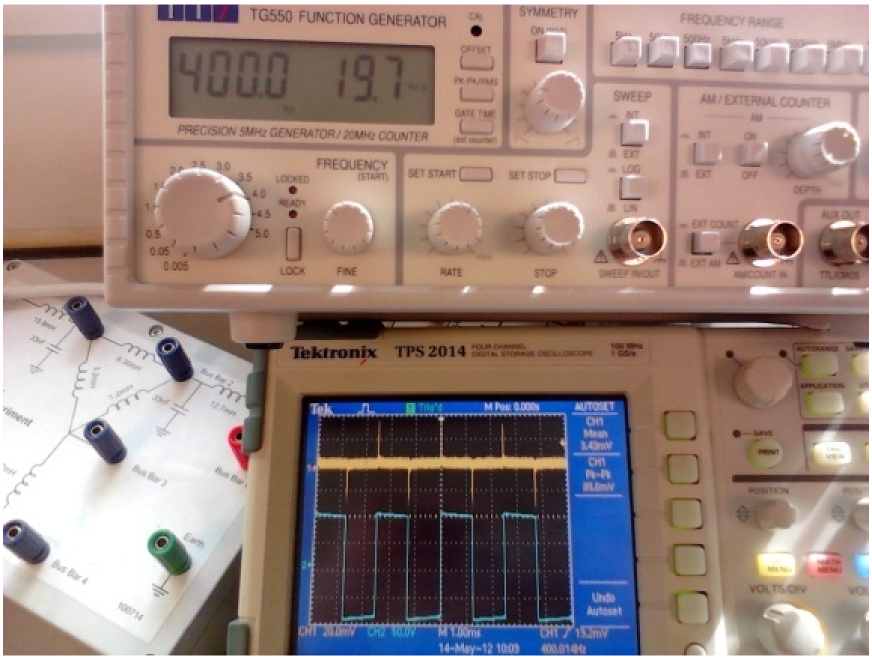

Figure 5.4: 400 Hz square waveform generator signal

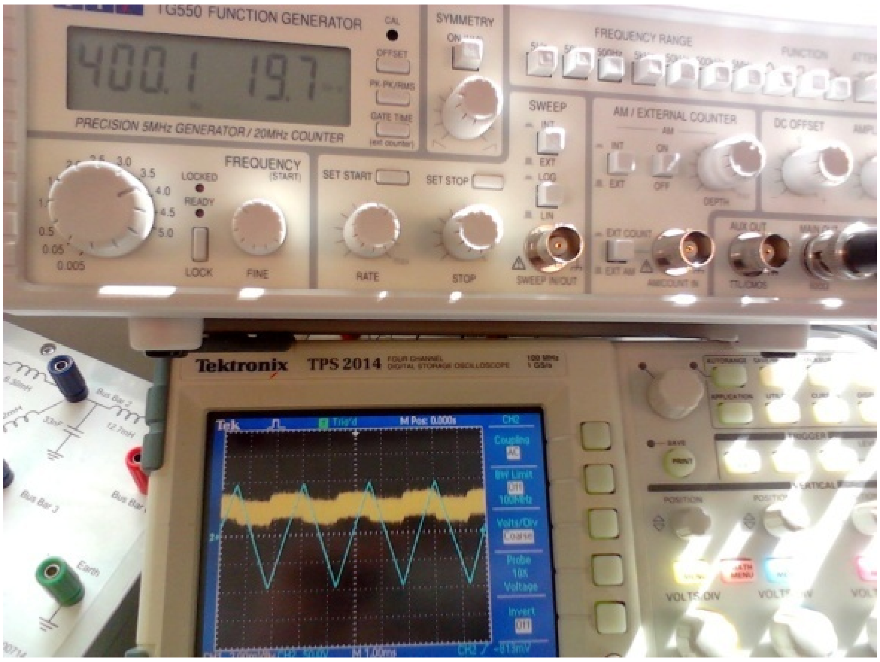

Figure 5.5: 400 Hz triangular waveform generator signal

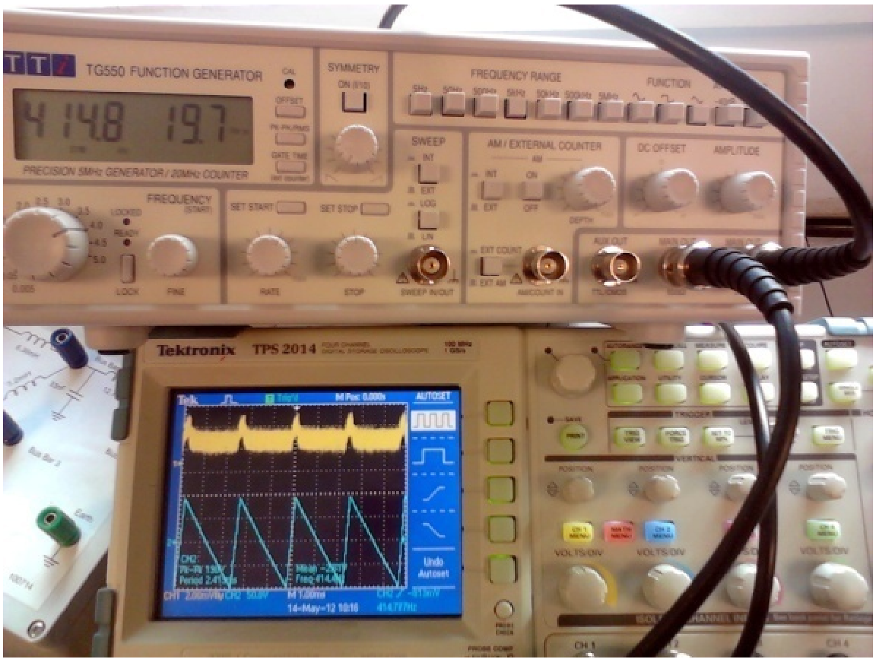

Figure 5.6: 400 Hz sawtooth waveform generator signal

During the experiments, the captured signals were observed, and preference was given to a rectangular (square) waveform because it was the most convenient waveform to detect on the surface of ground above the grounding grid. In comparison with the other waveforms, a square waveform signal had steep fronts that resulted in a higher value of electromotive force in sensors and a higher magnitude of the output sensor's voltage. It can be easily captured by an inductive coil used as a sensor. The steeper the signal front was the easier it was to identify and process it.

5.3 Field study on the grounding

In order to verify the results of the mathematics and computer modelling described in Chapter 3 and Chapter 4, experimental work on the grounding was set up and conducted. The grounding device consisted of two meshes of steel horizontal elements bonded to each other by means of bolt connection (see Figure 5.7). The horizontal element's (*E2*) integrity and failure were imitated by the switch position (*S*) located in the middle of the element. Open position of the switch *S* meant damaged element condition. Closed position of the switch meant that the element was integrated.

All elements of the experimental grounding device were buried into soil to a depth of 30-40 cm. The soil structure had sandy loam top stratum (15 cm) and clay as the bottom one. The diameter of round cross section conductors was 10 mm.

The grounding device area was approximately 16 sq. m.

A snapshot of the experimental setup is shown in Figure 5.8. A horizontal element in the centre of the grounding had a switch to imitate a physically integrated or damaged element.

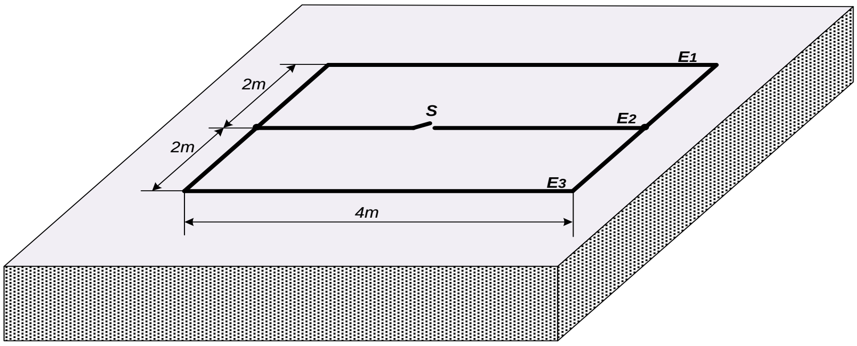

Figure 5.7: Experimental grounding device grid

Figure 5.8: Experimental grid (top view)

Impulses of square waveform injected in the grid were used since the signal had steep fronts that can be easily detected by inductive coils which were used as sensors above the elements.

In order not to create forced outages of power supply and eliminate noise of the fundamental frequency, a frequency of an even number harmonic was adopted for the test current injected into the grounding grid.

The sensors used in the experimental part to capture the test signal were solenoids with 8mm diameter core made from ferrite with the magnetic permeability much higher than of steel. Over the core, there were 3 layers of coil 127 turns each. The copper wire with

0.2mm radius was used to make the coil for each layer. The sensitivity of sensors was detected through the experimental way by adding layers of the coil. The setup (see Figure 5.2) consisted of a current-carrying conductor with 1A in it. The sensor was located 1m away of the wire in perpendicular direction to it. The layers of the coil were added until enough to be detected on the screen of the oscilloscope potential was captured. The electromotive force value or the sensor's potential value induced in sensors and its phase was under investigation within the experimental part.

During the experiment AC source was connected in different ways so there were a number of circuits for analysis.

In the first part of the experiment the generator was connected between two points of the grid at a maximum distance from each other. The sensors were moving along A-B line in the vicinity of the surface as shown in Figure 5.9.

Magnitudes of sensors' potentials detected by the oscilloscope were measured at points 1-11. Measurements were made at both positions of the switch (*S*): switched on (imitation of the horizontal element integrity) and switched off (damaged element). The source current was maintained constant (1.5 A), but at different frequencies.

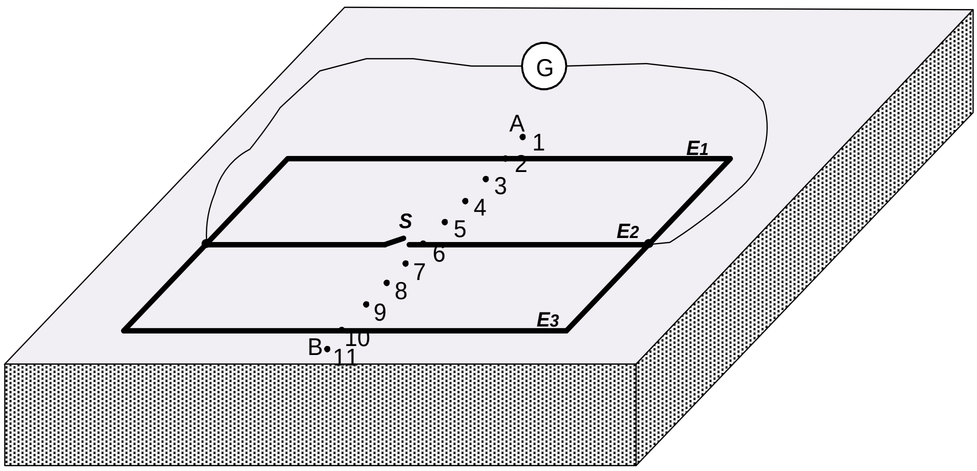

Figure 5.9: Grounding device under test

The results of the experiments are presented in Table 5.2and Figure 5.10 respectively.

In Figure 5.10, the curves (magnitudes in volts) with different frequencies are presented. Curve 1 represents potential distribution when Element 2 (E_2) is integrated (*S* is in the "ON" position). It means that current flows through all three horizontal elements almost equally. That is why there are peaks at points 2, 6 and 10 over the horizontal elements. Profile 3 is shown for the case when Element 2 (E_2) is damaged (*S* is switched off) that is why the potential at point 6 has the lowest value and almost the same as at points 5 and 7 where there is no any current-carrying conductor. At points 2 and 10 one can observe the increase of the sensors' potentials in comparison to the value at point 6. Again, that increase takes place above the integrated conductors with current.

Higher values of potentials detected on the surface of the ground were registered at the frequency of 1000 Hz. Indeed, as one can see from Figure 5.10 curves 2 and 4, potentials at all points are higher compared with the frequency 400 Hz.

When Element 2 (E_2) is integrated (*S* is "ON") for the point 2 for example at the frequency 400 Hz (see curve 1) the value of potential is 1.6 V. At the same time at frequency of 1000 Hz the potential of the same point is 3.0 V (see curve 2) which is almost 2 times higher.

Table 5.2: Sensors' potentials over grounding grid

Point Number	**Position of *S***	
	ON	**OFF**
F=400 Hz	***Curve 1***	***Curve 3***
1	0.7	1.2
2 (E1)	1.6	2.2
3	0.8	1.1
4	0.4	0.7
5	0.9	0.3
6(E2)	1.5	0.1
7	0.9	0.2
8	0.5	0.4
9	0.7	0.9
10(E3)	1.2	1.4
11	0.5	0.7

F=1000 Hz	***Curve 2***	***Curve 4***
1	1.2	2.1
2 (E1)	3.0	4.1
3	1.6	2.3
4	1.0	1.2
5	1.4	0.6
6(E2)	2.7	0.4
7	1.3	0.4
8	0.9	1.1
9	1.4	1.7
10(E3)	2.1	2.6
11	1.0	1.5

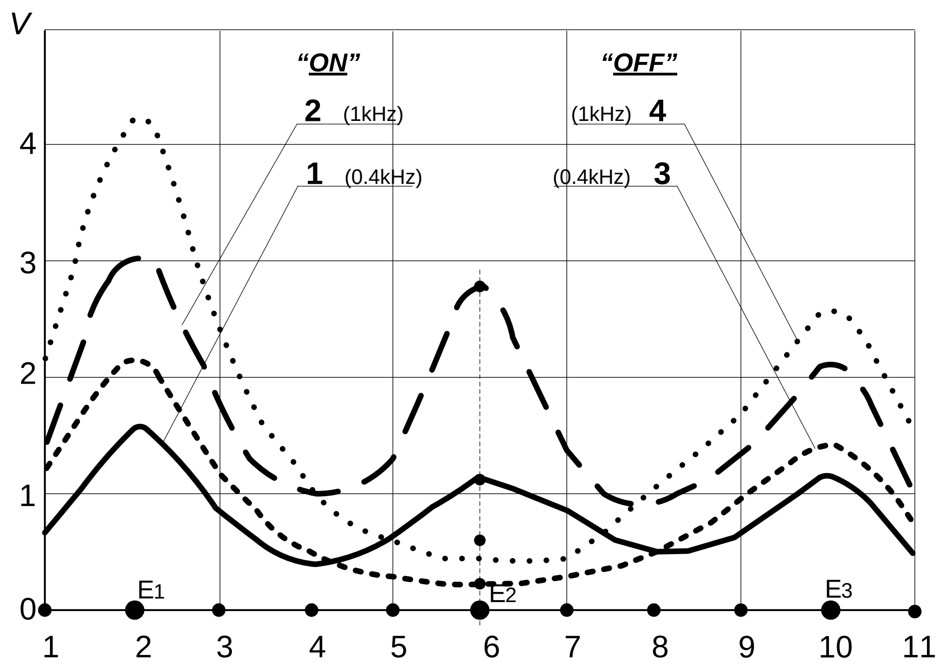

Figure 5.10: Potentials on surface of soil

Thus, to register signals on the surface of the ground by means of electromagnetic sensors (solenoids), which detect the induced potentials, it is more preferable to use a high-frequency signal.

But the higher the frequency of the injected signal is, the greater the difference in impedances' (resistance and reactance) magnitudes of the elements compared with the fundamental frequency 50 or 60 Hz one can have and as a result the greater the discrepancy of the signal distribution pattern compared with the common mode will be.

As a final choice with regards to the experimental investigation of the grounding grids it was decided to use a 400 Hz signal since it was the 8th harmonic and unlikely to be close to the fundamental frequency. Moreover, it is noted that the chosen frequency does not substantially change the characteristics of the elements in comparison with the fundamental one.

In order to determine a pattern of current distribution through the grounding grid's elements, two schemes of the generator connection were used.

The first scheme is similar to the circuit in Figure 5.9 but sensors potentials' values and currents' directions were analyzing not across the elements but along them. The generator was connected with its two leads to the grounding device's grid. The circuit is presented in Figure 5.11.

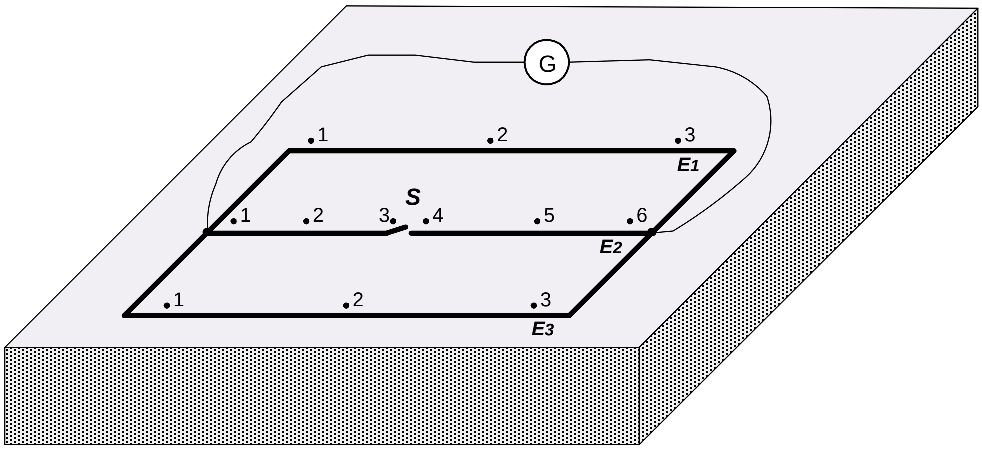

Figure 5.11: Current and potential distribution

While moving along the horizontal elements on the surface of the ground, signals of 400 Hz were observed on the screen of the oscilloscope. The results of the sensors potential measurements are presented in Table 5.3. Figure 5.12 depicts the results of the potential distribution along Element 2 (E_2) with length L.

Table 5.3: Sensors' potential distribution along elements

Position of *S*	**Element**	**Point Number**					
		1	2	3	4	5	6
ON	E_1	1.7	1.6	1.6	-	-	-
	E_2	1.6	1.5	1.5	1.5	1.6	1.6
	E_3	1.4	1.4	1.3	-	-	-
OFF	E_1	2.0	2.2	2.2	-	-	-
	E_2	1.2	0.4	0.1	0.1	0.2	0.9
	E_3	1.7	1.5	1.6	-	-	-

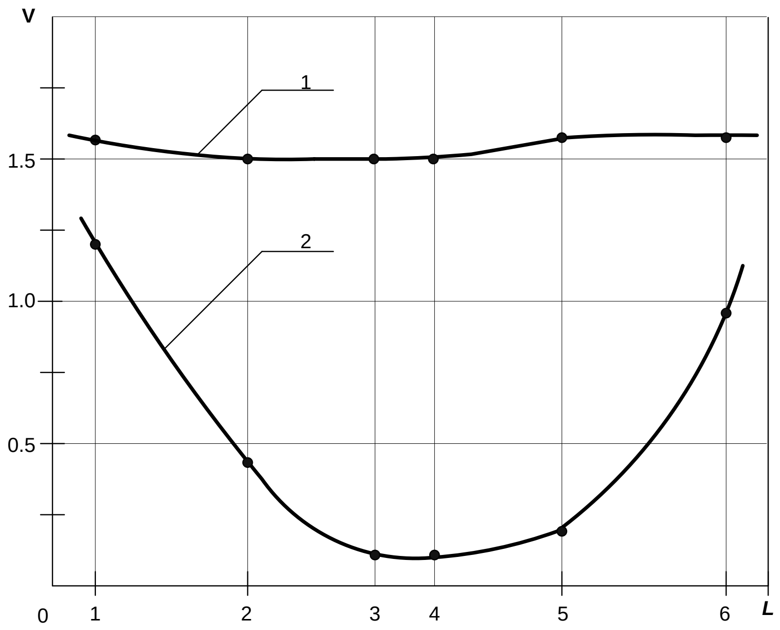

Figure 5.12: Potential distribution along element

1 – undamaged element, 2 – damaged element

As can be seen from the Figure 5.12 when the element is without damages, values of the sensors potentials over the conductor on the surface are almost the same at all points of the element. On the other hand, when the element is damaged the curve has a minimum between points 3 and 4 which is the point of failure.

The results of this experimental part prove the results of mathematical and computer modelling from Chapter 3 and Chapter 4 since according to Bio-Savart law, values of magnetic field strength vary linearly with the conductor current.

One more scheme was used to detect the current direction in elements of the grounding device. The circuit is shown in Figure 5.13. The generator was connected with one of its lead to the grounding device and with the other one to a vertical element of 2m length located outside of the grounding device. The vertical element had a round cross-section of approximately 10mm diameter. This element was buried in soil to depth of 1m. The location of the vertical electrode represents a remote ground so it should be at least several meters away from the grounding grid.

During the experiment when the switch was in the “ON” position, the directions of currents in different parts of the conductor were the same (see Figure 5.14 and Figure 5.15).. On the contrary, when the switch was “OFF”, the currents before and after the point of failure flowed against each other or in other words, they had opposite directions (see Figure 5.16 and Figure 5.17).

This effect could be caused by the higher resistance of the failure in comparison with the resistance of the rest of the circuit. In such a case, the current will flow through the smaller resistance which is the metal elements in parallel to E_2.

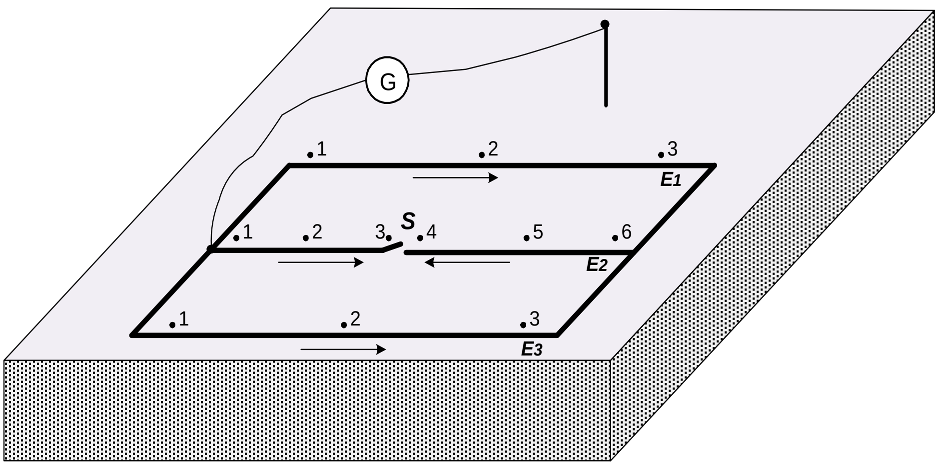

Figure 5.13: Current distribution

Figure 5.14: Setup with integrated element

Figure 5.15: In phase direction of currents in integrated element

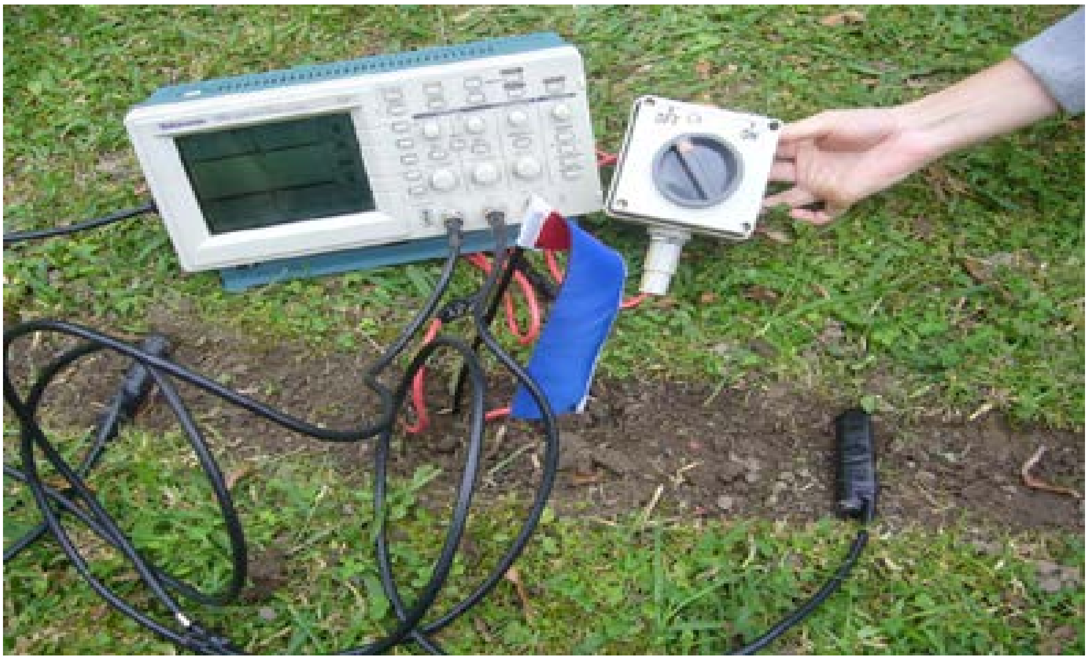

Figure 5.16: Setup with damaged element

Figure 5.17: Out of phase direction of currents in damaged element

The equivalent circuit of such a scenario can be presented as in Figure 5.18.

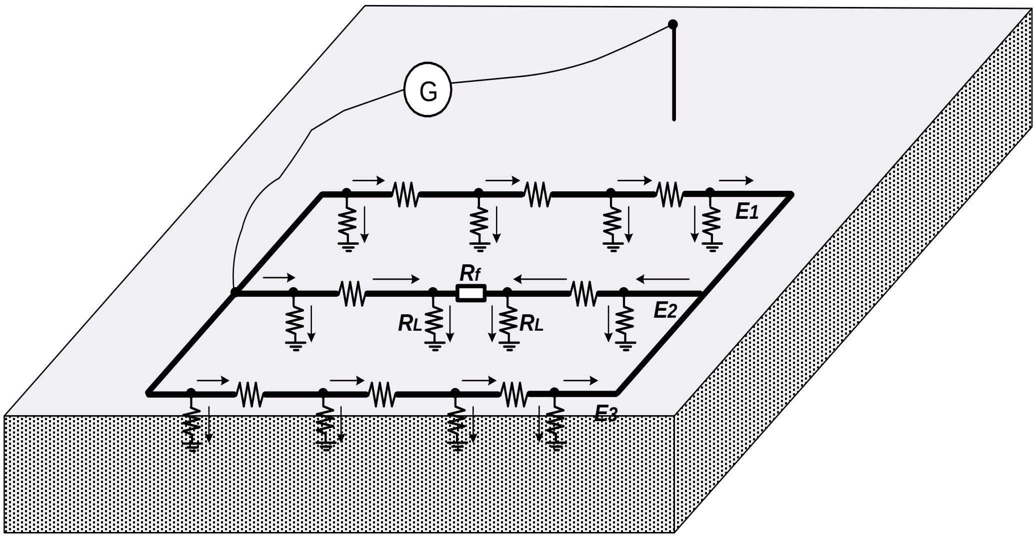

Figure 5.18: Equivalent circuit

R_f in Figure 5.18 is the resistance of the failure or the resistance of the soil between two metal parts of the damaged horizontal conductor. R_L is to represent a part of the current which flows from the current-carrying element into the soil. It is so called leakage current. All elements are shown as equal parts with distributed parameters. Such presentation can show currents that flow not only in the element itself but also currents flow in to the soil.

As it can be observed from Figure 5.18, when R_f has a big value (*S* is "OFF") which imitates failure of the element, the current distribution is as shown Figure 5.18. In this case, the currents in the damaged element E_2 flow from the ends of the damaged element to the place of failure and to the soil which is the return circuit for them through elements R_L. Since the impedance of the failure is substantially higher than the resistance of rest of the circuit, the current do not flow through R_f and almost all the current distributes between R_L elements of the circuit. That is why the direction of the current in different parts of the conductor is opposite to each other and signals captured by sensors are out of phase as shown in Figure 5.17.

On the contrary, when S is “ON”, the resistance of R_f is close to zero and can be neglected. In this case, due to a very small resistance of all cascaded parts of the metal conductor, the current will have the same direction at all points. It happens because the resistance of metal current-carrying element is much smaller than the resistivity of soil around it. One can see in phase signals captured by the sensors in Figure 5.15.

5.4 Concluding remarks

During the work of the horizontal elements failures’ detection it is necessary that the effect of electromagnetic fields generated by the equipment of the power plant (noise) and currents flowing through its grounding device was kept at a minimum value.

This requirement can be satisfied if the level of a measured signal is much higher than the magnitude of noise. It is possible when heavy duty source of signals is used. The other way is to use signal of frequency different from the fundamental one (50 or 60 Hz).

It is preferably to use the second option because a captured signal on the surface of ground in this case can be processed and point of failure can be detected without tripping of the electric power plan.

During the grounding devices’ monitoring the most suitable waveform of the test current is a square (rectangular) waveform of impulses. Such a type of signal has steep fronts that can be easily detected by means of electromagnetic sensors on the surface.

The higher the frequency of the test signal injected into the grounding device, the more substantial signal can be detected on the surface of ground. At the same time, the current distribution in the grounding devices at high frequencies can differ from the common mode distribution.

It is well known that symmetrical signals (including sine waveform) have only odd spectrum of harmonics in them. It means that frequencies presented with respect to electric power plants are frequencies of 1st, 3^{rd}, 5^{th}, 7^{th} and etc harmonics. Thus, the frequencies that likely to be detected at the territory of 50 Hz electric power plants are: 50 Hz, 150 Hz, 300 Hz, 450 Hz and etc respectively. In order to eliminate noise's influence for the investigated grounding devices, it is better to use the test signal of even frequency that is far from the fundamental one. As one of the best options is 400 Hz control frequency signal. It is 8th harmonic which is pretty far from the fundamental one and do not substantially change the elements' impedances.

During the experiment, the pattern of the potential distribution over the grounding device was investigated. It was shown that one can detect the maximum value of the potential in sensors over the current-carrying conductors crossed by perpendicularly (see Figure 5.9 and Figure 5.10). This value subsides with increase of distance from the conductor. The higher frequency of the signal injected was the higher level of the detected signal could be detected.

If the horizontal element did not have failures the pattern of the potential distribution is almost even without substantial differences of the value along the element. On the other hand, if the element is damaged there is a substantial drop of voltage at the point of failure with increase of the potential to the ends of the element. The same features of the even distribution of the current and as a result potential distribution over the element were revealed in Chapter 3.3, Figure 3.13 and Figure 3.14 and also in Chapter 4.2, Figure 4.11 and Figure 4.12.

The experimental studies showed and proved the validity of provisions obtained from the mathematical and computer modelling. As one can see from Figure 5.12, if the horizontal element in the grounding grid does not have any failures, the distribution of the potential through its length and electromagnetic field over it will have even character without steep drops. On the contrary, if the element is damaged, there will be a drop at the point of failure since the resistance of ground in the gap is much bigger than the resistance of the element itself.

One can see that the pattern of the current distribution in Figure 4.13 for the integrated and in Figure 4.14 for the damaged element is the same as shown in Figure 5.12

When the generator is connected with one lead to the grounding device and with the other one to the separate vertical electrode, the directions of currents before and after the point of possible failure depends on the condition of the element. If it is physically solid, the currents will have the same directions. When the element is damaged, the currents will have opposite directions. This feature is caused by a higher soil resistance compared with resistance of the metal elements (see Figure 5.13 and Figure 5.18).

The results of the current potential distribution over the integrated conductor shown in Figure 4.16 are the same as in Figure 5.15. When the element is damaged one can see out of phase distribution in Figure 4.18, during modelling and the same out of phase captured signal during the experimental part in Figure 5.17.

Described features of the current and potential distribution in the damaged and physically integrated elements can be used for establishment of a new technique for the horizontal elements' monitoring. After the injection of the test current into the grid, signals captured on the surface of the ground above the grid can be processed and the damaged horizontal element and the location of its failure can be pinpointed.

CHAPTER 6: IMPLEMENTATION OF THE PROPOSED TECHNIQUE TO GROUNDING DEVICES' INVESTIGATION

To summarize the results obtained from the mathematical analysis, computer modelling and experimental justification of the processes in the grounding grids, there are two main features that should be emphasized:

1. The current and potential distribution along the damaged horizontal element has uneven distribution in comparison with the element without failure.

2. The directions of currents in the damaged element are different. They have the opposite direction compared with the element without failures where the current direction is the same along the entire length of the element.

These features may be used as a base for the technical device to monitor the grounding grids elements' physical integrity.

In order not to create forced outages to the power supply of the load, the main requirements for the proposed technique used for the grounding investigation are as follows:

1. The technique must be an universal tool for the grounding devices of the whole variety of power plants;

2. The power plant must be at a normal operation regime (common mode);

3. The "noise" of the power plant created due to appearance of the current of normal operation and faults must be canceled (eliminated) and must not have any influence on the test current injected into the grounding grid;

4. The proposed technique must provide opportunity for the monitoring of all the horizontal elements of the grid;

5. The proposed new device for the monitoring must be portable and easy to use.

In accordance with all these requirements, it is suggested the impulse square wave form with frequency 400 Hz signal from a separate source (generator), which is connected to the grounding grid be utilized. After the injection of this impulse current into the grid and detecting it on the surface of the ground above the grid by means of two electro-magnetic sensors, captured signals from sensors are processed in the proposed device. The results can be seen on the front panel of the device as LEDs illumination.

6.1 Development of device's functional scheme

The proposed technical device consists of two main parts: an impulse square wave form generator which is connected to the grounding and a processing unit carried by an operator.

A circuit of the impulse generator is presented in Figure 6.1.

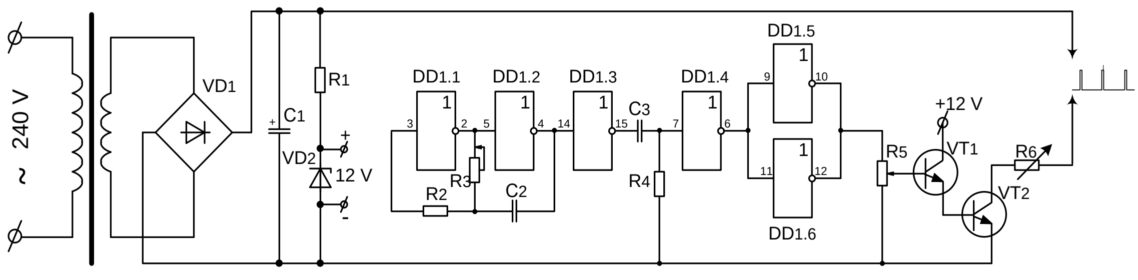

Figure 6.1: Circuit of pulse generator

The generator in Figure 6.1 consists of a tiny square wave form impulse multivibrator made on elements DD1.1 –DD1.6 and two bipolar transistors to form the output current signal (Schuler, 2003). The scheme has a resistor R_3 to vary impulses' frequency. As an example, the CD4049 microchip was used for the initial pulses generation.

A snapshot of the Generator is presented in Figure 6.2.

Figure 6.2: View of pulse generator

A snapshot of sensors is presented in Figure 6.3. To ease the investigation of the grounding devices' condition, the sensors are located on an auxiliary measuring rod made of insulated material (wood and plastic) as shown on in the same figure Figure 6.3.

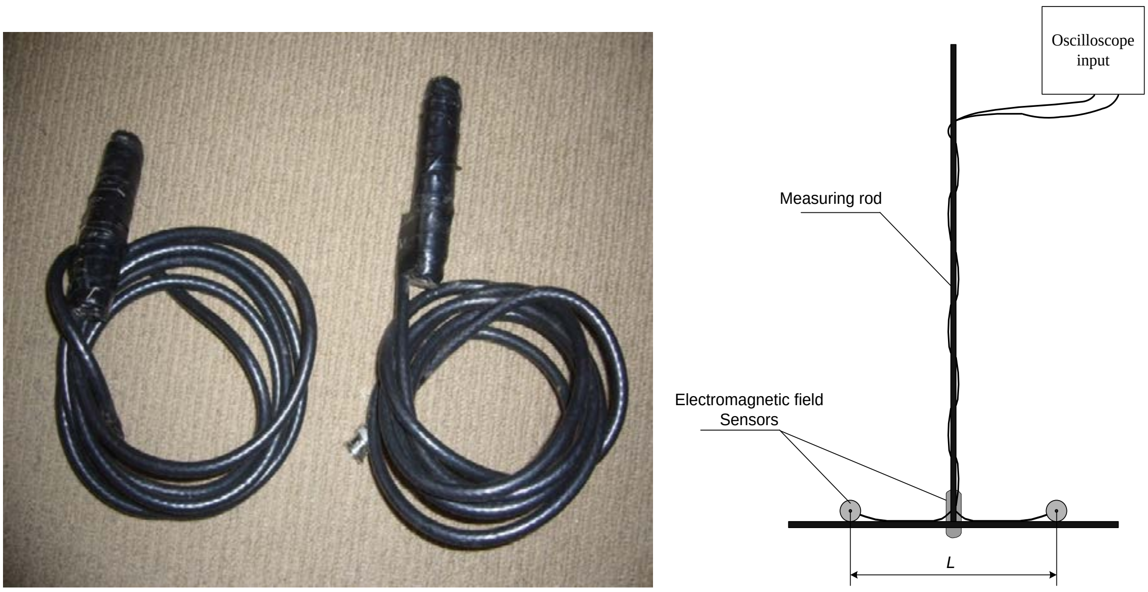

Figure 6.3: View of sensors and measuring rod

In line with all the above requirements the functional diagram of the processing unit can be presented as shown in Figure 6.4.

In order to obtain a magnitude of the captured sensors' signals enough to process, the future device should have not only the logical part but also a part to amplify the captured signals. As a base of such amplification, operational amplifiers (OpAmps) can be used (Predko, 2002).

After amplification the signal from each sensor is sent to a processing unit and the results are indicated on the screen of the device or can be heard by means of a small speaker. The functional diagram schematically can be presented as shown in Figure 6.4.

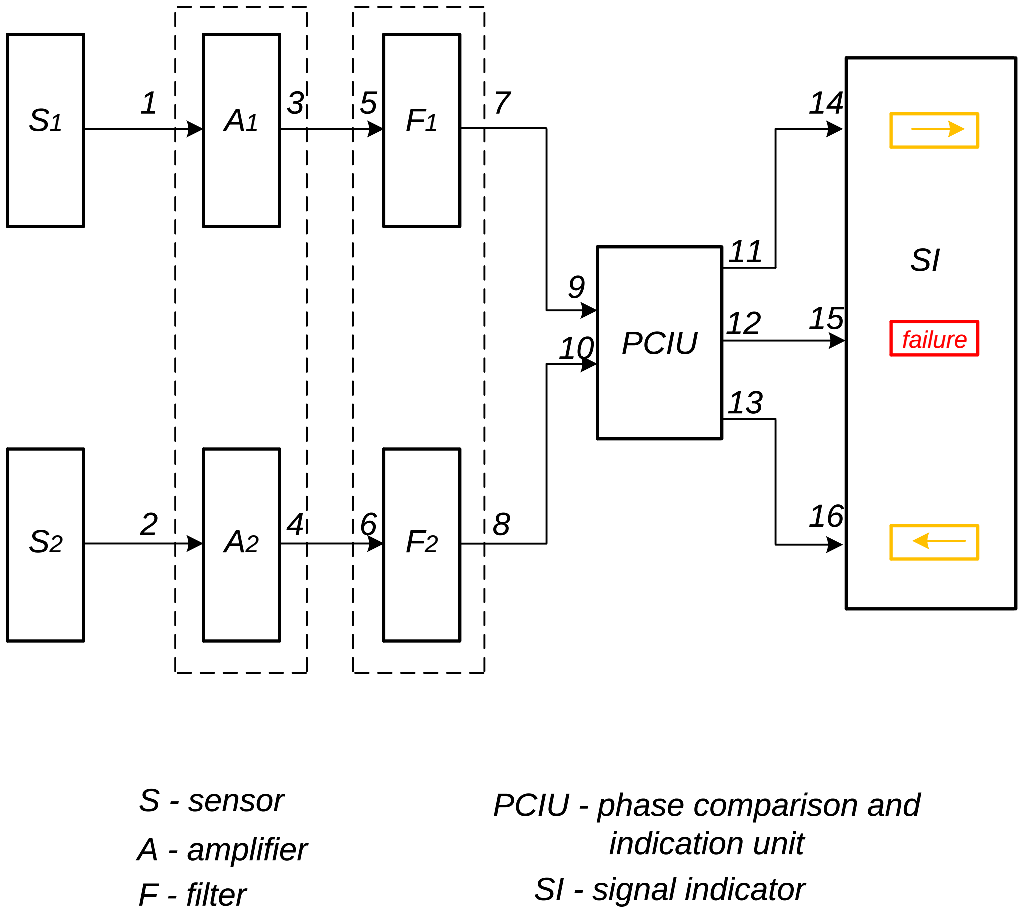

Figure 6.4: Functional diagram of device

As one can see from the scheme (see Figure 6.4) the captured signals from each sensor above the horizontal element arrive to the input of the amplifier units (A_1 and A_2). The main goal of the amplifier units is to increase a peak to peak value of the captured signals for the further processing.

After that, the amplified signals of required frequency are peaking out by means of filters (F_1 and F_2). The rest of the sensors' signals are noise which doesn't proceed beyond filters and they are not processed.

Further, the amplified and filtered signals are applied to inputs of a logical part of the device, so called phase comparison and indication unit (*PCIU*). This part provides a logical processing of the captured signals. It compares phases of the captured signals above the horizontal element and sends a signal to trigger the signal indicator (*SI*) if a damaged horizontal element of grounding is detected. The module also indicates a level of the captured signal above the horizontal element in order to find where it is located.

The signal indicator has two parts: (i) yellow LEDs to visualize the current direction in the horizontal elements and level of the captured signal above the element; (ii) a red LED plus a speaker as the failure detector in order to locate the point where the horizontal element is damaged. During the investigation of the grounding by observing the changes of the current directions and hearing the sound of the speaker (or by observing the active red LED), one can detect the damaged element and to locate the point of failure itself.

Figure 6.5 represents an internal structure of the *A1* and *A2* units. Each part of the unit consists of a chain with two operational amplifiers. Despite operational amplifiers theoretically have a huge gain; in practice it is useful to have two chains of amplifiers. It will ease the process of amplification and reduce the signal distortions.

As one can see from Figure 6.5, there are 3 resistors connected to the input of the first amplifier in each chain. They provide a step change of the gain value depending on the soil resistivity thereby providing sensitivity of the device. Different values of apparent soil resistance correspond to different values of gain. Each time during the grounding investigation, the gain can be adjusted up to the most suitable value. It can be done by arranging the sensors above the current-carrying conductor for instance, above one of the impulse generator’s leads.

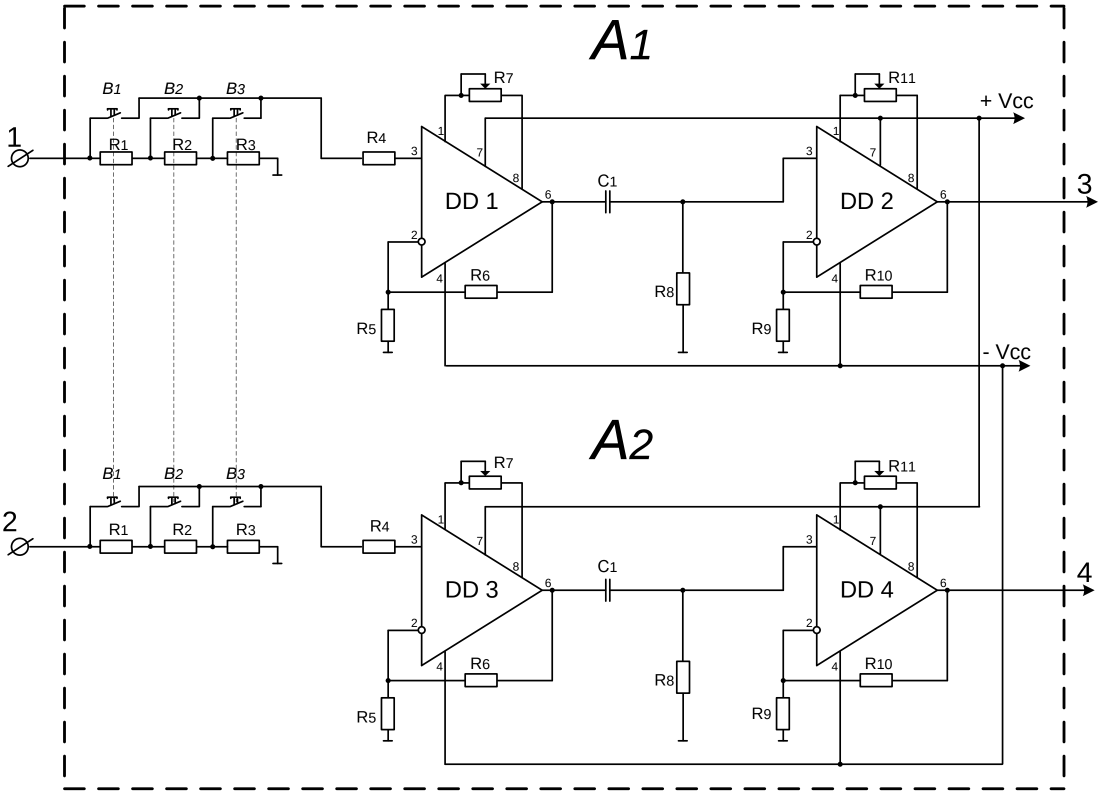

Figure 6.5: Amplification units of device

As an example, µA740C or 741, LM324, TL084, LM358 or TL082 operational amplifiers can be used. Chip pinout shown in Figure 6.5 is for µA740C or 741. Gain of the first OpAmp in each chain is 120 (but depends on the buttons position). The second OpAmp gain is 180 but it is also adjustable.

Each operational amplifier in Figure 6.5 has a non-inverting circuit with negative feedback which keeps the same original form of the sensors' signals. A capacitance C_1 and resistance R_8 in Figure 6.5 is a preliminary low pass filter and is needed to eliminate a DC offset and noise that can take place in the grounding.

Units F_1 and F_2 show in Figure 6.4 contain the active filter as a base for getting the peak out of the control signal. Different types of filter designs achieve different types of frequency responses, which are typically characterized by having a particularly flat passband frequency response (Butterworth filters) or by a very rapid transition between passband and stopband (Chebyshev filters, and Cauer, or elliptical, filters), or by some other characteristics, such as a linear phase response (Bessel filters). Achieving each of these properties usually involves tradeoffs; for example, a very flat passband response will usually result in a relatively slow transition from passband to stopband (Winder, 1997).

In addition to selecting a filter from a certain family, it is possible to select the order of the filter. In general, the higher the order, the faster the transition from passband to stopband but it will be at the cost of greater phase shifts and amplitude distortion.

All above-described types of filters perform well with a sinusoidal signal but have some distortion of the output signals when the input is a square-wave.

One of the possible circuits for the band-pass filters of certain frequency is shown in Figure 6.6. The same type OpAmps as shown in Figure 6.5 can be used.

The circuit shown in Figure 6.6 is a combination of a low pass filter (R_2, C_2) and a high pass filter (R_1, C_1).

If $C_1 = C_2 = C$ and $R_1 = R_2 = R$ (Williams & Taylor, 2006) a cutoff frequency of such a filter can be obtained as

$$f_0 = \frac{1}{2\pi \cdot C \cdot R}. \tag{6.1}$$

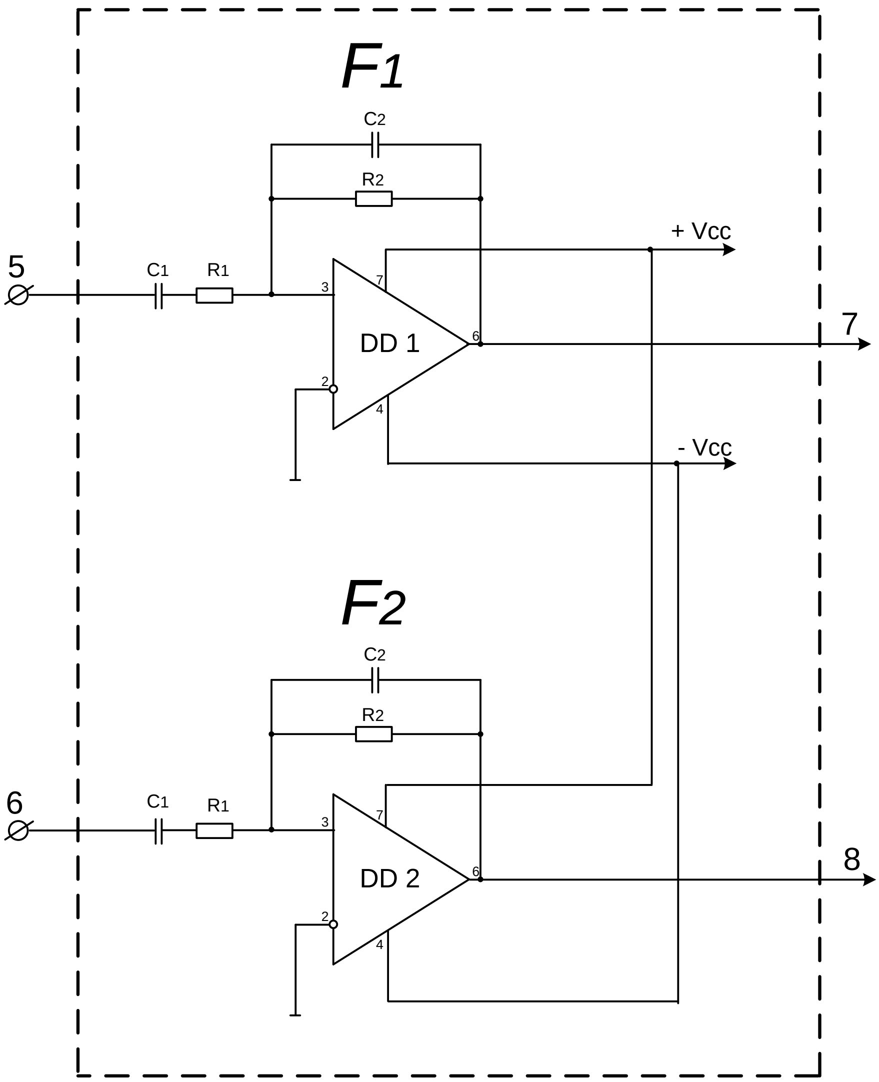

Figure 6.6: Filters unit of device

Setting the value of capacitance for the certain frequency one can find

$$R = \frac{1}{2\pi \cdot f_0 \cdot C}. \tag{6.2}$$

For the filter with 400 Hz resonant frequency, setting the value of gain $H_0 = 1$ in order to have equal magnitudes of input and output signals and the value of the capacitor C=0.33μF, one can obtain:

$$R = \frac{1}{2 \cdot 3.14 \cdot 33 \cdot 10^{-9} \cdot 400} = 1206\ \Omega.$$

Computer modeling of the above-described processes was fulfilled in MICRO-CAP software program with calculated parameters of filters (*Micro-Cap 10. Electronic circuit analysis program. User's guide*, 2010). In order to evaluate performance of the filter in circumstances close to the reality, the model comprises not only a filter itself and 10V peak to peak, 400 Hz source but also 3V peak to peak, 50 Hz noise source. The initial source has square-wave pulse signals. The results are shown in Figure 6.7.

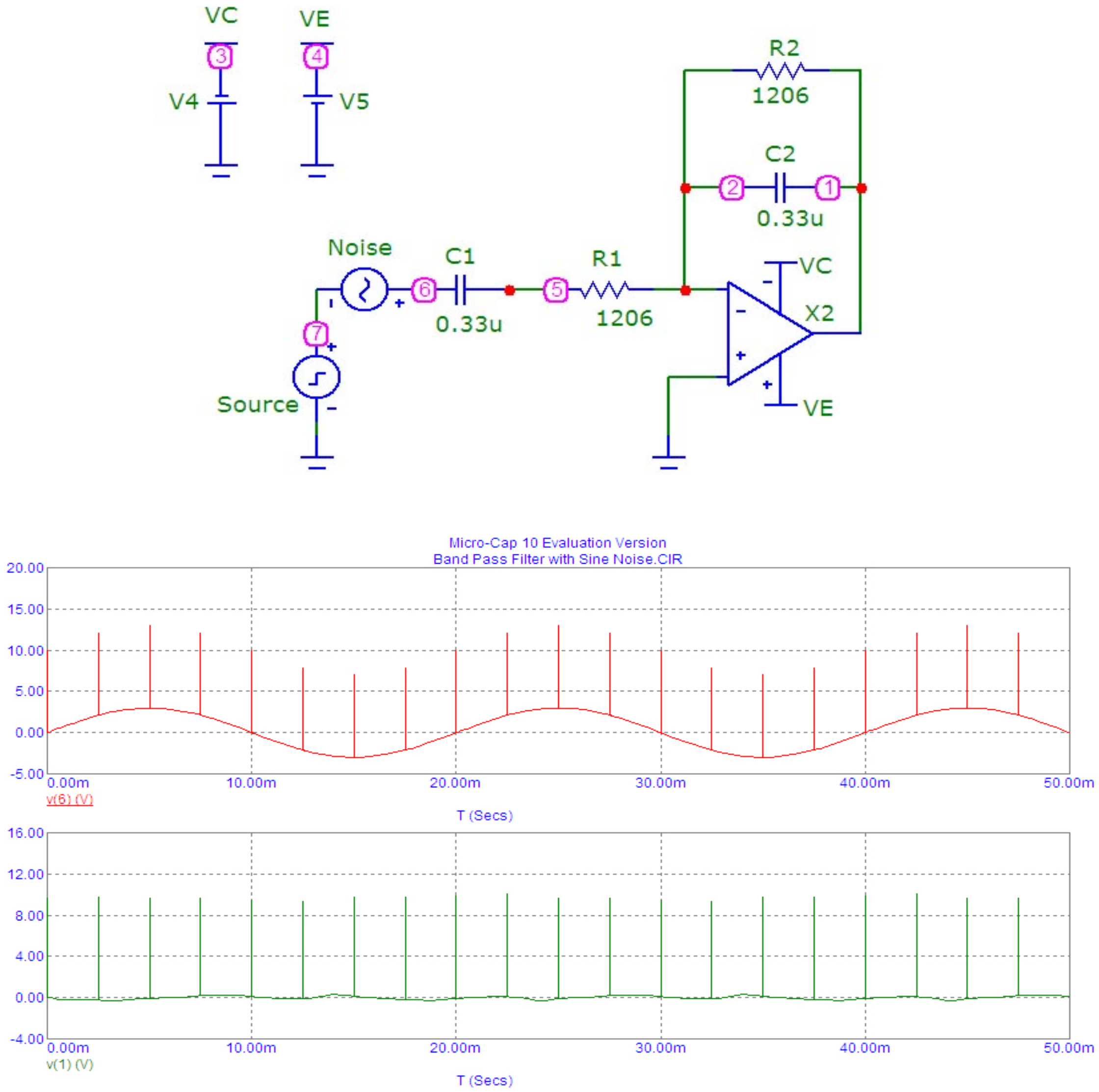

Figure 6.7: Filter modelling with sine noise

A frequency response and a phase shift of such type of filters for both types of noise made in MICRO-CAP AC ANALYSIS is depicted in Figure 6.8. The range of frequencies for the analysis was chosen from 10 Hz up to 1.5 MHz.

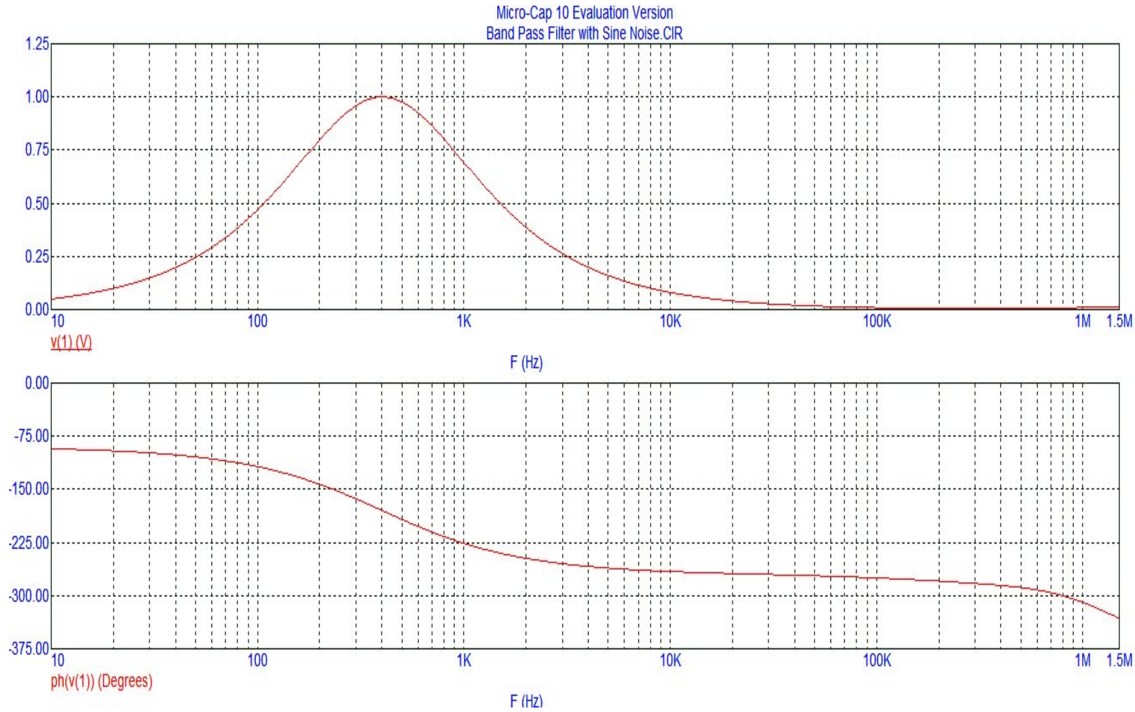

Figure 6.8: Frequency response of filters unit

6.2 Logical processing based on microchips

The main logical part of the device is *PCIU*. This unit provides logical processing of the captured signals. The *PCIU* compares phases of the signals and gives a digital output to trigger the signal indicator if the horizontal element of grounding is damaged. The unit also shows the directions of the current in the horizontal element and the level of the captured signal. The circuit is presented in Figure 6.9.

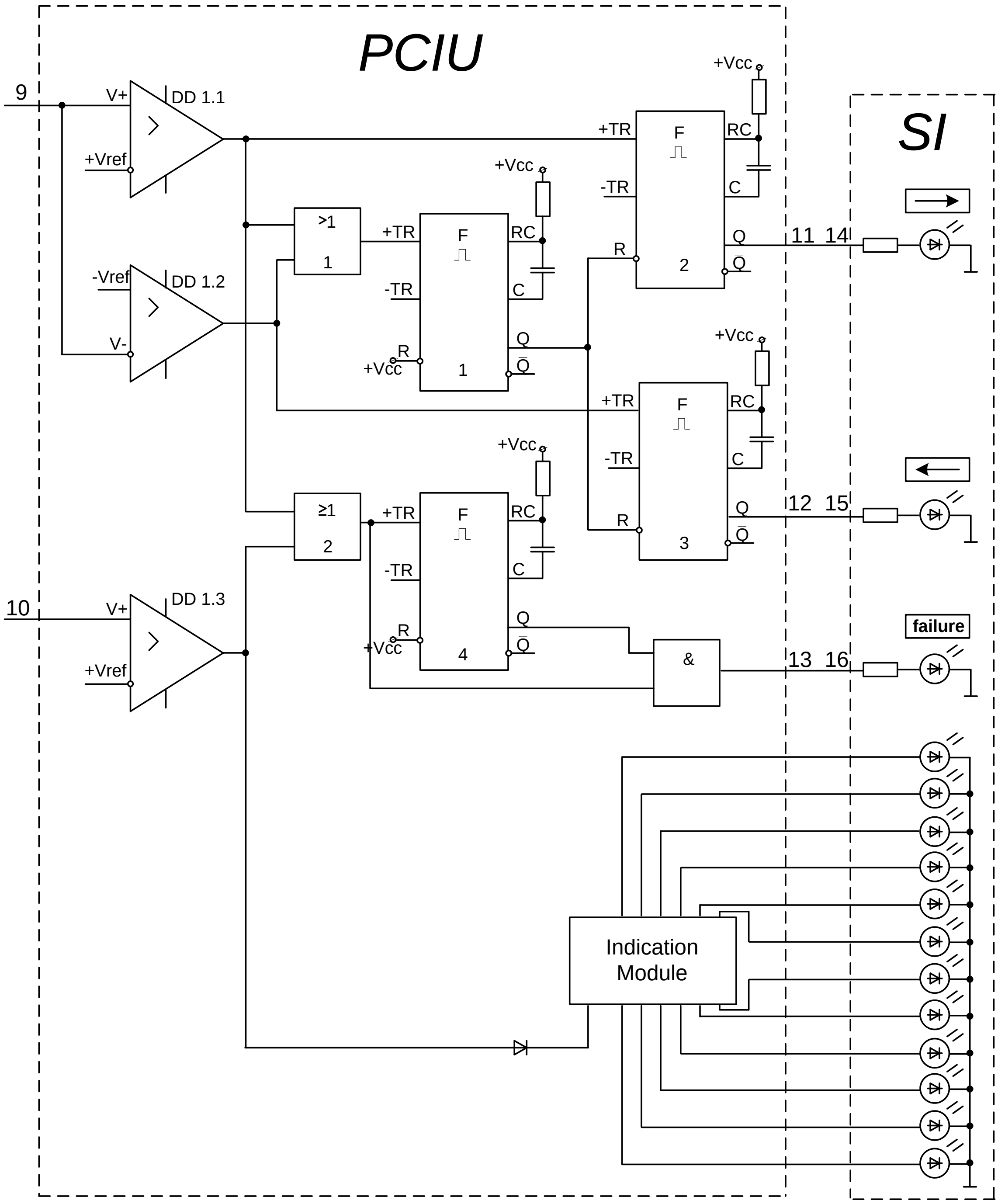

Figure 6.9: Logical part of device

The input signals from units F_1 and F_2 go to non inverting inputs of comparators DD1, DD2, DD3. The comparators convert the input signals into the digital “1” and “0” signals depending on levels.

A part of the scheme consisted of monostable multivibrators F_1-F_3 and a logical element "OR" number 1 is dedicated to the current direction control in the horizontal element. Depending on direction of current in the current-carrying conductor the operator will see the illuminated LED either from F_2 or F_3 multivibrators.

If one of the horizontal elements is damaged, one more part of the scheme will be activated. This part comprises another monostable multivibrator F_4 second logical element "OR" and element "AND". In this case the operator will see the active "failure" LED.

The Indication Module (*IM*) of the scheme is needed in order to evaluate the level of the detected signal above the horizontal elements. This unit has a band of LEDs made as display to visualize signal's level.

A full principal diagram of the logical part is shown in Figure 6.10.

The element *DD1* on the scheme is LM 2901 microchip. This device consists of four independent precision voltage comparators. The supply voltage V_{CC} can have a wide range from ±18 V for a single supply source to 36 V of a dual one. The microchip has TTL, DTL, ECL, MOS, CMOS compatible outputs.

Each pair of *DD2.1*, *DD2.2* or *DD3.1*, *DD3.2* elements is CD4098B microchip. It is a dual monostable multivibrator that provides resettable/retriggerable one-shot operation for any fixed-voltage timing application. An external resistor R_4 – R_6 and an external capacitor C_1 – C_3 control the timing for the circuit. S_1 and S_2 are the leading-edge-triggering and trailing-edge-triggering inputs of the microchip. The maximum voltage of the supply source is 18 V.

DD4 shown in Figure 6.10 is CMOS NAND microchip CD4011B. It is a quad 2 input NAND microchip that can have a DC supply source up to 20 V.

The value of the resistor R_7 depends on the type of LED chosen for indication but in general should be in the order of kΩ or higher.

The LED Driver for Light Band Displays – *DD5* is based on UAA180 microchip. This integrated circuit is made for driving 12 light emitting diodes. Corresponding to the input, the voltage LEDs forming a light band are controlled similar to a thermometer scale. Scale display by means of a growing light band is very suitable for the measuring of approximate signal level above the horizontal element. Pin 2 serves to determine the diode current which results in different light intensity. By using an appropriate circuitry, the light passage between two adjacent LEDs can be set between "smooth" and "abrupt".

The timing diagrams of the signals processing throughout the element and components of the circuit are shown in Figure 6.11 and Figure 6.12.

From Figure 6.11, it can be seen step by step processing of the Sensor 1 captured signal. The example shown in Figure 6.11 implies a failure of the horizontal element. In this case two digital signals from comparators K_1 and K_2 launch *DD2.2* comparator and one of the *DD2.1* and *DD3.1* comparators depending on the current direction. According to the result of such a processing, an operator will see one of the indicating LEDs glow. Thus, this part of the *PCIU* circuit indicates only differences in current directions and did not show the failure's position.

Processing of the signal for the horizontal element failure's indication is shown in Figure 6.12. As one can see, the "failure" LED flashing happens only if signals from both sensors are not overlapped as it is shown on the *DD3.2 (pin 11)* axes. In turn, signals do not overlap if they have different directions. Otherwise, if there is no failure and the current direction in the element is the same there will be no indication since a logical element *DD4* does not have activated inputs.

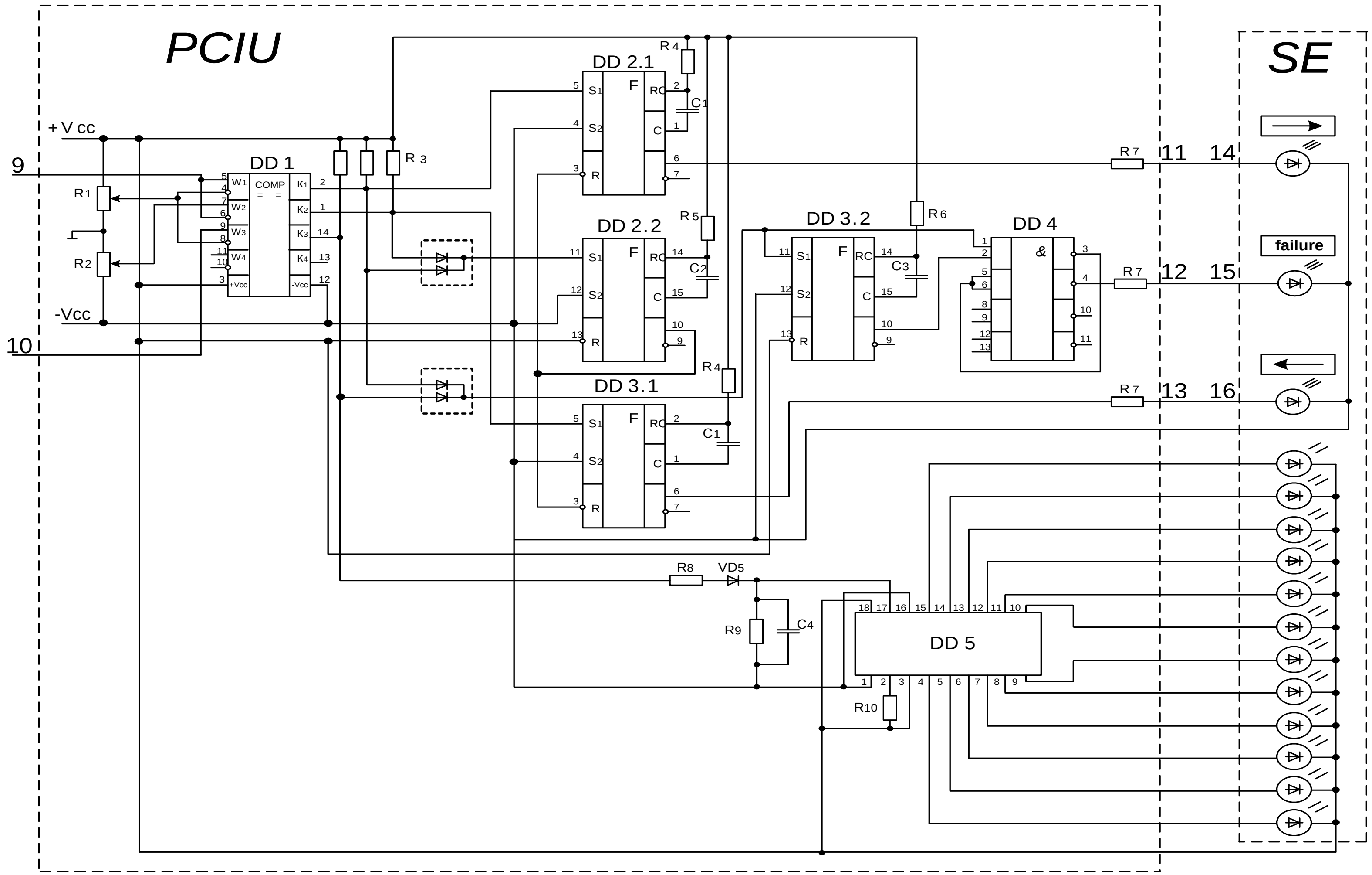

Figure 6.10: Principle diagram of device

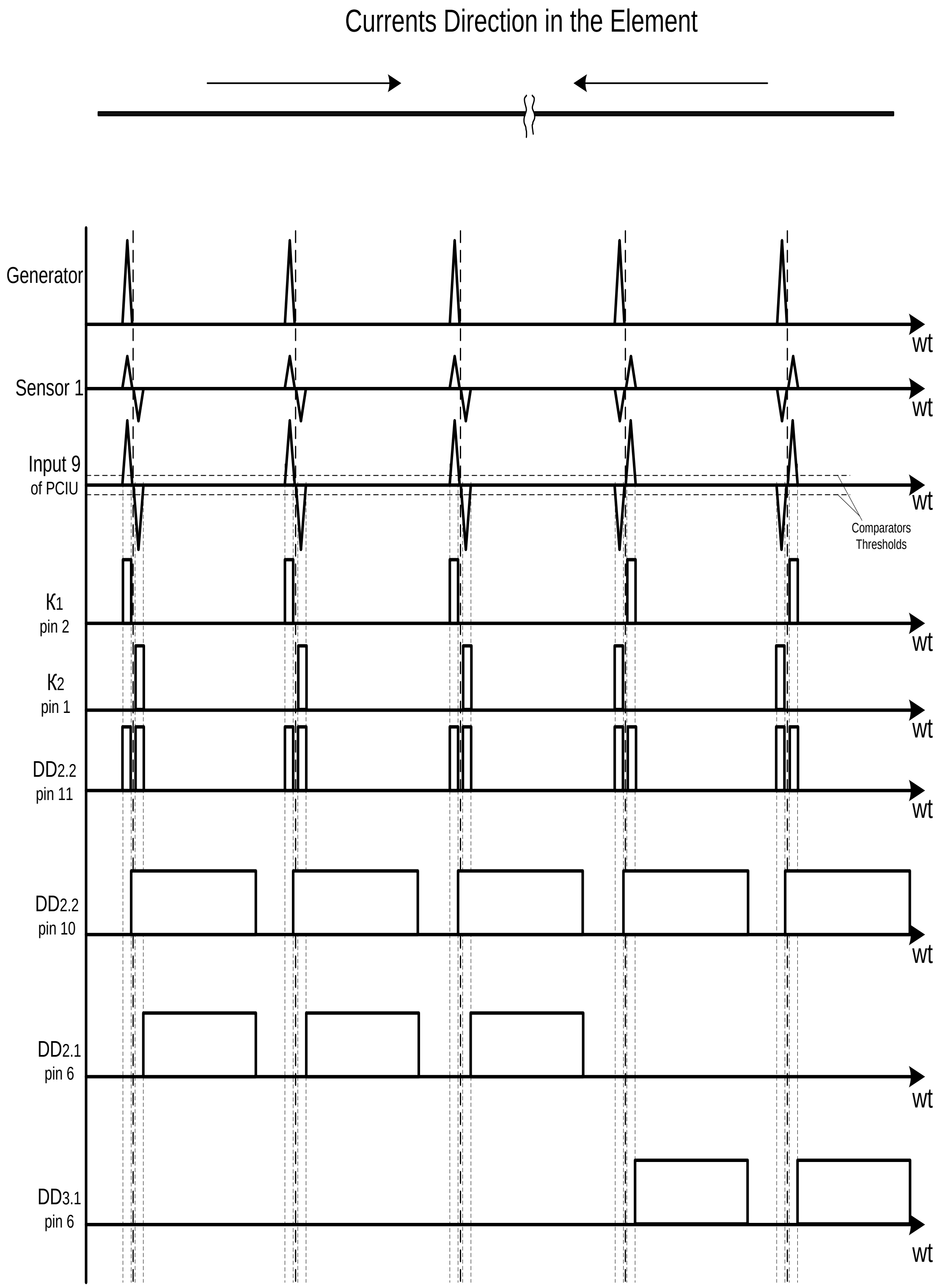

Figure 6.11: Timing diagram for currents direction indication

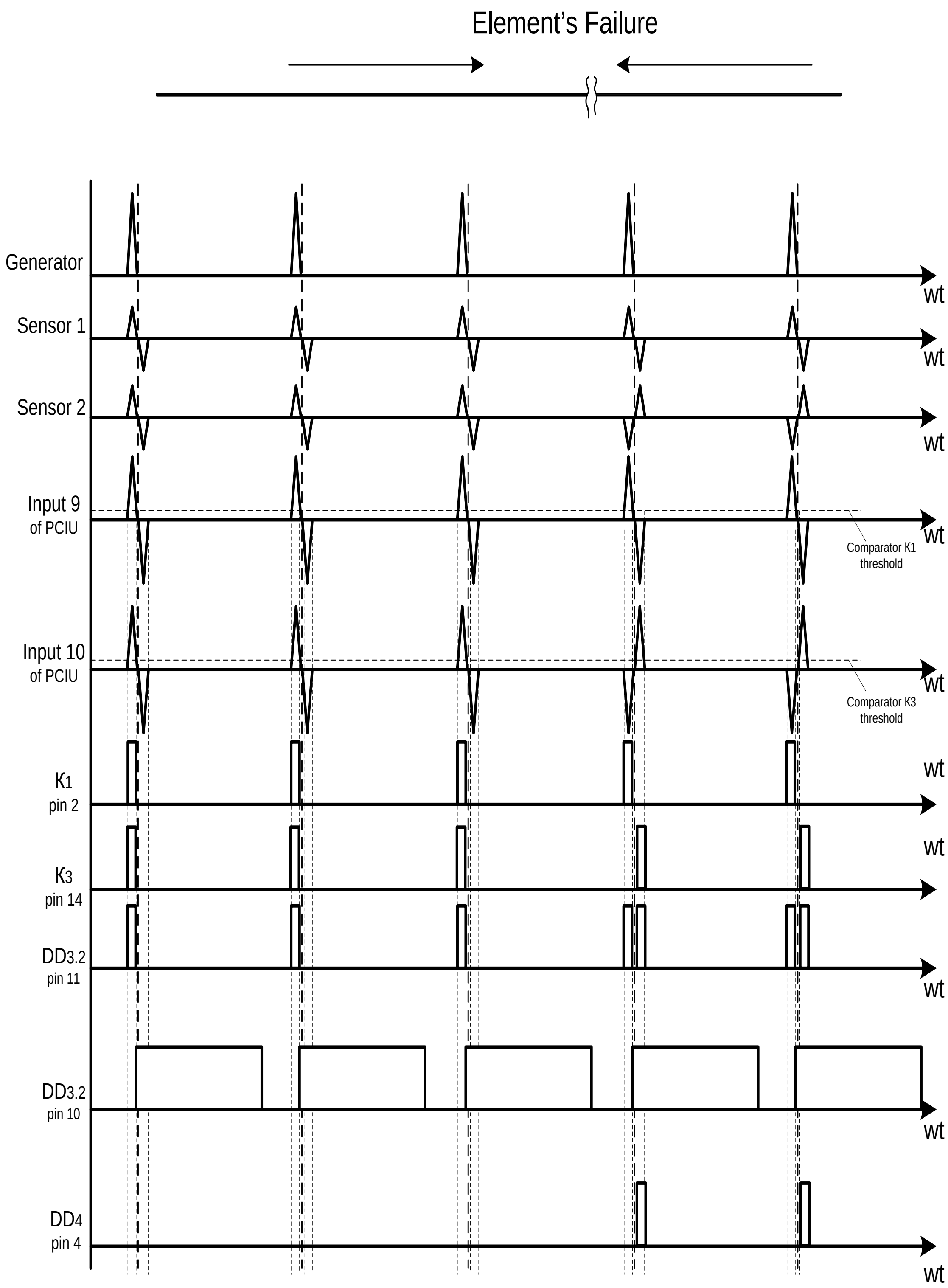

Figure 6.12: Timing diagram for failure indication

6.3 Logical processing based on microcontrollers (PLCs)

Despite an option of using microchips as a base for the future technical device as explained in the previous subsection, another way how to create such a device using programmable logic controller (PLC) can be developed.

A PLC is a digital computer used in many areas especially for automation and control of the processes in industry. A PLC is an example of a real time system since output results must be produced in response to input conditions within a limited time. PLCs are very convenient not only for industrial needs but also in such areas as relay control, motion control, process control, distributed control systems and networking. The data handling, storage, processing power and communication capabilities of some modern PLCs are approximately equivalent to desktop computers. The PLCs are well adapted to a range of automation tasks. These are typically industrial processes in manufacturing where the cost of developing and maintaining the automation system is high relative to the total cost of the automation, and where changes to the system would be expected during its operational life.

As an example, Programmable Logic Relay (PLR) Zelio Logic SR2 E121BD of Schneider Electric was used (see Figure 6.13) (*Smart relays Zelio Logics catalogue*, 2008). This family of PLRs includes a wide range of devices with different voltages of supply source and numbers of inputs and outputs (I/O). The supply source voltage can be up to 24 DC or 240 AC volts. The maximum number of I/O is 26 but can be easily extended by applying a needed number of extension blocks. This certain PLR contains 4 discrete inputs, 4 analogue inputs and 4 relay outputs.

This PLR can be programmed by using either Ladder Diagrams (LD) or Functional Block Diagrams (FBD) language. For a technical description of the programming, FBD way was chosen as more visual representation of the afore-described schemes and timing diagrams. Elements contained in FBD programming are close to those described earlier in a microchip base part of this work.

SR2 E121BD

Figure 6.13: Programmable logic relay SR2 E121BD

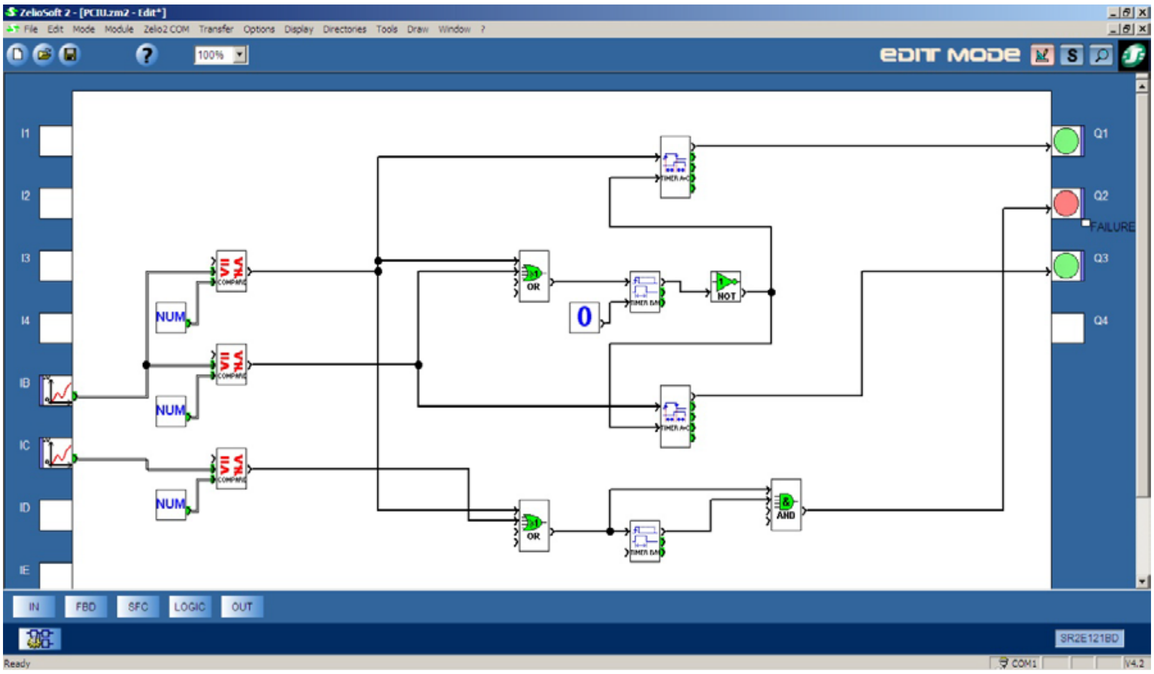

Figure 6.14: *PCIU* programming in Zelio Logic software

The result of *PCIU* programming in Zelio Logic software is shown in Figure 6.14.

Signals to be processed arrive from analogue inputs *IB* and *IC* to three comparators shown in the left-hand side of the Figure 6.14. Blocks *NUM* determine adjustable thresholds of comparators. In two comparators connected to the input *IB* both parts (positive and negative) of the processed signal are converting into digital signals corresponding to signal's polarity. The comparator connected to *IC* input digitizes only positive part of the captured signal since only this part is using for the future processing.

After that, the digital signals from first two comparators are used for the currents direction evaluation. This part is similar to three elements *DD2.1*, *DD2.2* and *DD3.1* of Figure 6.10. The main idea of the part is the same, first of two impulses launches a middle timer and the second one determines lighting of one of the green LEDs at the outputs *O1* or *O3* depending upon the current phase or direction.

A bottom part of the circuit has also the same principle of signal processing as in Figure 6.10. It compares phases of two signals from both sensors of the device. If signals phases are different, it will result in red LED activation at output *O2*.

A complete setup of the PLC and a laptop in order to download *PCIU* scheme is shown in Figure 6.15.

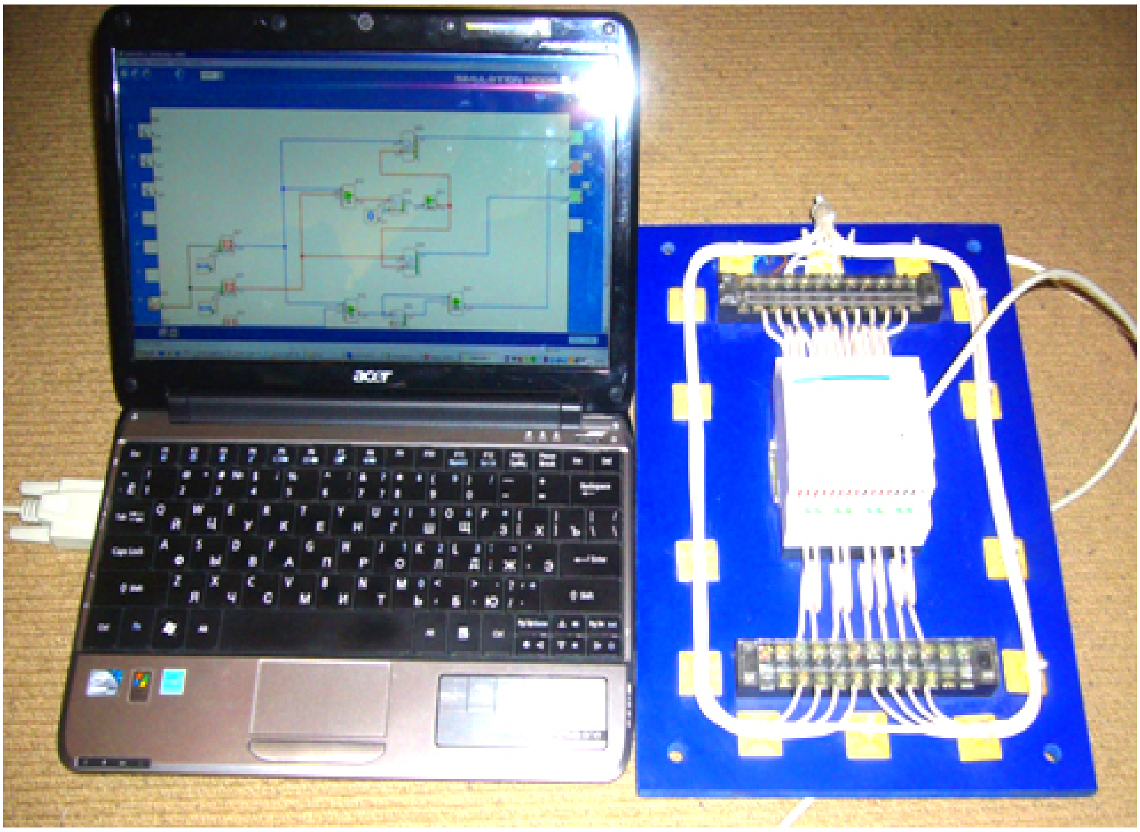

Figure 6.15: PC and laptop connection

Another example of PLC for the logical part can be SIEMENS LOGO series of controllers. This family of PLCs is similar to Zelio with a wide range of supply voltage (*Siemence Logo catalogue*, 2008).

A possible solution for the logical part of device can be presented as in Figure 6.16.

All the elements in Figure 6.16 have the same logical processing goal as explained earlier.

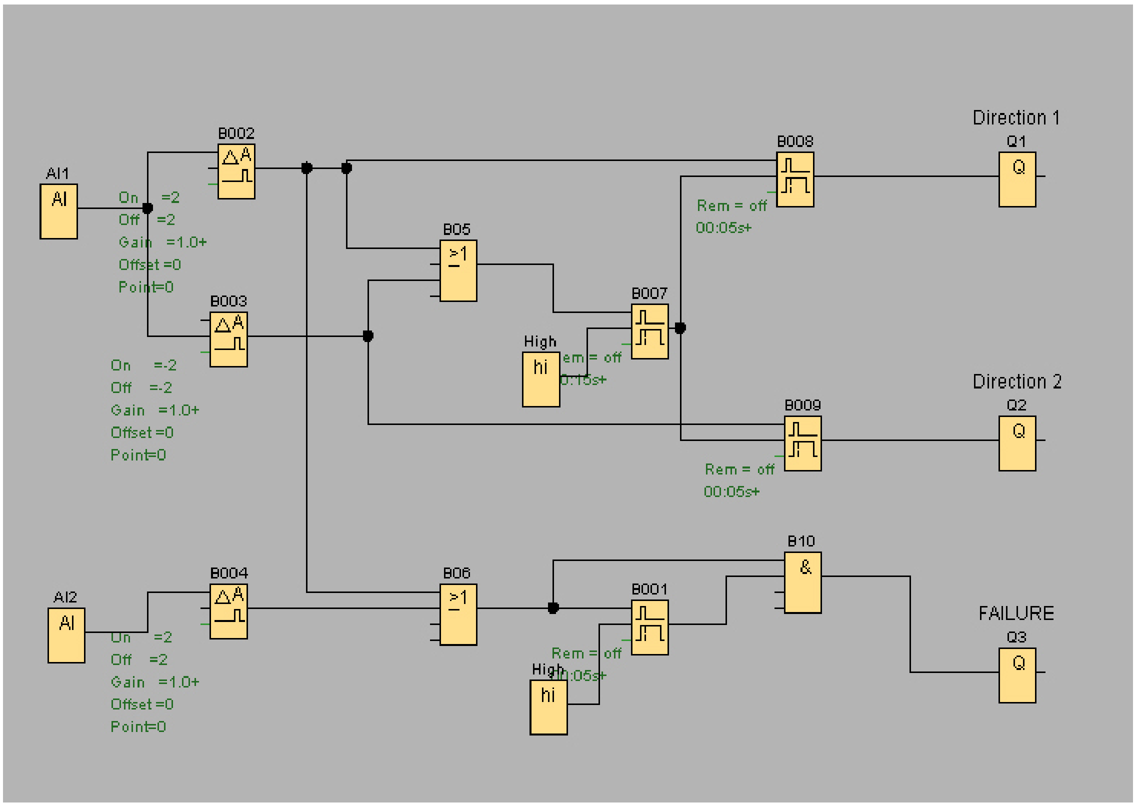

Figure 6.16: *PCIU* programming in SIEMENS LOGO software

6.4 Method of testing the horizontal elements integrity

Based on the features of the current and potential distribution in the grounding that have been revealed and explained earlier, in order to monitor the technical condition of the grids, detect damaged horizontal elements and their failures' positions, it is suggested to use a technique (sequence of steps) of the grounding devices investigation as described below. This number and content of steps in the procedure will allow full investigation of the horizontal elements' trace in the grids along with the damaged elements detection.

The monitoring technique comprises two main parts to be fulfilled.

During the first step of investigation, an impulse signal generator is connected with its both ends to the most remote points (enclosures' pigtails) at the territory of electric power plant. By means of such a connection, this scheme provides current flow through all elements of the grounding grid as shown in Figure 6.17. The current value is adjusted to be high enough for the detection on the surface of ground.

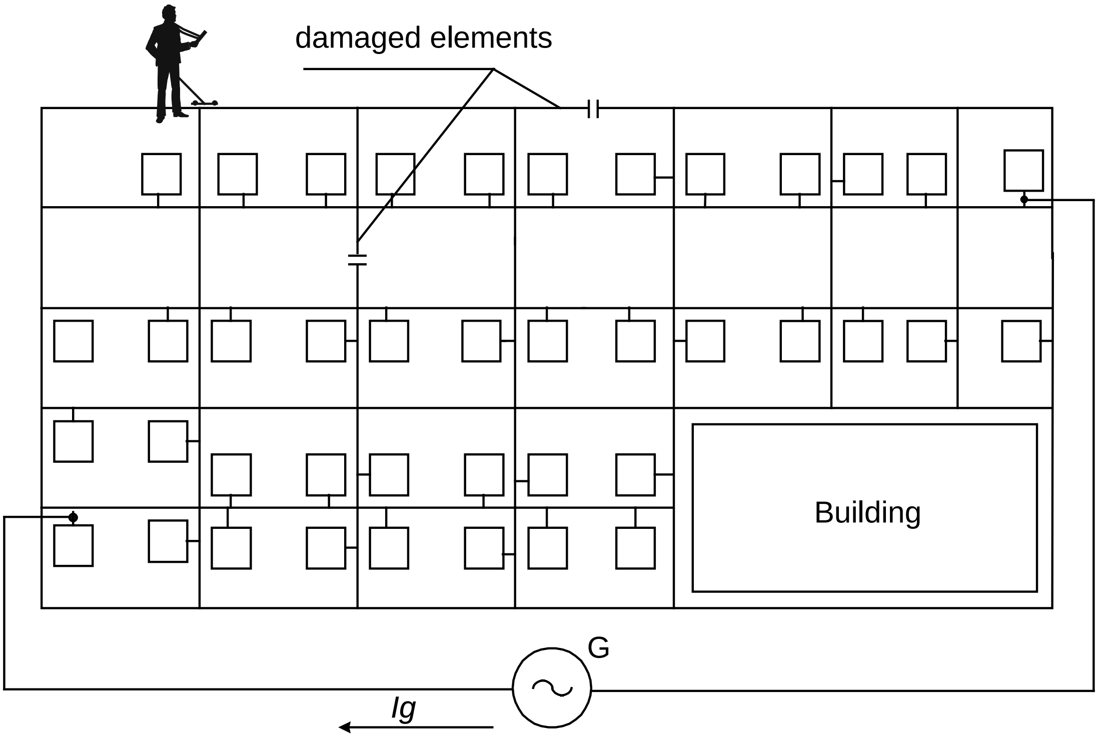

Figure 6.17: Grounding device investigation. Step 1.

While moving above the grounding grid, an operator is able to see the maximum readings of the Indication Module of the device above the horizontal elements. Thus, the operator determines the trace (location) of the grounding elements. It is important since within years the real position of the elements may change due to variations in the grounding scheme which is not always noted in the documentation.

At the same time while moving along the horizontal elements, the operator notices areas and elements with a substantial drop of the captured signal potential values. At this point, this sign may indicate a fact of the damaged horizontal element location. Horizontal elements without failures will not have such a noticeable potential drop.

The second step implies another circuit when one terminal of the generator is connected to any enclosures' pigtail and the other one to the remote probe (vertical electrode). The length of the vertical probe should be at least 2m to provide a good contact with soil. The location of the probe should be at least several meters away from the grounding grid. In this case, the scheme provides current from the horizontal elements of the grounding grid into the soil structure and then to the probe as shown in Figure 6.18.

.

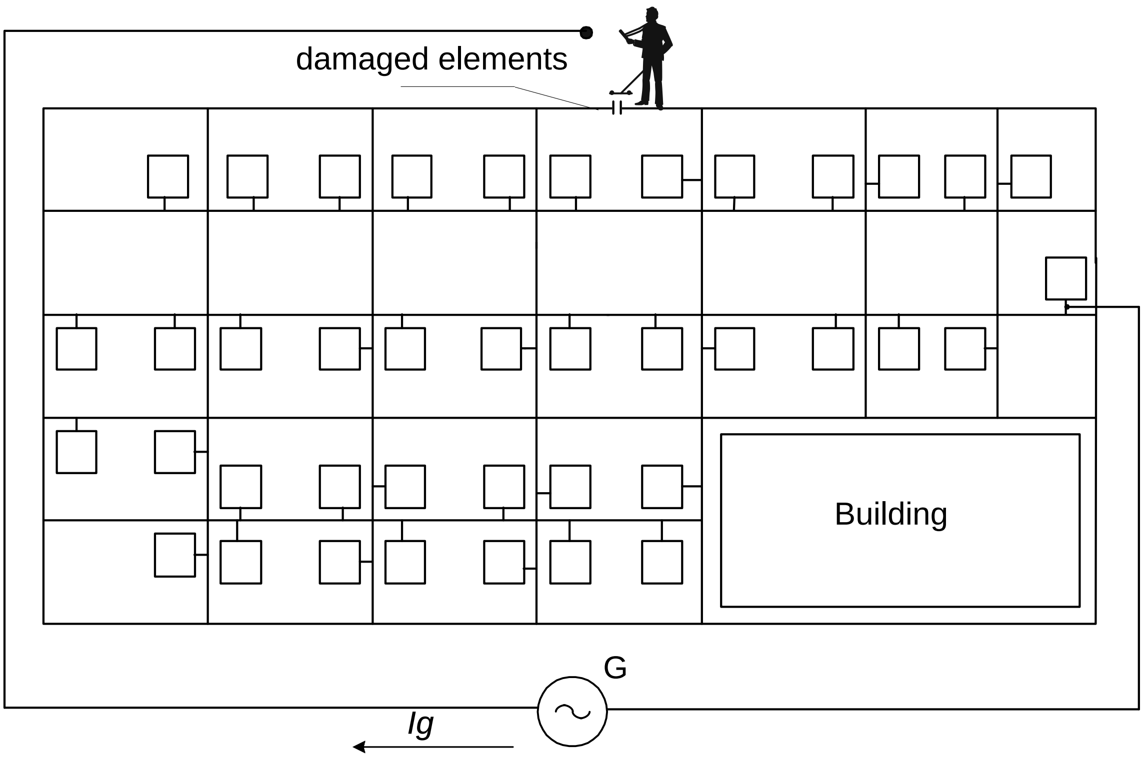

Figure 6.18: Grounding device investigation. Step 2.

At this stage, the operator moves along the "suspicious" horizontal elements detected at the previous step of the grounding investigation procedure. The Indication Module of the device shows the location of failure when the operator is moving over it by means of sound or light signal.

In general, regardless of the grounding device type, the algorithm of the described technique can be presented as shown in Figure 6.19.

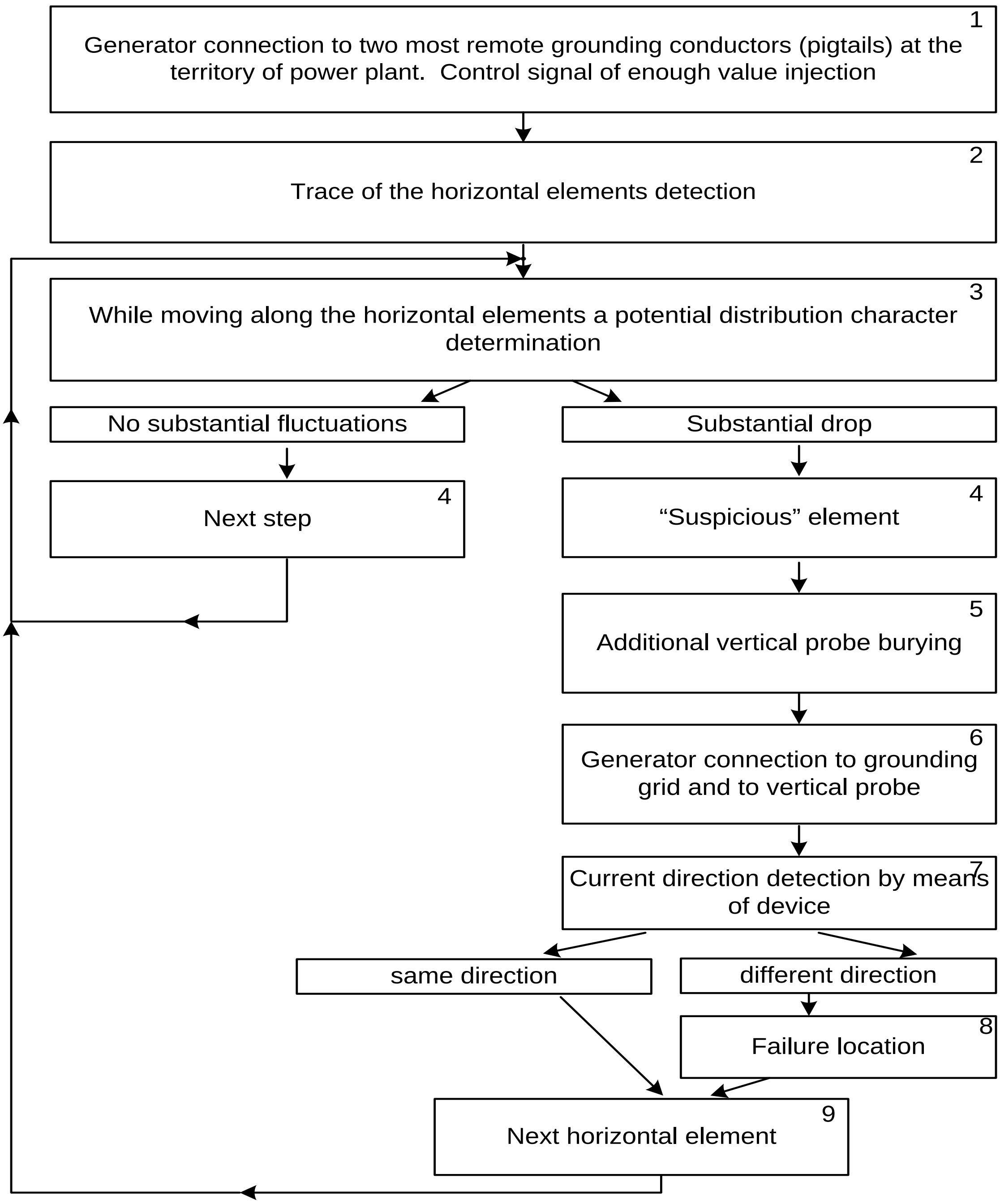

Figure 6.19: Algorithm of grounding investigation

The shape of the grounding grid and meshes configuration does not change the way of investigation or the device's performance. The only parameters that matter are the direction and character of the current in the horizontal elements or potential distribution over them. But with decrease of the length in one of the parts (bits) of the damaged horizontal conductor, the sensitivity of the device is not good enough to detect the current due to its small value.

6.5 Concluding remarks

There are two main aspects presented in this chapter; (i) a full description of the proposed device for the grounding monitoring and the damaged elements' detection and (ii) a sequence of actions for a complete examination of the horizontal grid.

It is described that as a base of the proposed device either microchips or programmable logical controllers (PLCs) can be used. Both ways of the device development have pros and cons. The main characteristics of the PLCs are: reliability, versatility, affordable and intuitive interface, the ability of reprogramming for needed operation along with a higher cost in comparison to the microchips. At the same time, not all the functions of analogue processing of the captured signals can be made by the available types of PLCs. Meanwhile, the integrated circuit base is more affordable but, at the same time, is more difficult to set it up and tune and it is not easy to reprogram.

The processing of the captured on the surface of ground test signal in the proposed device is explained in the chapter. The operation of all the units of the device along with the main timing diagrams is also described.

Finally, the algorithm of the grounding monitoring technique is presented in this chapter.

CHAPTER 7: CONCLUSIONS AND FUTURE RECOMMENDATIONS

7.1 Summary and conclusions

The main result of the study is the development of a new approach to the grounding devices' monitoring technique along with analysis of the fundamental processes in grounding grids with and/or without damaged horizontal elements. Considerable benefits such as time and labour reduction for the grounding devices' investigation with increase of accuracy of failures location can be obtained by using the proposed methods described in the thesis. Meanwhile, the main safety criteria prognosis can be made in case of damaged horizontal elements and this is due to the analysis suggested in this work.

Several evaluations were conducted in the study, i.e. the current and potential distribution in a separate conductor and in the grounding grid as whole, features of these processes in damaged elements, safety parameters evaluation in case of damaged elements presence, frequency response on grounding elements etc. These investigations required different analytical methods. The thesis presented step by step approach for each analysis. The methodology comprised mathematical, computer modelling and experimental studies of the processes in the grounding.

A mathematical analysis was carried out to set out frequency dependent characteristics of the grounding elements in grids. The results presented showed that elements' impedance could be substituted by its resistance for a low range frequencies analysis. But with a high frequency (megahertz) scenario, the conductor behaved more like the inductance rather than a pure resistance. It was also shown that the effect of frequency that has influence on the soil resistivity and permittivity must be taken into account.

During the magnetic field analysis over the horizontal element, the curves of patterns of the magnetic field and potential distribution along the horizontal element were shown to be quite different for integrated and damaged elements. The study demonstrated that there was a significant drop of the field and potential values at the point of the element's failure. Meanwhile, the curve of distribution was quite even over the elements without failures.

A mathematical model of the elements with lumped and distributed impedances and their interchange ability enabled the estimation of the processes for different scenarios of the grounding operation. The effect of the elements mutual coupling was also discussed and the mathematical analysis also provided. The findings from this research had led to further investigation of the processes in grids with or without damaged elements as a whole.

A network model and its analysis based on graphs theory and matrix analysis is presented in Chapter 4. It showed features of the current and potential distribution in the grid as a whole. A graph theory and a matrix analysis were very useful for the study.

A computer model of the grounding grid was presented to simulate the processes with damaged horizontal elements. The calculations and modelling results provided showed that even if the grounding devices initially had been made in accordance to all standardized permissible safety parameters, due to the horizontal elements destruction, hazardous potentials for personnel could appear. The study also revealed the main features of the current and potential distribution processes in the grids with damaged horizontal elements.

Experimental investigation of the processes in grounding was carried out to validate and justify the main outcomes of the theoretical part. The analysis presented showed that it is more convenient to use an impulse current for the grounding investigation with the frequency different from the fundamental one. This will benefit in reduction of the power plant noise influence on this impulse current. It will also allow of any digging, tripping and forced outage elimination at the plant.

Analysis carried out during the experimental part revealed the same principals and features of the current and potential distribution in grids as that discussed in the theoretical analysis of the thesis.

A new technical device's structure for the grounding monitoring was described in Chapter 6. Principal diagrams and schemes of the main units and blocks of the device along with timing diagrams of its operation were shown in the chapter. At the same time, a sequence of steps of a new grounding monitoring technique was presented.

7.2 Suggestions for future work

The findings of the experimental part with respect to the horizontal elements failure impedance can establish further investigation of this phenomenon in different scenarios of the grounding grids operation. It is necessary to derive empirical description, expression or formula to calculate such failure impedance as a function of distance, soil resistivity, form and shape of electrodes etc. It will be interesting to provide an evaluation of possible variations of this gap impedance for different types of horizontal elements as a function of the gap's distance. In addition, it can be useful to carry out the study for impulse impedance behaviour evaluation of the "failure" for different types of soil.

It was shown in the study that in case of the damaged element's presence in the grid, the currents before and after the point of failure had opposite directions. Moreover, the magnitudes of the potential and magnetic field strength at this point were significantly lower compared with the rest along of the element. It will be beneficial to explore the edge conditions of the failure position in the horizontal element since the closer the point of the failure to the end of the conductor the more substantial the influence from the adjacent elements on the processes will be.

Moreover, it would be very useful to evaluate the possibility of combining the functional capabilities of the device with the existing equipment for the grounding devices investigation.

REFERENCES

Audin, M. l. (2003). *Geometry*. New York: Springer.

Bayliss, C. R. (1996). *Transmission and distribution: Electrical engineering*. Oxford: Butterworth Heinemann.

Bernard Lacroix, & Calvas, R. (1998). Earthing systems worldwide and evolutions *173*, 1-24.

Berube, R. H. (2004). *Computer simulated experiments for electric circuits using Electronics workbench multisim* (3 ed.). Upper Saddle River, N.J: Pearson/Prentice Hall.

Betts, J. E. (1981). *Physics for technology*. Reston Va: Reston Pub. Co.

Bourg, S., Sacepe, B., & Debu, T. (1995, 14-18 Aug 195). Deep earth electrodes in highly resistive ground: Frequency behaviour Symposium conducted at the meeting of the Electromagnetic Compatibility, 1995. Symposium Record., 1995 IEEE International Symposium on doi:10.1109/isemc.1995.523625

Cavka, D., & Poljak, D. (2011, 15-17 Sept. 2011). Analysis of grounding electrode input impedance calculation. Symposium conducted at the meeting of the Software, Telecommunications and Computer Networks (SoftCOM), 2011 19th International Conference on

Celli, G., Ghiani, E., & Pilo, F. (2012). Behaviour of grounding systems: A quasi-static EMTP model and its validation. *Electric Power Systems Research, 85*(Journal Article), 24-29. doi:10.1016/j.epsr.2011.07.004

Chikarov, Y., Lie, T. T., & Nair, N. (2013). Safety parameters of grounding devices at an electric power plan. *Electrical and Electronics Engineering, 2*(1), 1-20.

Chikarov, Y., Lie, T. T., & Nair, N. K. (2012). Mathematical modelling for assessing integrity of power systems grounding devices. *Journal of Energy and Power Engineering, 6*(7), 1097-1105.

Cooper, W. F., & Dolbey Jones, D. A. (1997). *Electrical safety engineering*. Oxford: Newnes.

Dawalibi, F. (1986). Electromagnetic fields generated by overhead and buried short conductors. Part 2 - ground networks. *Power Delivery, IEEE Transactions on, 1*(4), 112-119. doi:10.1109/tpwrd.1986.4308037

Dzapo, H., & Giannini, R. (2003). Program support for earth surface potentials measuring system. *Measurement Science Review, 3,* 25-28.

Electrical Installations for Buildings, &. (2005). [IEC 60364]. Geneva, Switzerland: IEC.

Giannini, R., & Dzapo, H. (2004, 18-20 May 2004). Earth surface potentials measuring device for large grounding systems testing Symposium conducted at the meeting of the Instrumentation and Measurement Technology Conference, 2004. IMTC 04. Proceedings of the 21st IEEE doi:10.1109/imtc.2004.1351511

Grcev, L. (2007, 24-28 Sept. 2007). Impulse efficiency of simple grounding electrode arrangements Symposium conducted at the meeting of the Electromagnetic Compatibility, 2007. EMC Zurich 2007. 18th International Zurich Symposium on doi:10.1109/emczur.2007.4388261

Grcev, L., & Dawalibi, F. (1990). An electromagnetic model for transients in grounding systems. *Power Delivery, IEEE Transactions on, 5*(4), 1773-1781. doi:10.1109/61.103673

Grcev, L., & Popov, M. (2005). On high-frequency circuit equivalents of a vertical ground rod. *Power Delivery, IEEE Transactions on, 20*(2), 1598-1603. doi:10.1109/tpwrd.2004.838460

Grcev, L. D. (1996). Computer analysis of transient voltages in large grounding systems. *Power Delivery, IEEE Transactions on, 11*(2), 815-823. doi:10.1109/61.489339

Grigsby, L. L. (2001). *The electric power engineering handbook*. Boca Raton, FL: CRC Press.

Haddad, A., Warne, D. F., & Institution of Electrical Engineers. (2004). *Advances in high voltage engineering*. London: Institution of Electrical Engineers.

Hickey, R. B. (2002). *Electrical construction databook*. New York: McGraw-Hill.

Hu, J., Zeng, R., He, J., Sun, W., Yao, J., & Su, Q. (2000, 2000). Novel method of corrosion diagnosis for grounding grid Symposium conducted at the meeting of the Power System Technology, 2000. Proceedings. PowerCon 2000. International Conference on doi:10.1109/icpst.2000.898168

Huang, L., & Kasten, D. G. (2001). Model of ground grid and metallic conductor currents in high voltage a.c. substations for the computation of electromagnetic fields. *Electric Power Systems Research*, *59*, 31-37.

IEEE Guide for Measuring Earth Resistivity, Ground Impedance, and Earth Surface

Potentials of a Grounding System, &. (2012). [IEEE Std 81-2012 (Revision of IEEE Std 81-1983)].

IEEE Guide for Safety in AC Substation Grounding, &. (2000). [IEEE Std 80-2000].

IEEE Recommended Practice for Grounding of Industrial and Commercial Power Systems, &. (2007). [IEEE Std 142-2007 (Revision of IEEE Std 142-1991)].

IEEE Standard for Qualifying Permanent Connections Used in Substation Grounding, &. (2003). [IEEE Std 837-2002 (Revision of IEEE Std 837-1989)].

Jambak, M. I., & Ahmad, H. (2000, 2000). Measurement of grounding system resistance based on ground high frequency behavior for different soil type Symposium conducted at the meeting of the TENCON 2000. Proceedings doi:10.1109/tencon.2000.892251

Jones, R. A. P. E., Jones, J. G., & Mastrullo, K. G. (2011). *The electrical safety program guide*. Sudbury, Mass: Jones & Bartlett Learning.

Jordan, P. (2012). *Foundations of Excel: for engineers and scientists*. Auckland, N.Z: Pearson.

Jowett, J. (2008). Ground grid integrity. *Neta World Magazine* 1-3.

Kaiser, K. L. (2005). *Electromagnetic compatibility handbook*. Boca Raton: CRC Press.

Li, Z.-X., Chen, W., Fan, J.-B., & Lu, J. (2006). A novel mathematical modeling of grounding system buried in multilayer Earth. *Power Delivery, IEEE Transactions on, 21*(3), 1267-1272. doi:10.1109/tpwrd.2006.875857

Liu, Y., Xiao, L., & Tian, J. (2010, 25-29 July 2010). Optimized corrosion diagnosis of large-scale grounding grid Symposium conducted at the meeting of the Power and Energy Society General Meeting, 2010 IEEE doi:10.1109/pes.2010.5589464

Llovera, P., Lliso, J. A., Fuster, V., & Quijano, A. (2008). Improved methodology for high-frequency low-current measurement of grounding rod impedance. *Power Delivery, IEEE Transactions on, 23*(4), 1954-1960. doi:10.1109/tpwrs.2008.923812

Ma, Y., & Karady, G. G. (2009, 4-6 Oct. 2009). Investigating grounding grid integrity based on the current injection method Symposium conducted at the meeting of the North American Power Symposium (NAPS), 2009 doi:10.1109/naps.2009.5484048

Ma, Y., Karady, G. G., & Kucuksari, S. (2010, 25-29 July 2010). Testing continuity of grounding grid using the AC current injection method Symposium conducted at the meeting of the Power and Energy Society General Meeting, 2010 IEEE doi:10.1109/pes.2010.5590219

Melipoulos, A. P. S., Feng, X., Joy, E. B., & Cokkinides, G. J. (1993). An advanced computer model for grounding system analysis. *Power Delivery, IEEE Transactions on, 8*(1), 13-23. doi:10.1109/61.180314

Mentre, F. E., & Grcev, L. (1994). EMTP-based model for grounding system analysis. *Power Delivery, IEEE Transactions on, 9*(4), 1838-1849. doi:10.1109/61.329517

Micro-Cap 10. Electronic circuit analysis program. User's guide. (2010). (10 ed.). Sunnyvale, CA: Spectrum Software.

Natarajan, R., Imece, A. F., Popoff, J., Agarwal, K., & Meliopoulos, P. S. (2001). Analysis of grounding systems for electric traction. *Power Delivery, IEEE Transactions on, 16*(3), 389-393. doi:10.1109/61.924816

Nekhoul, B., Labie, P., Zgainski, F. X., Meunier, G., Morillon, F., & Bourg, S. (1996). Calculating the impedance of a grounding system. *Magnetics, IEEE Transactions on, 32*(3), 1509-1512. doi:10.1109/20.497536

O'Riley, R. P. (2002). *Electrical grounding: bringing grounding back to earth*. Albany: Delmar Thomson Learning.

Olhoeft, G. R. (2003, 14-16 May 2003). Electromagnetic field and material properties in ground penetrating radar Symposium conducted at the meeting of the Advanced Ground Penetrating Radar, 2003. Proceedings of the 2nd International Workshop on doi:10.1109/agpr.2003.1207309

Olsen, R. G., & Willis, M. C. (1996). A comparison of exact and quasi-static methods for evaluating grounding systems at high frequencies. *Power Delivery, IEEE Transactions on, 11*(2), 1071-1081. doi:10.1109/61.489370

Otero, A. F., Cidras, J., & Alamo, J. L. (1999). Frequency-dependent grounding system calculation by means of a conventional nodal analysis technique. *Power Delivery, IEEE Transactions on, 14*(3), 873-878. doi:10.1109/61.772327

Papalexopoulos, A. D., & Meliopoulos, A. P. (1987). Frequency dependent characteristics of grounding systems. *Power Delivery, IEEE Transactions on, 2*(4), 1073-1081. doi:10.1109/tpwrd.1987.4308223

Pedrosa, A. G., Shroeder, M. A. O., Afonso, M. M., Ali pio, R. S., de Castro Assis, S., Oliveira, T. A. S., & Braga, A. R. (2010, 8-10 Nov. 2010). Transient response of grounding electrodes for the frequency-dependence of soil parameters Symposium conducted at the meeting of the Transmission and Distribution Conference and Exposition: Latin America (T&D-LA), 2010 IEEE/PES doi:10.1109/tdc-la.2010.5762982

Poliyanin, A. D., & Manzhirov, A. V. (2007). *Handbook of mathematics for engineers and scientists*. Boca Raton, FL: CRC Press.

Predko, M. (2002). *Digital electronics guidebook*. New York: McGraw-Hill.

Rudenberg, R. (1945). Grounding principles and practice I - Fundamental considerations on ground currents. *Electrical Engineering, 64*(1), 1-13. doi:10.1109/ee.1945.6440813

Schuler, C. A. (2003). *Electronics: principles and applications*. New York: Glencoe McGraw-Hill.

Sekioka, S., Sonoda, T., & Ametani, A. (2005). Experimental study of current-dependent grounding resistance of rod electrode. *Power Delivery, IEEE Transactions on, 20*(2), 1569-1576. doi:10.1109/tpwrd.2004.838660

Selby, A., & Dawalibi, F. (1994). Determination of current distribution in energized conductors for the computation of electromagnetic fields. *Power Delivery, IEEE Transactions on, 9*(2), 1069-1078. doi:10.1109/61.296292

Serway, R. A., & Jewett, J. W. (2004). *Physics for scientists and engineers*. Belmont, CA: Thomson/Brooks/Cole.

Short, T. A. (2003). *Electric power distribution handbook*. GB: CRC Press Inc.

Siemence Logo catalogue, &. (2008). Nurnberg, Germany: Siemence AG.

Skiling, H. H. (1967). *Electrical engineering circuits* (2 ed.). New York, NY: Wiley.

Skilling, H. H. (1974). *Electric networks*. New York, NY: Wiley.

Smart relays Zelio Logics catalogue, &. (2008). Rueil-Malmaison Cedex, France: Schneider Electric Industries SAS.

Sunde, E. D. (1949). *Earth conduction effects in transmission systems.* . New York, NY D. Van Nostrand Company, Inc. doi:10.1002/sce.3730340336

Terman, F. E. (1943). *Radio engineers' handbook.* New York, NY: Mc Graw-Hill Book Company.

U.S. Department of Health and Human Services. (2008). Worker deaths by electrocution.

Vautier, G., Consulting, C., & New Zealand Institute of Chartered, A. (2008). *Excel: tips and techniques that make you say 'wow'!* (Vol. no. S.885.). Wellington, N.Z: New Zealand Institute of Chartered Accountants.

Visacro, S., & Portela, C. M. (1987). Soil permittivity and conductivity behavior on frequency range of transient phenomena in electric power systems. *Proceedings of Symposium High Voltage Engineering*.

Williams, A. B., & Taylor, F. J. (2006). *Electronic filter design handbook*. New York: McGraw-Hill.

Winder, S. (1997). *Filter design*. Boston: Newnes.

Yacobs, A. I. (1981). *Electrical safety in agriculture*. Moscow: Kolos.

Yang, H., & Pan, D. (2008, 2-5 Nov. 2008). A numerical calculation method of substation grounding grids based on a new mathematical model Symposium conducted at the meeting of the Antennas, Propagation and EM Theory, 2008. ISAPE 2008. 8th International Symposium on doi:10.1109/isape.2008.4735339

Zhang, B., Zhao, Z., Cui, X., & Li, L. (2002). Diagnosis of breaks in substation's grounding grid by using the electromagnetic method. *Magnetics, IEEE Transactions on, 38*(2), 473-476. doi:10.1109/20.996125

Zhang, L., Pan, Z., Tan, B., & Wen, X. (2009, 27-31 March 2009). Computer Modeling and Simulation of Impulsive Grounding Symposium conducted at the meeting of the Power and Energy Engineering Conference, 2009. APPEEC 2009. Asia-Pacific doi:10.1109/appeec.2009.4918233

Appendix: List and relevant research outputs

Chikarov, Y. (2011, October). Development of New Control Techniques for Grounding Devices of Electric Power Plants. Oral Presentation at the Engineering Lunchtime Seminar Series (19/10/2011), School of Engineering, Auckland University of Technology, Auckland, New Zealand.

Chikarov, Y., Lie, T. T., & Nair, N. (2012). Mathematical Modelling for Assessing Integrity of Power Systems Grounding Devices. Journal of Energy and Power Engineering, 6(7), 1097-1105.

Chikarov, Y. (2012, September). A New Approach to Monitor the Integrity of the Grounding Grids' Horizontal Elements. Paper presented at the Earthing, Bonding, Lightning & Surge Protection Conference, Auckland, New Zealand.

Chikarov, Y., Lie, T. T., & Nair, N. (2012). Modelling and Analysis of Current and Potential Distribution Paths for Grounding Devices. Accepted for publication in the IET Proceedings: Generation, Transmission and Distribution.

Chikarov, Y. (2011, December). New Approach to Monitor Integrity of Grounding Devices. Oral Presentation at the Engineering Lunchtime Seminar Series (06/12/2012), School of Engineering, Auckland University of Technology, Auckland, New Zealand.

Chikarov, Y., Lie, T. T., & Nair, N. (2013). Safety Parameters of Grounding Devices at an Electric Power Plan. Electrical and Electronics Engineering, 2(1), 1-20.

Chikarov, Y., Lie, T. T., & Nair, N. (2013, July). Safety Parameters at an Electric Power Plant in case of the Grounding Devices' Elements Failures. Proceedings of the IEEE PES General Meeting, Vancouver, Canada.